TECHNISCHE UNIVERSITÄT MÜNCHEN

FAKULTÄT CHEMIE

LEHRSTUHL ORGANISCHE CHEMIE II

UNRAVELING BACTERIAL INTERKINGDOM SIGNALING BY TARGETING PHOSPHOASPARTATE WITH CHEMOPROTEOMICS

DISSERTATION ZUR ERLANGUNG DES AKADEMISCHEN GRADES EINES DOKTORS DER NATURWISSENSCHAFTEN VON

PATRICK WOLFGANG ANTON ALLIHN

MÜNCHEN 2021

TECHNISCHE UNIVERSITÄT MÜNCHEN

FAKULTÄT CHEMIE

LEHRSTUHL ORGANISCHE CHEMIE II

UNRAVELING BACTERIAL INTERKINGDOM SIGNALING BY TARGETING PHOSPHOASPARTATE WITH CHEMOPROTEOMICS

Patrick Wolfgang Anton Allihn

Vollständiger Abdruck der von der Fakultät für Chemie der Technischen Universität München zur Erlangung des akademischen Grades eines

Doktors der Naturwissenschaften (Dr. rer. nat.)

genehmigten Dissertation.

Vorsitzender:		Prof. Dr. Franz Hagn
Prüfer der Dissertation:	1.	Prof. Dr. Stephan A. Sieber
	2.	Prof. Dr. Kathrin Lang

Die Dissertation wurde am 03.11.2021 bei der Technischen Universität München eingereicht und durch die Fakultät für Chemie am 16.11.2021 angenommen.

Danksagung

An dieser Stelle möchte ich mich bei denjenigen bedanken, die diese Arbeit ermöglicht und den Weg dorthin erfolgreich und so kurzweilig gemacht haben.

Zuallererst möchte ich mich bei Prof. Dr. Stephan Sieber für die Möglichkeit bedanken, an seinem Lehrstuhl meine Doktorarbeit anzufertigen und an spannenden Projekten arbeiten zu dürfen. Vielen Dank für die hervorragende Betreuung, das Vertrauen und die hilfreiche Unterstützung bei sämtlichen wissenschaftlichen Herausforderungen.

Ein riesengroßes Dankeschön gilt Dr. Stephan Hacker, der mir von Tag eins an mit Rat und Tat zur Seite stand, um in unzähligen Meetings und Versuchen mit Hilfe seiner isoDTB Strategie einen optimierten Workflow und die bestmögliche Analyse-Methodik für das Phosphoaspartat-Projekt zu erarbeiten. Neben der erfolgreichen Zusammenarbeit danke ich ihm für Bürounterkunft und die stets unterhaltsame und kollegiale Zeit außerhalb des Labors. In seiner neuen Position als Juniorprofessor an der Universität Leiden wünsche ihm nur das Beste. Weiterhin möchte ich besonders großen Dank an Dr. Christina Ludwig vom BayBioMS aus Freising aussprechen. Ich hätte mir keine bessere Mentorin vorstellen können und von ihr habe ich sehr viel lernen dürfen. Durch ihre Expertise und kompetenten Ratschläge wurde eine erfolgreiche Methodik-Entwicklung und somit mein Promotionsabschluss erst möglich.

Außerdem möchte ich Dr. Robert Mayer und Dr. Armin Ofial von der LMU für die erfolgreiche Kooperation danken. Des Weiteren danke ich den weiteren Kooperationspartnern Dr. Sam Asami, Patrizia Bratrich und Prof. Dr. Michael Sattler vom Bayerischen NMR Zentrum sowie Dr. Ana Gasperotti und Prof. Dr. Kirsten Jung von der LMU für die gute Zusammenarbeit.

Ein großer Dank geht an Dr. Mathias „Hacki“ Hackl für die ausgezeichnete Betreuung und Übergabe des Phosphoaspartat-Projektes, sowie die herausragende Vorarbeit hierzu. Ich danke Angela Weigert-Muñoz vielmals für die tolle Teamarbeit und wünsche ihr viel Erfolg für die Fortführung des Cystic Fibrosis Gender Gap Projektes.

Ein riesiges Dankeschön geht an die „Drübners“ (Dr. Ines Hübner und Dr. Jonas „Johnny“ Drechsel) für die unglaubliche Hilfsbereitschaft, enge Freundschaft, täglichen Diskussionen und stets unterhaltsame Zeit seit Beginn des Masterstudiums. Vielen Dank an Dr. Patrick Ralph Angelo „Zani“ Zanon für die unvergesslichen Patrick A bis Z Seminare. Auch, wenn man sogar als Bayer von seinem Genuschel vor allem mit Maske nichts verstanden hat, hatte der harte Kern eine Fetzen-Gaudi mit ihm und all seinen Geschichten (meist begünstigt durch kräftige Unterstützung seines Mexikaners). Und wenn es wie des Öfteren etwas „Wichtiges“ zu besprechen gab, waren Ines, Johnny, Zani, Robs, Angela und Till als harter Kern immer für einen da. Merci für die ur-griabige Zeit!

Vielen Dank an Dr. Theresa „Thesi“ Rauh für den bestmöglichen Start in den Tag beim Radeln in die Uni, aber auch für die fatalen Versuche als Wetterfrosch für einen „sicheren“ Heimweg. Danke auch an den Rest der Radl-Crew, die Squasher, die Kicker und die morgendlichen Boulder-Sessions mit Thesi, Zani, Thommy G, Tilli und Stewie. Es war mir zudem eine Ehre, Teil des guten alten LabBs gewesen zu sein mit Akteuren wie Hacki, Thommy G, Babsi, Weining und nicht zuletzt Stewie.

Danke für die schönen Zeiten, als Konferenzen noch persönlich stattfinden konnten, mit Caro, Mareike, Laura und Moritz der Barcelona-Crew bei der MaxQuant Summer School, mit Paaavel in Venedig beim SFB Retreat und mit Ines, Johnny, Zani und Hackerooo in Heidelberg bei der EMBL Konferenz.

Herzlichen Dank an die alte Generation, von der ich mir vieles abschauen durfte, vor allem von Dr. Dóra Balogh, Dr. Markus Lakemeyer, Dr. Philipp Le, Dr. Volker Kirsch, Dr. Matthias Stahl und Dr. Pavel Kielkowski. Außerdem vielen Dank an Mona Wolff, ohne die der Laden niemals laufen würde. Ebenso gilt mein Dank Katja Bäuml, Christina Brumer und Barbara Seibold für die herausragende Unterstützung des ganzen Arbeitskreises.

Ich möchte natürlich dem gesamten AK Sieber danken für die tolle Arbeitsatmosphäre und die heiteren Abende in der Kaffee-Küche, beim Grillen, im Kleinwalsertal und natürlich bei allen Doktorfeiern. Schee war’s!

Großes Merci an die Schöffel-Crew und vor allem die Weißbierseekopfadler Dr. Johannes Kremser und Kevin Vincze für die griabige Zeit während des Bachelors in Innsbruck.

Mein größter Dank jedoch gilt meiner FAMILIE für die sensationelle Unterstützung und den außerordentlichen Rückhalt über all die Jahre, und ROXANA RAAB, die mich seit dem Abitur ebenso liebevoll unterstützt und mir täglich Kraft und Motivation für alle Herausforderungen gibt. Vielen vielen Dank für einfach alles!

Abstract

Antimicrobial resistance is a major threat for human health and will become the number one cause of deaths worldwide, if no action is taken. Thus, there is an urgent need to find new druggable targets for antibiotics. In this process, the identification of the microbe's resistance and virulence regulating enzymes is crucial.

Two-component systems are indispensable for the survival and pathogenicity of bacteria, as they can sense a multitude of external signals like antibiotics and respond by triggering adaptive resistance. Within these signal transduction systems, consisting of a sensor histidine kinase and a response regulator (RR), the latter contains a key posttranslational modification essential for its activity, phosphoaspartate (pAsp). To infer the role of these systems in disease associated signal transduction pathways, analysis of the conserved pAsp modification is mandatory. However, this posttranslational modification is hydrolytically unstable, impeding its detection via common analytical methods.

The goal of this thesis was to establish a chemoproteomic method to capture transient pAsp with a tailored nucleophilic probe for activity-based protein profiling (ABPP). The trapping strategy was optimized using a recombinant model RR, revealing an acidic pH as prerequisite for hydroxylamine turnover. Subsequently, a reverse polarity ABPP platform was established to detect pAsp sites using a desthiobiotin (DTB) tag. Application of a refined workflow to lysates of *B. subtilis* and *P. aeruginosa* proteomes allowed the successful identification of multiple annotated pAsp sites of known RRs in addition to many new potential pAsp sites by mass spectrometry (MS).

The validated strategy was further advanced by incorporating the newly developed isotopically labeled DTB (isoDTB)-tags into the workflow enabling accurate quantification of pAsp levels under varying treatments. The goal of implementing this method was to decipher molecular details of *P. aeruginosa* cationic peptide signaling. Investigating the signaling of the human peptide stress hormone dynorphin A, which is sensed by highly pathogenic *P. aeruginosa* to induce adaptive resistance, revealed CprR as an unprecedented RR in dynorphin A interkingdom signaling. This finding was substantiated

by varying treatment durations and the application of targeted mass spectrometry with enhanced sensitivity. Overall, the illustrated mass spectrometry-based method is widely applicable for the exploration of various signaling systems involving pAsp in both prokaryotes and eukaryotes.

Furthermore, in-depth analysis of DTB-tag MS-fragmentation behavior allowed the identification of distinctive patterns and signature fragment ions that were used to significantly boost the sensitivity of the method.

Zusammenfassung

Antimikrobielle Resistenz stellt eine große Bedrohung für die menschliche Gesundheit dar und wird zur weltweiten Todesursache Nummer eins werden, wenn keine entsprechenden Maßnahmen ergriffen werden. Daher besteht ein dringender Bedarf, neue Angriffspunkte für Antibiotika zu finden. Dabei ist die Identifizierung der Resistenz- und Virulenz-regulierenden Enzyme der Mikroben von zentraler Bedeutung.

Zweikomponentensysteme sind für das Überleben und die Pathogenität von Bakterien unverzichtbar, da sie eine Vielzahl von externen Signalen wie Antibiotika wahrnehmen und daraufhin adaptive Resistenz auslösen können. Innerhalb dieser Signaltransduktionssysteme, welche aus einer Sensor-Histidinkinase und einem Antwortregulator bestehen, enthält letzterer eine für seine Aktivität wesentliche posttranslationale Modifikation, Phosphoaspartat (pAsp). Um die Rolle dieser Systeme in krankheitsbedingten Signaltransduktionswegen zu ermitteln, ist die Analyse der konservierten pAsp-Modifikation unerlässlich. Dass diese posttranslationale Modifikation jedoch hydrolytisch instabil ist, erschwert ihren Nachweis mit den üblichen Analysemethoden.

Ziel dieser Arbeit war es, eine chemoproteomische Methode zum Abfangen der kurzlebigen pAsp-Modifikation mit einer maßgeschneiderten nukleophilen Sonde für die aktivitätsbasierte Proteinprofilierung (ABPP) zu entwickeln. Die Abfangstrategie wurde durch Zuhilfenahme eines rekombinanten Modell-Antwortregulators optimiert. Dabei stellte sich ein saurer pH-Wert als Voraussetzung für den Umsatz mit Hydroxylaminen heraus. Anschließend wurde eine ABPP-Plattform mit inverser Polarität zum Nachweis von pAsp-Stellen unter Verwendung eines Desthiobiotin-Tags eingerichtet. Die Anwendung des ausgefeilten Arbeitsablaufs in Lysaten von *B. subtilis* und *P. aeruginosa*-Proteomen ermöglichte die erfolgreiche Identifizierung zahlreicher annotierter pAsp-Stellen bekannter Antwortregulatoren sowie vieler neuer potenzieller pAsp-Stellen durch Massenspektrometrie (MS).

Die validierte Strategie wurde durch die Einbeziehung der neu entwickelten isotopenmarkierten markierten DTB (isoDTB)-Tags in den Arbeitsablauf weiterentwickelt, um eine genaue Quantifizierung der pAsp-Modifikationen bei unterschiedlichen Behandlungen zu ermöglichen. Das Ziel der Implementierung dieser Methode war die Entschlüsselung der molekularen Details der Signalübertragung durch kationische Peptide in hochpathogenem *P. aeruginosa*. Das humane peptidische Stresshormon Dynorphin A wird von *P. aeruginosa erkannt*, um adaptive Resistenz zu induzieren. Bei der Untersuchung der Wirkung dieses Hormons auf Antwortregulatoren von *P. aeruginosa* wurde entdeckt, dass CprR als bis dato unbekannter Antwortregulator für die Dynorphin A-Signalübertragung zwischen den Organismen zuständig ist. Dieser Befund wurde durch unterschiedliche Behandlungsdauern und die Anwendung der gezielten Massen-spektrometrie mit erhöhter Empfindlichkeit bestätigt. Insgesamt ist die gezeigte Massenspektrometrie-basierte Methode zur Untersuchung verschiedener Signaltransduktionsssysteme, an denen pAsp beteiligt ist, sowohl in Prokaryoten als auch bei Eukaryoten umfassend einsetzbar.

Darüber hinaus ermöglichte eine tiefgreifende Analyse des MS-Fragmentierungsverhaltens der DTB-Tags die Identifizierung charakteristischer Muster und signifikanter Fragment-Ionen, welche die Empfindlichkeit der Methode erheblich steigern ließen.

Introductory Remarks

This doctoral dissertation was completed between October 2017 and October 2021 under the supervision of Prof. Dr. Stephan A. Sieber at the Chair of Organic Chemistry II of the Technical University of Munich.

Parts of this thesis have been published in:

Allihn, P. W. A, Hackl, M. W., Ludwig, C., Hacker, S. M., Sieber, S. A. A tailored phosphoaspartate probe unravels CprR as a response regulator in *Pseudomonas aeruginosa* interkingdom signaling. *Chem. Sci.,* **2021**, *12*, 4763-4770.

Parts of this thesis were reproduced with permission from Allihn, P. W. A, Hackl, M. W., Ludwig, C., Hacker, S. M., Sieber, S. A. A tailored phosphoaspartate probe unravels CprR as a response regulator in *Pseudomonas aeruginosa* interkingdom signaling. *Chem. Sci.,* **2021**, *12*, 4763-4770.

Contributions:

P.W.A.A., M.W.H., S.M.H. and S.A.S. conceived the project. Nina C. Bach performed cloning experiments. P.W.A.A. and M.W.H conducted organic synthesis, gene overexpression, protein purification, IPMS experiments, gel-based labeling experiments. P.W.A.A., M.W.H. and S.M.H. performed MS-based labeling experiments. P.W.A.A. performed biochemical assays, western blots, signaling experiments, PRM experiments and site-ID analyses. P.W.A.A. and C.L. developed PRM methods and analyzed PRM experiments.

Contributions by M.W.H. have additionally been published as part of the publication: Hackl, M. W., Phenyl Esters as Inhibitors of *S. aureus* ClpP and Hydroxylamine-based Reverse Polarity ABPP. **2018**. http://mediatum.ub.tum.de/doc/1415620/1415620.pdf (Doctoral dissertation, Technical University of Munich).

Publications

Journal Publications

Allihn, P. W. A, Hackl, M. W., Ludwig, C., Hacker, S. M., Sieber, S. A. A tailored phosphoaspartate probe unravels CprR as a response regulator in *Pseudomonas aeruginosa* interkingdom signaling. *Chem. Sci.,* **2021**, *12*, 4763-4770.

Mayer, R. J.; Allihn, P. W. A.; Hampel, N.; Mayer, P.; Sieber, S. A.; Ofial, A. R. Electrophilic reactivities of cyclic enones and α,β-unsaturated lactones. *Chem. Sci.*, **2021**, *12*, 4850-4865.

Conferences

Allihn, P. W. A., Hackl, M. W., Mayer, R. J., Hacker, S. M., Ofial, A. R., Sieber, S. A. Reactivity and binding dynamics of small molecules at active sites. *SFB 749 Conference*, Venice, Italy, Mar 11-14, **2019**. (Poster presentation)

Allihn, P. W. A, Hackl, M. W., Hacker, S. M., Sieber, S. A. Chasing phosphoaspartate by hydroxylamine based reverse polarity ABPP*. Expanding the Druggable Proteome with Chemical Biology (EMBL Conference).* Heidelberg, Germany, Feb 5-7, **2020**. (Poster presentation)

Table of Contents

1 Introduction

1.1. Antibiotic Crisis and Bacterial Signaling via Two-Component Systems

1.1.1. Antibiotic Crisis

The assumption, that microbial infections do not pose a major health risk and can be treated with appropriate medication, holds true in most cases to this date. However, if antimicrobial agents are not applied properly, pathogens are capable of acquiring resistance and common infections become life-threatening. Already back in 1945, in his Noble lecture for the discovery of the first broad-spectrum antibiotic penicillin, Sir Alexander Fleming illuminated this phenomenon by the detection of resistant microbes upon penicillin underdosage and warned about the danger of antimicrobial resistance (AMR).[1] Despite Fleming's early warning and the development of a multitude of antibiotics foremost in the last century, the emergence and spread of drug-resistant pathogens could not be stopped. Especially the misuse and overuse of antimicrobial agents in agriculture, aquaculture and animal as well as human health-care drove this evolution.[2] One major danger is the alarming appearance and potential spreading of pan-resistant bacteria, so-called superbugs, that are resistant to all existing antibiotics.[3, 4] Common infections or minor surgeries would therefore illustrate serious threats. By the year 2050, antimicrobial infection will be the number one cause of death with around 10 million cases worldwide, if no new medication is developed.[5] Therefore, AMR displays one of the greatest and most complicated global threats facing humanity. Already at this point, annually in the United States, more than 2.8 million antibiotic-resistant infections occur and more than 35 thousand people die from them.[6] The cost of AMR to the U.S. economy is enormous at more than US$4.6 billion per year.[7] Aside from disability and death, the cost factor also accounts for those affected, since prolonged disease leads to longer hospital stays and more expensive treatments.[7] Therefore, it is crucial to prevent antimicrobial infections in the first place and contain their spread, accompanied by responsible use of antibiotics.[6] On the other side, new antibiotics have to be developed. However, this intention is not attractive to most pharmaceutical companies for financial reasons. On the one hand, the complex process of drug development takes many years, leading to high research costs of around US$1.5 billion.[8] On the other hand, new antibiotics are solely prescribed for late-stage treatments over a short period of time,

resulting in low revenue expectancies. To account for the lack of financial incentives, new strategies are needed. A key approach to this is funding by governments and international institutions along with their collaboration with the pharmaceutical industry. Accordingly, a number of initiatives have been launched to fund and drive antibiotic research and development, like the German Antibiotic Resistance Strategy (DART 2020)[9], Global Antibiotic Research & Development Partnership (GARDP),[10] Combating Antibiotic-Resistant Bacteria (CARB-X)[11] and the AMR Action Fund.[12]

The development of effective drugs against multidrug-resistant bacteria is often based on the identification of new bacterial targets, mostly enzymes, whose inhibition restricts bacterial growth or prevents the pathogen from becoming virulent. However, the function of the target is often unclear. In fact, a large proportion of the genomes of WHO priority pathogens is composed of genes of unknown function (GUFs). This is particularly the case for *Pseudomonas aeruginosa*, for which 70% of GUFs (1470) are identified only in *Pseudomonas* species (specific), while 30% (633) are also present in other organisms (non-specific).[13] Since this bacterium is particularly dangerous, it is vital to identify its essential, specific and virulence expressing enzymes and understand their functions. Consequently, these enzymes can display interesting targets for the development of new drugs that impair them and thus lead to death or virulence attenuation of the pathogen.

1.1.2. *Pseudomonas aeruginosa* Infections

P. aeruginosa is a Gram-negative, rod-shaped and facultative anaerobic bacterium that is found primarily in soil and water.[14] Possessing a versatility of regulatory genes and virulence factors, its large genome (5.5-7 Mb) enables the bacterium to adapt to changing environmental conditions and become highly resilient.[15] *P. aeruginosa* is one of the most dangerous Gram-negative pathogens, causing severe diseases such as pneumonia and cystic fibrosis, which are associated with reduced quality of life and increased mortality.[16, 17] Furthermore, it is a common cause of catheter-associated infections and in burn wounds.[18, 19] Being designated by the WHO as a critical priority for the development of new antibiotics to combat multidrug resistance, *P. aeruginosa* possesses sophisticated pathogenesis mechanisms, enabled by a large variety of virulence factors, and antibiotic defense mechanisms for resistance development.[20, 21] Pathogenesis mechanisms include

acute virulence factors like the type III secretion system to secrete exotoxins (ExoS, ExoT, ExoU, ExoY)[22] and quorum sensing (e.g. the Las and Rhl systems), describing the coordination of cell population density, to secrete pyocyanin, rhamnolipids, elastase and cyanide.[23-25] Phenotypic virulence factors belonging to this group consist of flagella-mediated swimming and swarming and type IV-pilus-mediated twitching motility.[26] In contrast, chronic virulence factors comprise the siderophore pyoverdin, alginate, type VI-secretion and biofilm formation.[21, 27, 28] Together, this repertoire of virulence factors demonstrates the danger to humans, resulting in diseases such as cystic fibrosis.

1.1.3. The Cystic Fibrosis Gender Gap

Cystic fibrosis (CF) is a genetic disorder caused by mutations in the cystic fibrosis transmembrane conductance regulator (CFTR) gene.[29] The CFTR protein represents a chloride channel that conducts chloride ions across epithelial cell membranes. When it is not functional, chloride ions cannot be transported and water diffuses into the cells by osmosis. Consequently, the secretions become thicker and can no longer be transported adequately, which applies to all glands in the body.[30] Thus, CF mostly affects the lungs in addition to the pancreas, liver and intestine. As a result, displaying ideal conditions for pathogens like *P. aeruginosa*, chronic biofilm infections occur. These are difficult to treat, since affected patients have to be medicated with antibiotics over a long period of time and thus *P. aeruginosa* can become highly resistant, eventually leading to premature mortality due to respiratory failure.[31] However, over the last 80 years, life expectancy of a new-born increased from only a few years to 53 years by now.[32]

Remarkably, women with CF were found to die significantly earlier than compared to men, which has not changed despite increased life expectancy.[33] This phenomenon is called CF gender gap.[34] However, the reason for this is unknown to this point and might be due to chromosomal or hormonal differences between the sexes.[35-37] Since it has been shown that pulmonary exacerbations correlate with the estrogen concentration during the menstrual cycle, a hormonal influence was assumed.[36] Nevertheless, it is not known how the influence of estrogen can explain the exacerbations. One possibility could be that estrogen influences the CF affecting bacteria, mainly *P. aeruginosa*, and thus activates their virulence. Interestingly, showcasing bacterial interkingdom signaling, it has been

shown that *P. aeruginosa* is able to recognize a human peptide hormone and control virulence in response, which is outlined in the following section.[38, 39]

1.1.4. Dynorphin A Signaling and Adaptive Resistance

When eukaryotic cells are exposed to stress, such as antibiotic infections, antimicrobial peptides and hormones are secreted to combat the threat. [38, 40, 41] Interestingly, when the human peptide hormone dynorphin A is released, which exhibits only moderate antibiotic activity, *P. aeruginosa* can sense it and respond by inducing virulence mechanisms.[38, 39] This interkingdom signaling between a human stress hormone and *P. aeruginosa* gives the pathogen a competitive advantage as it listens in on the human defense mechanism to prepare for an impending attack.

Recently, it was shown that dynorphin A is sensed by the two-component system (TCS) ParRS, which belongs to a family of TCSs that can recognize cationic antimicrobial peptides (CAMPs) such as the antibiotic polymyxin B and trigger adaptive resistance.[42] This finding was plausible, since dynorphin A shows similar properties like CAMPs, bearing five positive charges. In the course of adaptive resistance, the ArnBCADTEF operon is induced, which mediates the addition of positively charged 4-aminoarabinose to the lipid A moiety of lipopolysaccharide (LPS).[39, 42, 43] Thereby, the negative charge of LPS is masked that is responsible for the binding and uptake of cationic antimicrobial peptides.[44] Consequently, this illustrates the importance of TCS signaling for bacterial survival.

1.1.5. Two-Component System Bacterial Signaling

The most common multi-step signal transduction pathways found in nature are two-component systems (TCSs).[45] They are particularly prevalent in bacteria, although TCSs exist in all three domains of life.[46-48] Being vital for the bacteria's survival and virulence, TCSs can sense and respond to a multitude of external signals. For instance, they perceive the presence of antibiotics and therefore initiate resistance mechanisms.[42] To demonstrate their variety, they can detect even small differences in their environment, including changes in nutrient supply, temperature, pH, light, osmolarity, redox potential, chemoattractants and quorum signals.[49-51]

Canonical TCSs consist of a usually membrane-bound histidine kinase (HK) and an intracellular response regulator (RR) (Figure 1). The HK comprises an *N*-terminal sensor domain connected to the cytoplasmic *C*-terminal HK domain by a transmembrane region.[52] The signaling occurs via a multi-step mechanism and starts by sensing external stimuli through the HK's sensor domain. Subsequent ATP hydrolysis leads to autophosphorylation of a conserved histidine residue in HK domain, forming a high energy bond between the phosphoryl group and the imidazole ring.[53] Next, the phosphate group is transferred from the HK to a conserved aspartate (Asp) residue in the receiver (REC) domain of its cognate RR. The REC domain is predominantly located on the sequential conserved *N*-terminus and linked to the *C*-terminal effector domain by a flexible linker.[54] RR phosphorylation causes a long-range conformational change activating the effector domain and thereby inducing the biological response.[53]

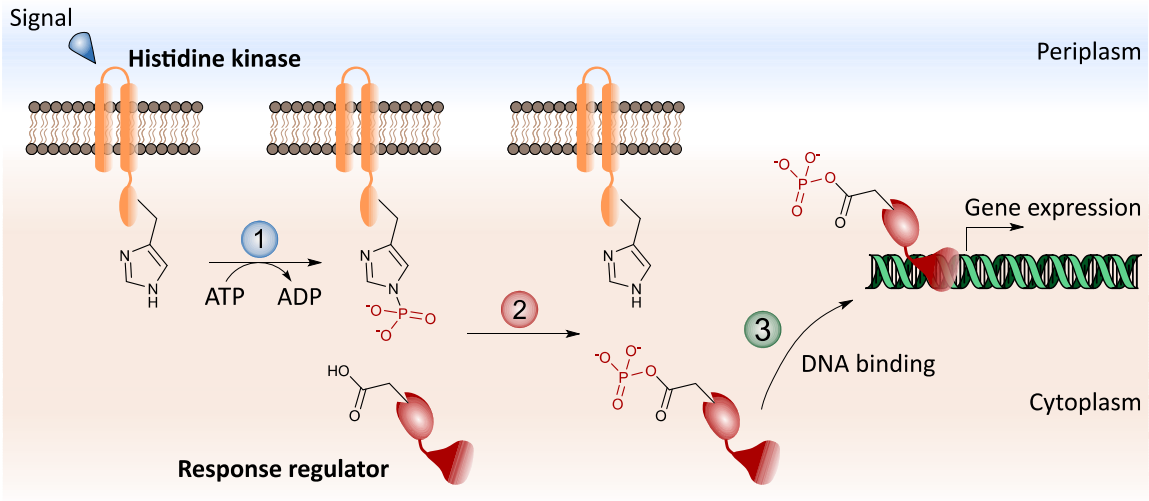

Figure 1: Architecture of two-component system signaling. (a) The membrane-bound histidine kinase senses an external signal and is autophosphorylated on a conserved His residue (1), followed by phosphotransfer to a conserved Asp residue of its cognate response regulator (2). Upon a conformational change, the response regulator binds to target genes and regulates their expression or induces chemotaxis (3). Adapted from Allihn *et al.*[55]

Reflecting the significance of responding to environmental changes through transcriptional regulation, the majority of RR effector domains bind target genes and thereby regulate gene expression.[53] However, RRs are highly diverse and aside from DNA-binding domains, they can contain RNA-binding, protein-binding or ligand-binding

effector domains to control a multitude of transcriptional and (post-) translational processes.[56] For example, chemotaxis can be regulated by effector domain binding of phosphorylated CheY to the flagellar motor FliM resulting in a flagellar rotational switch.[57, 58] Moreover, displaying about 8% of RRs effector domains, enzymatic domains can directly participate in signal transduction, *e.g.* as methylesterases or c-di-GMP-specific phosphodiesterases.[59, 60]

Apart from canonical TCSs there also exist phosphorelays involving numerous pHis- and phosphoaspartate (pAsp)-containing proteins that undergo multiple phosphorylation steps.[61] Being more prevalent in eukaryotes, these can also include hybrid kinases that contain the sensor HK as well as the RR in a single protein.[62] Overall, this demonstrates the versatility of TCSs and the importance to study Asp phosphorylation in signal transduction.

1.1.6. Phosphoaspartate

Phosphorylation of aspartate (pAsp) is a posttranslational modification (PTM) known to occur mainly in RRs of TCSs in bacteria. Nevertheless, it is present in all domains of life in enzymes like phosphorylation-type adenosine triphosphatase (P-type ATPase) ion pumps or as a free amino acid in bacteria, fungi and plants, displaying a key intermediate in the biosynthesis of the essential amino acids lysine, methionine and threonine.[63-66]

pAsp is a mixed carboxylic acid-phosphoric acid anhydride (acyl phosphate) that is highly reactive due to activation of both the carboxyl as well as the phosphoryl group for nucleophilic substitution.[66] Nature exploits this activation to allow otherwise inaccessible carboxylates or phosphates to be transformed with nucleophiles. Due to this activation, free pAsp is prone to hydrolysis at neutral pH, but can also be converted to the hydroxamate with hydroxylamine.[67] Furthermore, pAsp hydrolysed to 30% within 30 min in the pH range 4-10 at 30 °C, which was war less pronounced at 15 °C. Interestingly, experiments with acetyl phosphate showed hydrolytic cleavage of the C-O bond at acidic and alkaline pH, while at neutral pH the P-O bond was cleaved.[68, 69] These early reactivity studies of free pAsp and its analogues were monitored by colorimetric analysis of the corresponding hydroxamates upon turnover with hydroxylamine.[67, 70] However, this

method and the later introduced reductive cleavage by sodium borohydride did not allow direct detection of pAsp, which is desired in direct analysis of proteins containing this PTM.[71]

Since pAsp is assumed to be more stable within proteins, other methods were developed to detect pAsp in proteins. Originally, methods such as Fourier transform infrared spectroscopy and X-ray crystallography showed sporadic successful results for individual proteins.[72, 73] However, for the analysis of pAsp-bearing RRs, other methods were applied. A method for the structural characterization of the RR's active site is NMR spectroscopy using beryllofluoride (BeF_3^-) to bind Asp and thereby serving as a mimic of the phosphoryl group.[74] The most common and direct method to study Asp phosphorylation of RRs is based on the use of isotopically labeled ^{32}P reagents, which are transferred to the Asp residue of the RR and visualized by autoradiography after SDS-PAGE.[75] On the one hand, [γ-^{32}P]ATP is used to facilitate autophosphorylation from a HK, which in turn transfers the isotopically labeled phosphoryl group from its conserved histidine residue to the conserved Asp residue of the RR. On the other hand, the ability of the REC-domain of the RR to utilize small [γ-^{32}P]-isotopically labeled molecules such as acetyl phosphate, phosphoramidate, and carbamoyl phosphate, however not ATP, as Asp phosphorylation agents can be exploited.[76] In both methods, point mutations have demonstrated that phosphorylation must occur at a particular conserved Asp residue in each case. Furthermore, this method allows the monitoring of time dependent phosphorylation events.[75] However, these methods are only suited for the study of isolated RRs or TCSs instead of whole bacterial cells. For this, PTMs like phosphorylations are typically analyzed via mass spectrometry (MS)-based proteomics experiments.[77] However, conventional analytical methods like the immobilized metal affinity chromatography (IMAC) followed by liquid chromatography coupled to tandem MS (LC-MS/MS) are not applicable due to the limited half-life of the pAsp modification during the common proteomic workflows. Therefore, Chang *et al*. reverted to the original indirect method of trapping pAsp by α-effect nucleophiles, such as hydroxylamine, and applied it to the investigation of whole *E. coli* proteome by activity-based protein profiling (ABPP), which is outlined in the following section. [78-80]

1.2. Activity-Based Protein Profiling and Mass Spectrometry-Based Target Identification

1.2.1. ABPP

Activity-based protein profiling (ABPP) is a robust chemoproteomic technique for the exploration of enzymatic activity and drug-protein interaction in complex proteomes. Initially inspired by Parker, the method was developed by Cravatt[81-83] and Bogyo.[84, 85] The method usually employs small electrophilic compounds, activity-based probes (ABPs), which are covalently linked to nucleophilic amino acid residues such as cysteines for target discovery.[80] Conversely, also nucleophilic compounds can be covalently attached to electrophilic sites in proteins, which is called reverse-polarity ABPP (rp-ABPP).[86] To enable target identification (target-ID), the probes are equipped with a linker for specificity and a reporter tag to enable visualization or enrichment of labeled proteins.

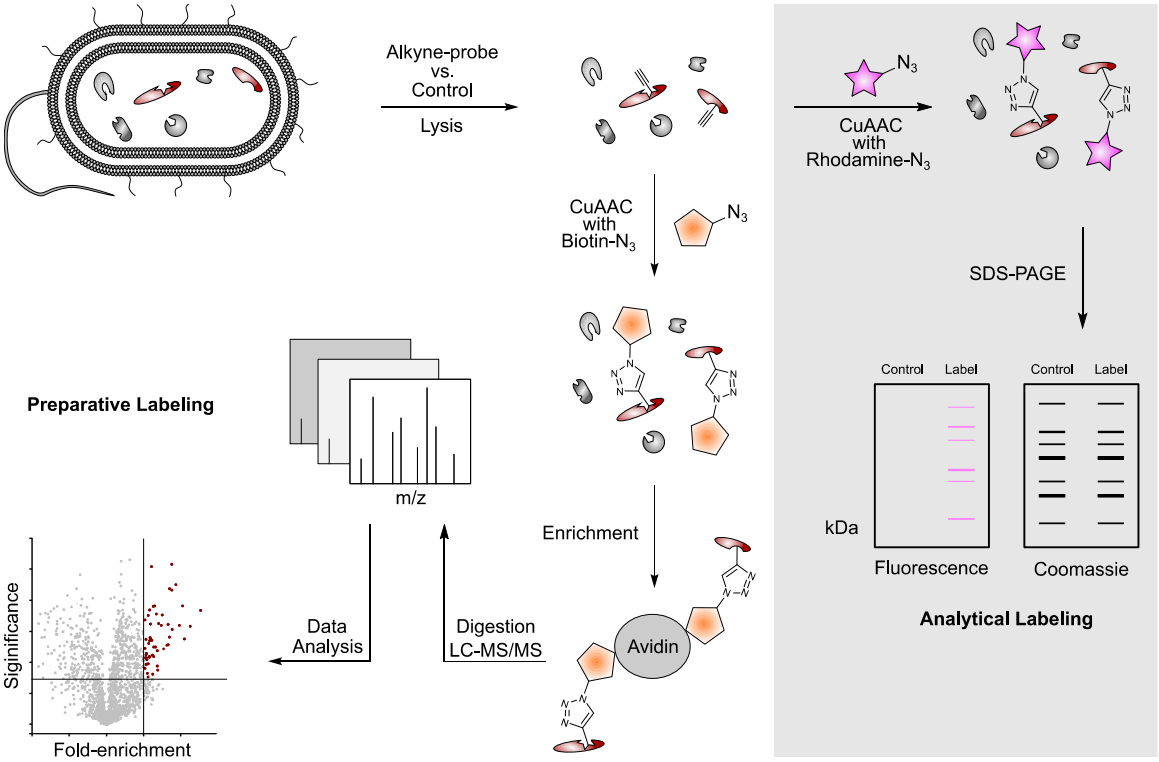

Figure 2: Schematic workflow of an ABPP experiment. Proteins are treated with a probe or a control by *in situ* labeling or after cell lysis. For analytical labeling, labeled proteins are conjugated to a fluorescent tag for SDS-PAGE and analysis by in-gel fluorescence scanning and Coomassie staining. For preparative labeling, labeled proteins are clicked to an affinity handle, enriched, digested and subjected to LC-MS/MS analysis.

Initially, reporter tags were directly attached to the probe. However, since probes were often not cell-permeable due to their polarity or bulk, other strategies had to be applied. Overcoming this limitation, *Huisgen*-[3+2] azide-alkyne cycloaddition, also called click reaction, allowed the introduction of the reporter tag at later stage during the workflow[83, 87, 88]. Hence, ABPs are equipped with either a terminal alkyne tag for covalently binding probes or an additional photo-crosslinker within the probe, allowing covalent attachment upon UV irradiation.[89] The latter approach is defined as affinity-based proteome profiling (AfBPP). Alkyne-bearing probes have several advantages. Besides their minor differences in size and reactivity to the original probe, various labels can be attached to the probe via click chemistry.[83, 88] Being important for many target identification experiments, the labeling conditions can be optimized in a cost-efficient way on analytical scale by "clicking" probe-labelled proteins to fluorescent tags like rhodamine azide, enabling readout by in-gel fluorescence SDS-PAGE (Figure 2). Utilization of an affinity tag allows the enrichment of probe-labeled proteins, which is required for their subsequent identification and quantification by high resolution mass spectrometry (HR-MS). The most widely-used affinity tag is biotin, showing high affinity to its natural binding partner avidin.[90] Therefore, probe-labeled and biotin conjugated proteins can be isolated from complex sample background by affinity pulldown on avidin beads, prior to enzymatic digestion and LC-MS/MS analysis. The MS-based quantification of enriched proteins allows the assessment of the target binding potency to a given probe and examination of binding differences under changing conditions. Several methods have been established for MS-based analysis and quantification, as discussed in the following section.

1.2.2. MS-Based Protein Analysis

MS- based protein analysis uses two common approaches, top-down and bottom-up proteomics.[91] Facilitating sample preparation, top-down proteomics implies the identification of intact proteins by direct LC-MS/MS measurement. Despite being less effective for protein identification than the bottom-up approach, top-down proteomics achieves complete sequence coverage and can therefore provide valuable information about site-specific mutations and PTMs.[91] Intact-protein MS (IPMS) additionally enables the fast evaluation of PTMs or covalently bound small molecules in single proteins.[92]

However, protein solubility, chromatography and spectra interpretation due to proteome complexity pose major challenges, preventing the majority of proteomics researchers employing despite recent advancements.[93, 94] Conversely, bottom-up proteomics involves the proteolytic cleavage of proteins into peptides prior to LC-MS/MS analysis (Figure 3).[91] Since proteins are cut into small fragments, the term "shotgun proteomics" evolved. As already indicated, digested peptides are separated by LC before measurement in order to reduce spectral complexity. The peptides are subjected to the mass spectrometer and analyzed via their mass-to-charge ratio (m/z). Since the m/z of a single peptide (MS1-level) of the digest does not inevitably allow a unique association to a protein, precursors are fragmented (MS2-level) that delivered the expression tandem MS. To gain information about the amino acid sequence and the association to a respective protein, bioinformatics software match the peptide sequence against an *in-silico* digest of the proteome of the organism under investigation.[95, 96] Thereby the identification of thousands of peptides is enabled within hours or even minutes.[97, 98]

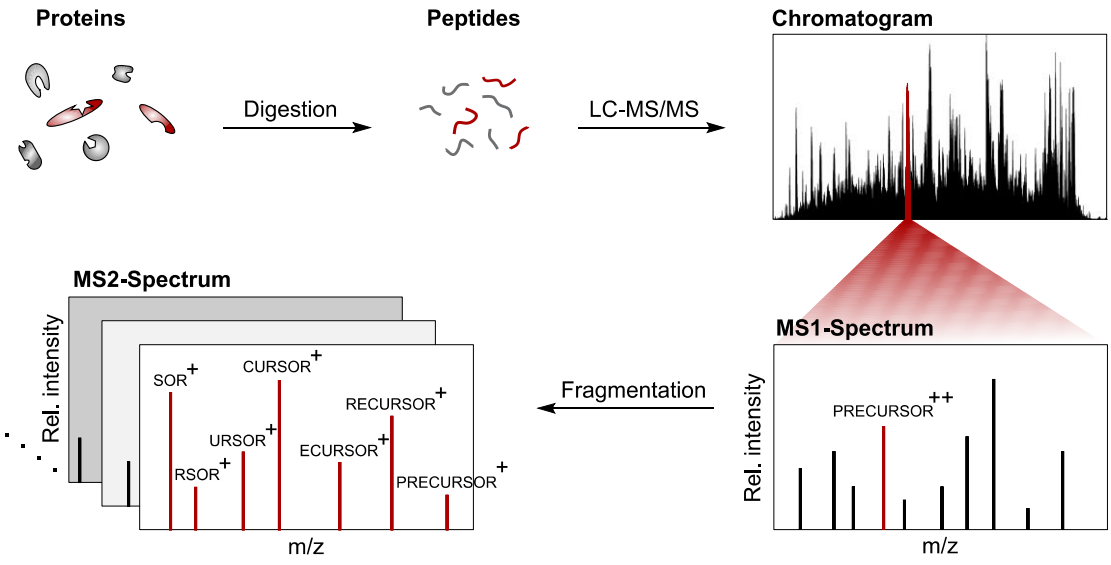

Figure 3: Schematic process of LC-MS/MS-based protein identification. Proteins are digested and peptides are separated by HPLC, followed by subjection to the mass spectrometer. Peptides are ionized and analyzed via their mass-to-charge ratio (m/z). The TopN most intense precursors (MS1) are selected for fragmentation (MS2).[99]

In order to draw conclusions about the differences between the various treatment methods, quantification is required in addition to identification. Quantification can take place at both the MS1, MS2 and even MS3 level using the respective signal intensities. At the MS1 level, the methods label free quantification (LFQ), stable isotope labeling by amino acids in cell culture (SILAC) and reductive dimethylation (ReDiMe) are the most established.[100-102] While LFQ is based on an algorithm that normalizes MS-runs and compares different runs with each other without the requirement of isotope labels, methods including isotope-labels (SILAC, ReDiMe) allow direct comparison of two conditions within a single run. For quantification at the MS2 level, isobaric labeling methods like tandem mass tags (TMT) and isobaric tags for relative and absolute quantification (iTRAQ) have been developed, allowing high throughput with up to 18 channels in one experiment.[103-105] However, the respective MS2 spectra are prone to interferences due to co-isolation of near-isobaric ions, resulting in ratio distortion. In turn, the interference effect can be overcome by a further isolation and fragmentation event (MS3).[106]

1.2.3. Binding Site Identification

The previously described methods addressed the identification of protein targets from covalent (ABPP, rp-ABPP) or non-covalent probes (AfBPP). However, to investigate the reactivity and binding of covalent probes at specific sites in proteins, and thus their mechanism of action, other techniques have to be employed.

The simplest way is full proteome analysis and does not require probe modification and hence, affinity enrichment. It consists merely of proteomic labeling with a probe, proteolytic digestion and LC-MS/MS measurement. Identification of the binding site is enabled by the specification of variable modifications in the search engine. If the mass shifts between potentially modified and unmodified peptides is not known, open search tools or the dependent peptides function in MaxQuant can provide information about putative mass shifts and the quantity of PSMs that contain these mass shifts.[98, 107] However, since complete proteomes represent highly complex samples, prior fractionation steps are required, which increases the measurement time several fold. This issue is even more pronounced when various conditions are assessed.

In contrast, ABPP methods can compensate for the drawbacks of full proteomic analyses by the enrichment of labeled proteins. However, in a target-ID approach, the measurement of all tryptic peptides of a protein is possible except for the one bound to avidin, which includes the site of interest. As this peptide is attached almost irreversibly to avidin, the information is lost, unless harsh conditions are used to detach the peptide of interest from the beads, which would destroy the peptide or the modification.[108] To overcome this limitation, two concepts are commonly applied. These include either the incorporation of a proteolytic cleavage site other than the one used in the general workflow or the introduction of an affinity tag that can be detached from the enrichment handle under mild conditions.[109, 110]

The former method is termed tandem orthogonal proteolysis-activity-based protein profiling (TOP-ABPP).[109] Compared to conventional ABPP, labeled probes are clicked to the tobacco etch virus (TEV)-biotin tag that additionally includes a TEV cleavage site. Upon avidin bead enrichment, proteins are sequentially digested by trypsin and TEV-protease and sequentially analyzed by LC-MS/MS to obtain identifications of both the labeled proteins (tryptic digest) and the sites of modification (TEV-protease digest), respectively.

The second ABPP method typically implies the use of desthiobiotin (DTB) containing probes or affinity tags and does not require an additional proteolytic cleavage step.[79, 110] Since DTB has a several fold lower affinity to avidin compared to biotin, an elution of enriched proteins from bead-bound avidin is allowed under acidic conditions.[108, 110, 111] Analogous to the TOP-ABPP method, analysis of both the labeled proteins (tryptic digest) and the sites of modification (elution) is enabled, respectively.

1.2.4. Quantification of Identified Binding Sites

To quantify the identified binding sites for the investigation of different conditions, there exist several possibilities. Of note, the introduced quantification methods from section “MS-based Protein Analysis” are all feasible. However, since only a single modified peptide can be used for identification and quantification, application of the most accurate method is recommended. The quantification method with the highest accuracy is assumed to be SILAC,[112] since differentially labeled cell populations can be pooled at the

earliest point during the workflow, directly after lysis.[101] However, in bacteria, SILAC can only be used by unconventional adjustment of culture media, since the *de novo* synthesis of amino acids renders reproducible incorporation difficult.

Therefore, refined versions of the previously introduced TOP-ABPP and DTB methods can be applied. For both affinity tags (TEV-biotin, desthiobiotin), isotopically labeled versions were established, resulting in the isoTOP-ABPP and isoDTB-ABPP methods, respectively.[110, 113] Both methods can be applied analogously to the former versions with the only difference that samples clicked to either light or heavy tag are pooled after the click reaction (Figure 4). This provides identical treatment under both conditions from the earliest possible point during the workflow, allowing for the highest possible accuracy in quantification on MS1 level.

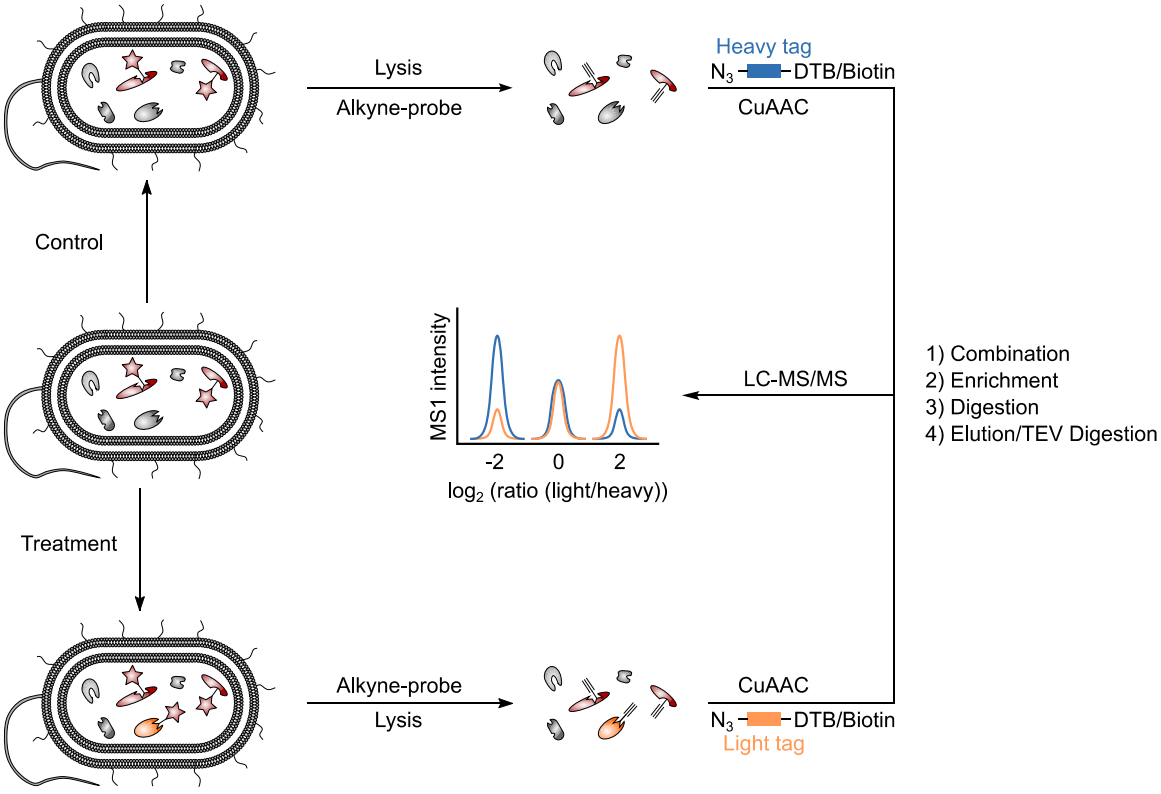

Figure 4: isoDTB and isoTOP-ABPP workflow for quantitative MS1 binding site-ID analysis using the reverse polarity approach. Cells are pre-treated or control-treated and labeled after cell lysis. Labeled proteins are either clicked to isoDTB- or TEV-Biotin tags, combined, enriched on avidin beads and tryptically digested. Peptides are either eluted from the avidin beads (isoDTB) or digested by TEV-protease and subjected to LC-MS/MS analysis. Samples are processed and probe binding sites quantified on MS1 level. Adapted from Allihn *et al.*[55]

The only possibility to further increase sensitivity, and therefore higher quantification accuracy, is the application of targeted proteomic methods like parallel (PRM) or selected reaction monitoring (SRM).[114-116] However, since these methods are not data dependent compared to conventional data dependent shotgun proteomics, prior information about the identified precursors (PRM) and fragments (SRM) analyzed by isoTOP-ABPP or isoDTB-ABPP is required, respectively. To account for the conventional data acquisition method, referred to as data-dependent acquisition (DDA), data is acquired based on dynamic alternation between MS1 and MS2 scans.[117] In one cycle, the topN most abundant precursors in an MS1 spectrum are sequentially fragmented and analyzed (MS2). To ensure the measurement of low abundant peptides, the precursors already measured are excluded from the fragmentation for a certain period of time (exclusion time). Therefore, for each precursor that makes it under the topN, there is only one suitable MS2 spectrum for its identification and quantification. In targeted proteomics methods, on the other hand, the mass spectrometer does not perform real-time decision making and therefore the analyte of interest must be determined in advance. Selected precursors are then fragmented either during the whole chromatographic run (unscheduled) or during defined retention time windows (scheduled).[118] This allows obtaining MS2 fragment data of selected precursors of interest over the complete elution time of a precursor. For instance, in isoDTB-ABPP experiments, increased sensitivity is particularly required when a specific site was found under only one condition (light or heavy). Accordingly, no ratio calculation between the conditions can take place. Targeted proteomics methods, on the other hand, could possibly detect appropriate signals in both light and heavy channels due to its increased sensitivity, thus enabling quantification and hence, correct data interpretation.

1.3. Objectives

Two-component systems are indispensable for the survival and pathogenicity of bacteria, as they can sense and adapt to a multitude of changes in their environment. Consisting of a sensor histidine kinase and a response regulator, the latter contains a key feature for its activity, phosphoaspartate. To infer the role of these systems in disease associated signal transduction pathways, analysis of the pAsp modification is mandatory. However, this

transient posttranslational modification is not accessible in living bacteria by common analytical methods.

As pAsp is known to react with α-nucleophiles, a reverse polarity chemical proteomic strategy was designed to trap pAsp with a tailored hydroxylamine probe, forming a stable hydroxamate. Stable covalent binding is necessary for the attachment of affinity tags by click-chemistry, allowing enrichment of probe-labeled proteins for subsequent identification and quantification by LC-MS/MS analysis. The initial use of a recombinant model response regulator for *in vitro* IPMS assays was intended to allow optimization of pAsp capture. Subsequently, application of the refined methodology in proteomes of *B. subtilis* and *P. aeruginosa* was envisaged to enable the detection of many known and potentially new pAsp sites with distinct sequence motifs.

With superior methodology in hand compared to the recently developed analogous rp-ABPP method by Chang *et al*.,[79] the ultimate goal was to gain insights into *P. aeruginosa* interkingdom signaling by employing the newly developed isoDTB-tags for the refined rp-ABPP workflow. Since a previous AfBPP showed that the human peptide hormone dynorphin A is sensed by the histidine kinase ParS, rp-ABPP was proposed to enable the elucidation of the RR involved during this interkingdom signaling process. Overall, the method should render valuable for the investigation of diverse signaling systems in different organisms.

2 Results and Discussion

Contributions:

See “introductory remarks.”

2.1. Trapping of Acyl Phosphates as Stable Hydroxamates

2.1.1. Introduction

Prior to the study of pAsp in whole proteomes, preliminary studies with a model RR containing a known pAsp site were required in order to optimize conditions for the conversion of pAsp to corresponding hydroxamates. In *E. coli*, the RR PhoB is well-studied as part of the TCS PhoBR, a key regulator of the organism's phosphate metabolism.[119-121] Under limiting phosphate concentration, the cognate HK senses the shortage and phosphorylates Asp53 of PhoB, which in turn regulates the transcription of target genes by binding to DNA and interacting with RNA polymerase.[122] It has been shown by fluorescence-based assays, that PhoB can also be phosphorylated by small molecule phosphor donors like ^{32}P-acetyl phosphate.[123] Using this *in vitro* phosphorylation strategy as a starting point, an IPMS assay was established to monitor the degree of PhoB phosphorylation and subsequent chemical trapping with hydroxylamines via IPMS.

First of all, PhoB was recombinantly expressed as a His_6-tagged construct in *E. coli* BL21 containing a tobacco etch virus (TEV)-cleavage site. Purification was carried out by HisTrap affinity and subsequent size exclusion chromatography. Since the His_6-tag did not affect PhoB activity, its removal by TEV protease was optional.

2.1.2. *In vitro* Phosphorylation and Phosphoaspartate Conversion of PhoB

Initial IPMS experiments were aimed at verifying the binding of one phosphoryl group to PhoB by *in vitro* treatment of 12.5 µM PhoB with 20 µM acetyl phosphate, followed by removal of excess phosphorylating agent with spin-colums and subjection to IPMS (Figure 5a). Although pAsp is considered unstable and prone to hydrolysis under common acidic LC/MS conditions,[69] the experiment turned out successful by showing a mass shift of +80 Da for almost 50% of the protein (Figure 5b). Confirming phosphorylation site specificity at Asp53, no adduct was observed for the respective Asp (D) to asparagine (N) mutation (D53N) (Figure S1).

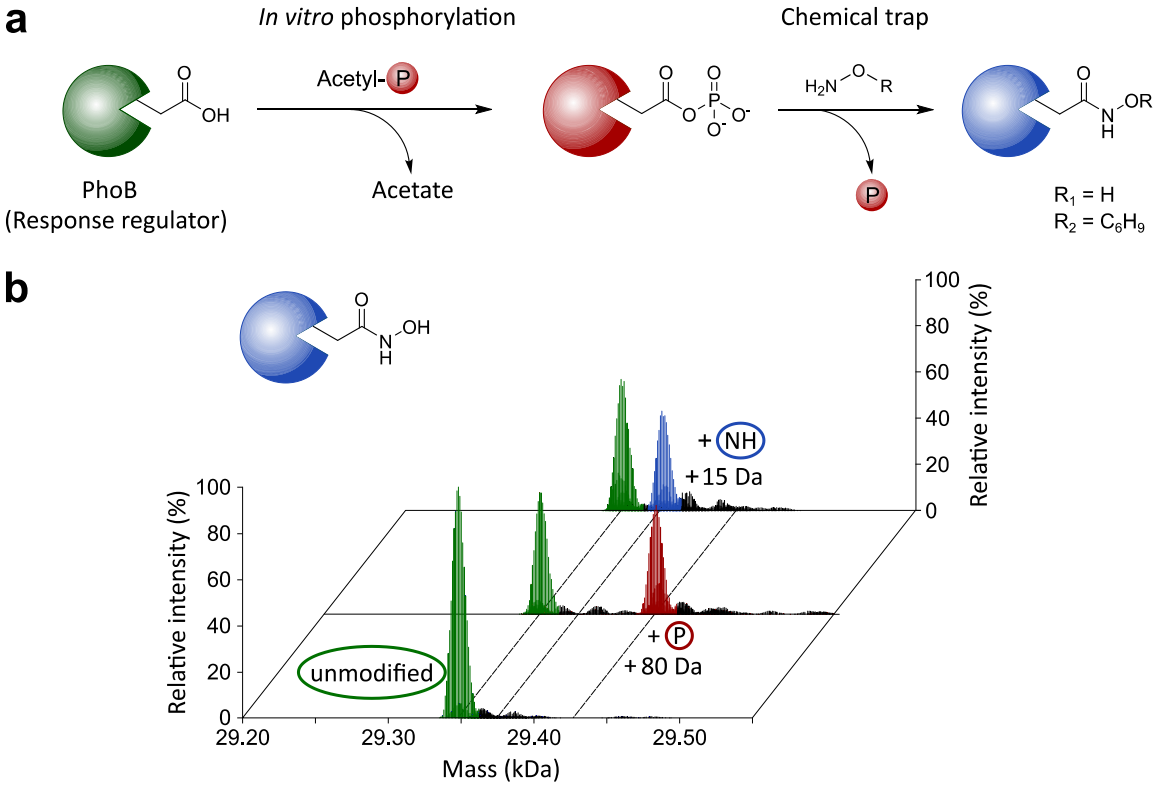

Figure 5: Intact-protein mass spectrometric (IPMS) assay for the *in vitro* phosphorylation and chemical pAsp capture of model response regulator PhoB in *E. coli*. (a) PhoB (green) was phosphorylated *in vitro* with acetyl phosphate (red) and converted with 500 mM hydroxylamine or HA-yne at pH = 4 (blue). (b) IPMS assay results using hydroxylamine. *In vitro* phosphorylation yielded around 50% pPhoB, which was quantitatively converted with hydroxylamine. Adapted from Allihn *et al.*[55]

For proof of concept experiments, the trapping of acyl phosphates as stable hydroxamates (Figure 5a), hydroxylamine should serve as a model nucleophile, showing α-effect properties and having no steric hindrance. However, incubation of phosphorylated PhoB with hydroxylamine (final concentration of $NH_2OH{\cdot}HCl$ = 0.5 M) at pH = 7 exhibited no conversion but pAsp hydrolysis instead (Figure S2). This finding seemed surprising at the beginning, since a previous study by Chang *et al.* used similar conditions for the labeling of pAsp in a whole proteome approach in *E. coli*.[79] One possible key difference might be their use of 6 M urea, which denatures the proteins and could thereby facilitate access to pAsp sites. However, early studies by *Daniel E. Koshland* suggest a nucleophilic attack at the phosphorous atom at neutral pH. Under acidic and alkaline conditions, on the contrary, a nucleophilic attack at the carbonyl carbon is proposed (Fig. 6).[68] Therefore, the

initial trapping experiment was repeated under acidic conditions (pH = 4). Time resolved IPMS analysis revealed fast reactivity and quantitative pAsp conversion to the hydroxamate *N*4-hydroxyasparagine after 30 minutes (Figure 5b, Figure S3a). Being vital for reasonable applications at a later stage, the reaction was also selective showing no unspecific background, because only a single mass shift of +15 Da was detected. Since an analogous experiment without prior *in vitro* phosphorylation of PhoB resulted in no adduct formation (Figure S4), the acidic pH was regarded as substantial for an effective pAsp conversion with hydroxylamines (Figure 6).

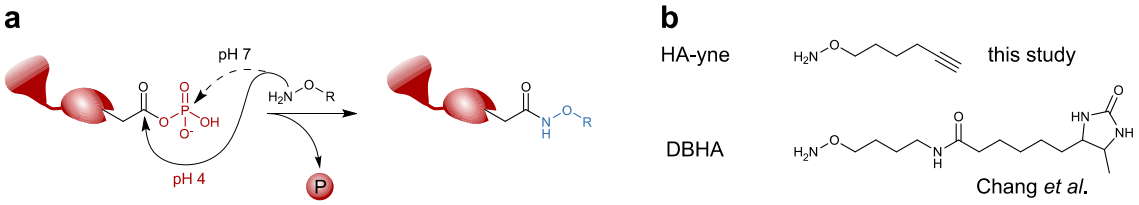

Figure 6: pH-dependent hydroxylamine reactivity at pAsp. (a) Hydroxylamine-based probes attack either the carbonyl-C (pH = 4) or the phosphate-P-atom (pH = 7) of pAsp. (b) rp-ABPP probes used for the detection of pAsp by Chang *et al.* (DBHA)[79] and in this study (HA-yne). Adapted from Allihn *et al.*[55]

For the successful application of this optimized trapping method in whole proteomes, a tailored probe was required, that enables an enrichment strategy and thereby maximum sensitivity for detection in proteomic analyses. Commonly, streptavidin bead enrichment is applied for ABPP experiments by binding to biotinylated proteins, which can be generated by coupling biotin-azide to a terminal alkyne bearing probe via click-chemistry.[83] To provide the best possible access to pAsp sites in proteins, a minimal hydroxylamine probe was synthesized containing a terminal alkyne (HA-yne) (Figure 5b). Interestingly, the same molecule was previously used for oxime ligations at acidic pH to find targets of lipid-derived electrophiles.[124] In the same way as hydroxylamine, the reaction of HA-yne with phosphorylated PhoB showed complete and fast conversion at pH = 4 by formation of a characteristic +95 Da adduct (Figure 7, Figure S3b).

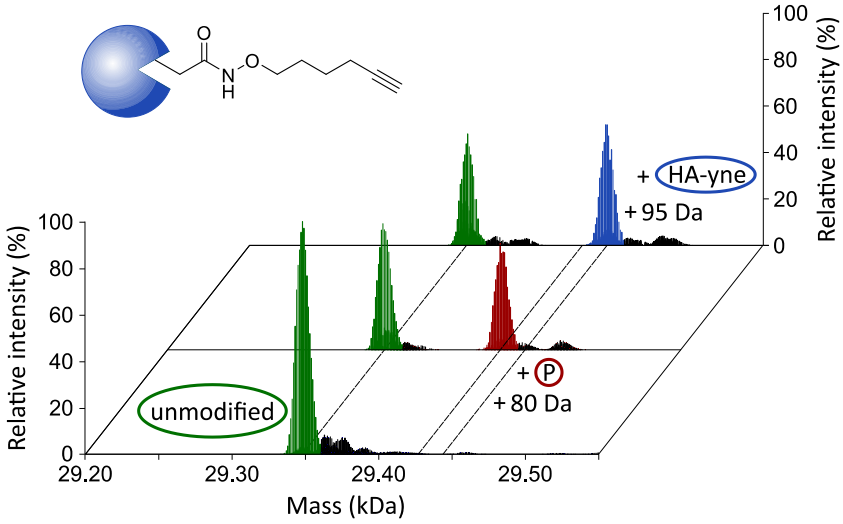

Figure 7: IPMS assay results for the *in vitro* phosphorylation and chemical trapping of pAsp of *E. coli* PhoB using 500 mM HA-yne at pH = 4. PhoB, pPhoB and converted PhoB are indicated in green, red and blue, respectively. Similarly to hydroxylamine, pPhoB was quantitatively converted with HA-yne. Adapted from Allihn *et al.*[55]

Having accomplished the development of optimized conditions for *in vitro* RR phosphorylation and pAsp conversion with a suitable ABP, the establishment of an rp-ABPP workflow applicable to more complex samples was approached. Showing the advantages of an alkyne bearing probe, besides its minor differences in size and reactivity to the original probe, various labels can be attached to the probe via click chemistry, enabling versatile detection methods like in-gel fluorescence SDS-PAGE or MS-based analyses.

2.2. RP-ABPP Workflow Establishment and Optimization

2.2.1. Gel-Based RP-ABPP Experiments for HA-yne Labeling Optimization

Before applying pAsp trapping to whole bacterial proteomes, the labeling conditions were optimized on analytical scale in gel-based rp-ABPP experiments in exponentially growing *B. subtilis* (Figure 8). To enable a readout by in-gel fluorescence SDS-PAGE, the probe was clicked to rhodamine azide upon labeling. A crucial factor for pAsp trapping is the transience of the modification. Therefore, the nucleophilic attack needs to occur as early as possible during the workflow. However, even if the probe is cell permeable in bacteria, a common *in situ* approach would not ensure pH = 4 inside the cells and is therefore not

feasible. To achieve a rapid pAsp conversion at pH = 4, cells were lysed in an acidic buffer (pH = 4) already containing the nucleophile (HA-yne) while cooling on ice. In the general rp-ABPP labeling setup on analytical scale, bacteria were grown over night to exponential phase, because pAsp-involving regulatory processes were expected to occur particularly in this phase. The cells were harvested and lysed (100 µL, OD_{600} = 40), followed by separation of the soluble and insoluble fraction. In order to remove excess

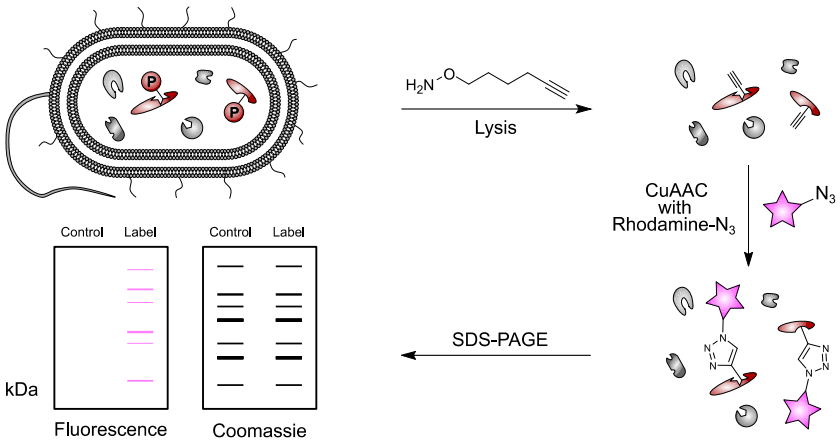

Figure 8: Gel-based rp-ABPP workflow for method optimization. *B. subtilis* cells were grown to exponential phase and lysed in a buffer containing the nucleophilic HA-yne probe (variables: pH value, detergent, HA-yne concentration). Labeled proteins were conjugated to rhodamine azide and SDS-PAGE analysis was performed by in-gel fluorescence scanning and Coomassie staining.

probe, the insoluble fractions were washed with PBS and soluble ones were precipitated in acetone and washed with methanol. Finally, labeled proteomes were clicked to rhodamine azide and subjected to fluorescence scanning with subsequent Coomassie Brilliant Blue staining for protein loading control. However, this first approach resulted in no labeling caused by precipitation of almost the entire proteome provoked by the high probe concentration of 0.5 M and the acidic pH (Figure S5). This observation was less pronounced at pH =7 and in particular at pH = 9. Interestingly, labeling at pH =7 and pH = 9 showed distinct labeling patterns, which presumably stem from other possible electrophilic PTMs appearing at the set pH. These include glutamate methylation, ADP-ribosylation or also transamidation, which is favored at alkaline pH.[125-127] Since the initial optimization methods were based on phosphorylation and labeling of only a single protein and because pAsp stability and reactivity might vary within the proteome, pAsp

modification and conversion cannot be excluded at pH =7 and pH = 9 *per se*. Nevertheless, because of successful initial pAsp conversion solely at pH = 4, labeling was continued to be carried out at acidic pH. Consequently, various detergents were tested at pH = 4 and the most suitable labeling conditions were obtained by the use of 1% (w/v) lauryldimethylamine oxide (LDAO) (Figure S6). Further optimizing the workflow, a screen of different probe concentrations showed sufficient labeling at 125 mM HA-yne (Figure S7).

In summary, optimized pAsp trapping in *B. subtilis* was achieved by the use of 125 mM HA-yne at pH = 4 in 20 mM HEPES and 1% (w/v) LDAO at OD_{600} = 40. These conditions were set as basis for the following MS-based proteomic analyses, the target and binding site identification in whole bacterial proteomes.

2.2.2. Target Identification in *B. subtilis*

In brief, common MS-based target identification by ABPP comprises varying treatments of proteomes, followed by enrichment like the streptavidin bead method, LC-MS/MS analysis and comparison of the different treatments.[90] By comparing probe- and DMSO-treated samples, targets of the probe can be identified. Optionally, the use of various competitors can give information about the selectivity of a probe's reactivity. Here, the goal was to obtain a first, though global, profile of the proteins that are labeled under the optimized pAsp-trapping conditions. Ideal results would confirm explicit enrichment of known pAsp proteins or additional reactivity of certain classes with so far unknown pAsp sites, whereas an unspecific labeling would suggest background binding, which was tried to be excluded by the preliminary rp-ABPP method optimization.

For rp-ABPP on preparative scale, the optimized conditions for analytical labeling were applied with only minor differences until the click reaction (Figure 9). In brief, overnight cultures of bacterial cells were grown to exponential phase, harvested, lysed and treated (HA-yne vs. DMSO). The fractions were separated, washed and recombined before the click reaction. The only differences were the adjusted protein amount (1 mL instead of 100 µL) and the recombination of the fractions in order to prevent biases caused by the different solubility upon different treatments. Furthermore, at least three technical

replicates were required under each condition to provide statistical significance. From that point on, the samples were treated according to a common ABPP workflow.[80]

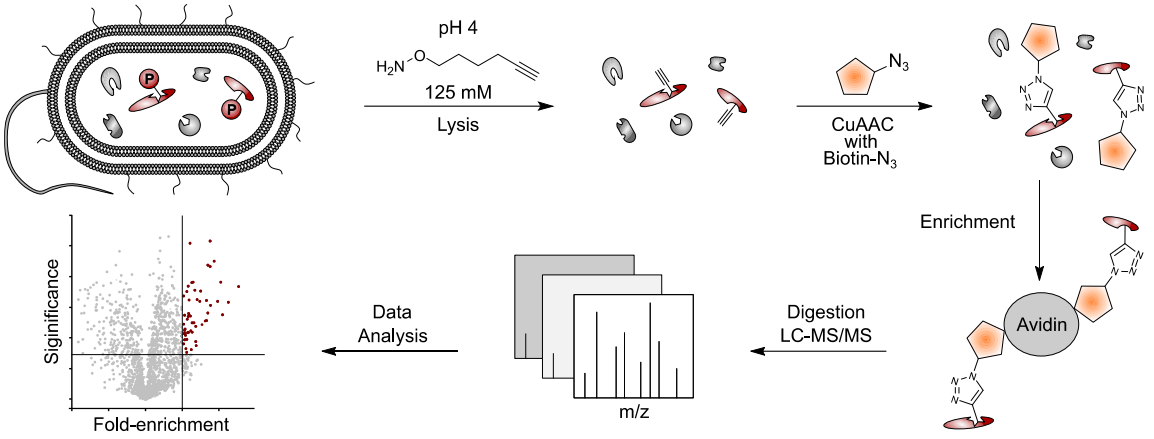

Figure 9: rp-ABPP workflow for the target identification of HA-yne. *B. subtilis* cells were grown to exponential phase and lysed in a buffer containing the nucleophilic HA-yne probe (125 mM) at pH = 4. Labeled proteins were conjugated to biotin azide and enriched on streptavidin beads. Enriched proteins were tryptically digested and subjected to LC-MS/MS analysis.

Hence, samples were clicked to biotin-azide, enriched on streptavidin beads, followed by on-bead tryptic digestion and subsequent desalting. Finally, the samples were subjected to LC-MS/MS analysis. The raw data were processed and evaluated by using MaxQuant and Perseus software, respectively.[97, 128] The output data is shown as volcano plots, displaying the statistical significance of protein enrichment as function of the logarithmic ratio of protein enrichment from HA-yne-treated and control cells (DMSO).

In general, the comparison of HA-yne- vs- DMSO-treated samples revealed the enrichment of a multitude of proteins (Figure S8). Notably, a few pAsp annotated proteins were significantly enriched, suggesting successful pAsp trapping. This result was not very surprising since RRs are often low abundance proteins and especially because high concentrations of pAsp are not expected in the cell.[129] Furthermore, methyl-accepting proteins as well as flagellar proteins are amongst the enriched hits. Although these proteins are not known to contain pAsp modifications, this finding also appeares plausible, since methylated glutamate and glutamine can possibly be trapped under the set conditions. The fact, that methyl-accepting proteins can be methylated on multiple

sites, supports this assumption.[125] Overall, the data showed no clear specificity, which is supposedly not due to undesirable unspecific binding of HA-yne, since initial IPMS assays of unphosphorylated PhoB showed no adducts upon HA-yne treatment (Figure S4). The presence of pAsp modifications on such a global level is also not expected and very unlikely. Therefore, in addition to putatively some so far unknown pAsp-modified proteins, other electrophilic modifications like ADP-ribosylation, glycosylation or glutamate and glutamine methylation might explain the outcome. Furthermore, isomerization processes induced by the detergent LDAO or elevated temperatures during cell lysis could play an additional role.[130] These and other possible reasons for unspecific HA-yne reactivity will be discussed in section "Binding Site Identification in *B. subtilis* and *P. aeruginosa*". Another important factor that affects and probably impedes the detection of HA-yne-modified proteins, is the proteomic workflow. Therein, unspecific binding during streptavidin bead enrichment displays the most crucial role, since its occurrence is supported by the existence of many down-regulated proteins, that are in principle not possible in an ABPP approach of alkyne-probe vs. DMSO.

Overall, this standard approach to profile the targets of HA-yne showed interesting results. But under the set conditions, no explicit clear conclusion could be drawn. Therefore, a more sophisticated method was conducted that investigates the covalent binding of HA-yne to certain residues in order to provide detailed explanations for HA-yne reactivity in bacterial proteomes.

2.2.3. Binding Site Identification of Spiked-in *E. coli* PhoB in *B. subtilis*

2.2.3.1 Introduction

Proving the feasibility of the established rp-ABPP method, the following experiments were intended to provide a conclusion about the direct site of HA-yne modification, the binding site-ID approach. Therefore, a further proof of principle experiment was designed to verify the binding of HA-yne to an annotated pAsp site in a complex biological background. Here, pAsp trapped and HA-yne converted *E. coli* PhoB was spiked into the proteome of *B. subtilis* to function as positive control. In principle, this spike-in approach would also be useful for the target-ID approach to prove the feasibility of the rp-ABPP method. However,

binding site-ID is more favorable for the purpose of HA-yne modification analyses, since it provides valuable information about the residue-specific localization of HA-yne-modified residues.

To enable the elution of HA-yne-modified peptides from streptavidin beads, desthiobiotin (DTB) tags were required.[108] Illustrating the feasibility of both tags, desthiobiotin azide as well as the recently developed isoDTB-tags were used.[110] Being relevant for later signaling experiments described in section ”Dynorphin A Signaling in *P. aeruginosa*”, the isoDTB-tags enable the analysis of two differently pretreated proteomes before probe-labeling. Apart from clicking to DTB-tags and the PhoB spike-in, further differences compared to the target-ID workflow are that desalting is not required and AspN is used in addition to trypsin digestion. AspN cleaves *N*-terminally of Asp residues and is required in order to obtain a pAsp trapped peptide with an appropriate size for MS detection, since omitted AspN employment would result in a 51 amino acid long peptide. Consecutive use of trypsin and AspN generates a convenient 19 amino acid long peptide, presupposing a missed cleavage of the HA-yne-modified residue within the sequence.

To account for the spike-in of *E. coli* PhoB, the protein was *in vitro* phosphorylated and converted with HA-yne, as already described in section “*In vitro* Phosphorylation and Phosphoaspartate Conversion of PhoB.” HA-yne-modified PhoB (5 µg) was precipitated and later resuspended together with soluble and insoluble fractions of *B. subtilis* prior to the click reaction. For the following *B. subtilis* binding site-ID workflow, bacteria were grown, harvested and labeled as described in the previous section. Afterwards, washed and reuspended pellets (including spiked-in PhoB) were clicked either to desthiobiotin azide or separately to the isoDTB tags. In case of the isoDTB tags, light and heavy samples were combined by consecutive precipitation in acetone. Samples were enriched on streptavidin beads, successively on-bead digested by trypsin and AspN, followed by elution of HA-yne-modified peptides. Finally, the samples were subjected to LC-MS/MS analysis and processing of the raw data by MaxQuant produced an output table with all HA-yne-modified peptides.

2.2.3.2 Binding Site-ID results

Binding site-ID analysis revealed successful HA-yne modification at the expected residue (Asp53) of PhoB both with commercially available desthiobiotin azide (Figure 10a) and the isoDTB-tags (not shown).

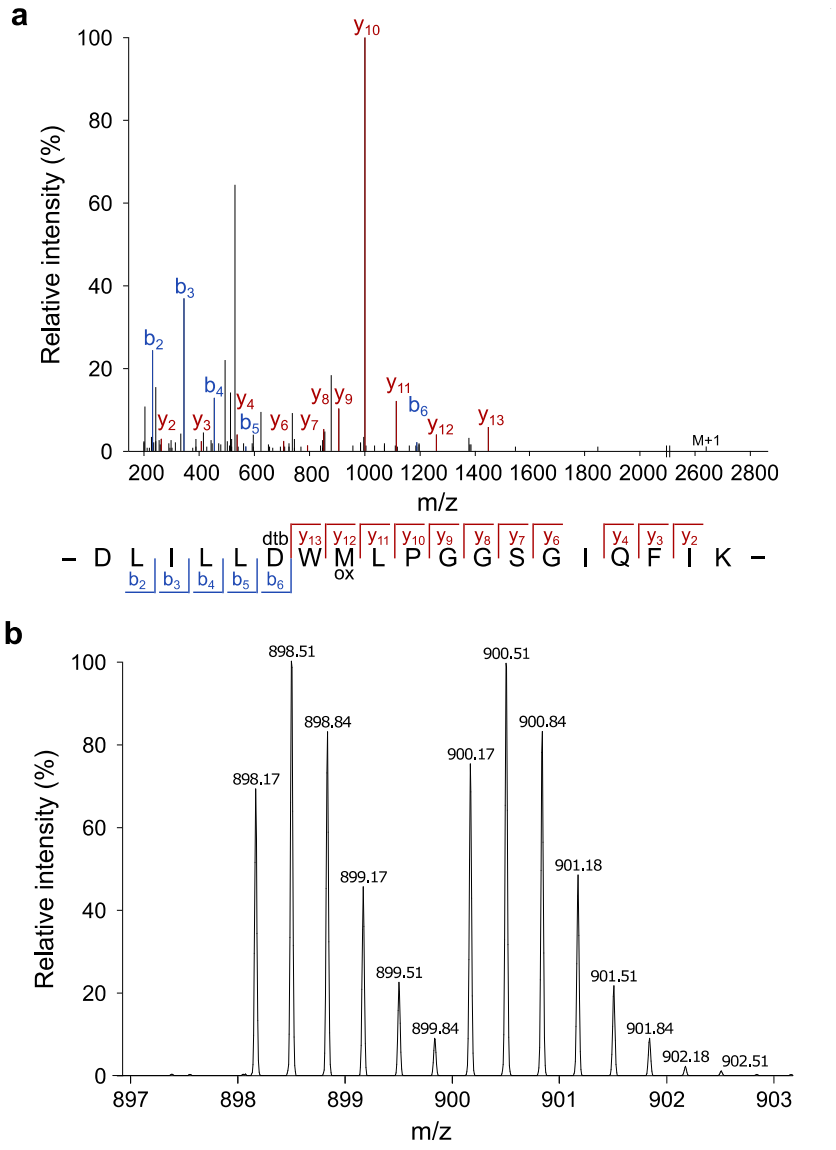

Figure 10: MS1 and MS2 spectra of the HA-yne-modified PhoB peptide. For rp-ABPP method development, HA-yne-modified *E. coli* PhoB (Fig. 2c) was spiked into a labeled proteome of *B. subtilis*, clicked to desthiobiotin-azide (a) or the isoDTB tags (b), enriched, digested and subjected to LC-MS/MS analysis. The predicted pAsp peptide was identified with the modification at the annotated position (D53) using MaxQuant software.[97] (a) MS2 spectrum of HA-yne-modified PhoB (DTB tags). The MS2 spectrum is almost identical when using the isoDTB tags (not shown). (b) MS1 spectrum of the light and heavy labeled PhoB precursor revealing the expected 1:1 ratio. Adapted from Allihn *et al.*[55]

Furthermore, analysis of the MS1 spectra of isoDTB samples affirmed the anticipated 1:1 ratio of light vs. heavy samples, providing the prerequisite for different treatment possibilities in later rp-ABB applications (Figure 10b). Interestingly, successful detection of the HA-yne-modified peptide of PhoB was only possible when enabling methionine oxidation as variable modification. Since this additional mass shift was not detected during IPMS assays, the oxidation must occur during the rp-ABPP worflow. Noteworthy, both acetone and the also performed Wessel-Flügge precipitations turned out applicable. Regarding the HA-yne-modified sites in the *B. subtilis* proteome, only very few sites were found in each sample. Nonetheless, the pAsp annotated site of the RR resD was found to be modified with HA-yne in each sample both with and without methionine oxidation.

Moreover, a supplementary approach was to identify the HA-yne-modified peptide of PhoB by using only trypsin during the rp-ABPP workflow, since this depicts the practicable condition for site-ID experiments in whole bacterial proteomes. To account for the large size of the 51 amino acid long and HA-yne-modified peptide, the maximum peptide mass was raised from 4600 to 6600 Da in MaxQuant. However, since the standard scan range for the MS1 data acquisition was 300-1500 m/z, the detection of the +5 or higher charged peptide would have been required, which is not unlikely depending on the sequence. Though, the modified peptide was absent. Nevertheless, an adjusted scan range of up to 2200 Th would allow detection of its +3 and +4 charged peptides, which possibly display more intense precursors than the +5 charged one. However, a measurement with an adapted scan range was not repeated, since the extremely large peptide depicts an unusual case and the vast majority of the expected pAsp and HA-converted tryptic peptides of RRs would still be detectable under standard MS acquisition and MaxQuant settings. For example, the RR resD in *B. subtilis* was again successfully detected at the annotated pAsp site. Thus, a drastic change of the scan range was not regarded beneficial for site-ID analyses.

2.2.3.3 Peptide Enrichment

Altogether, despite the correct identification of spiked-in *E. coli* PhoB and the RR resD at the annotated pAsp sites, both attempts failed to identify an adequate number of HA-yne-modified sites. Comparing the results to the target-ID approach, deficient and unspecific binding of peptides to the streptavidin beads might prohibit the successful enrichment of HA-yne-modified peptides. Interestingly, during the process rp-ABPP method development, a similar study was published by Chang *et al.*[79] Their study revealed the identification of 138 hydroxylamine probe modified sites from 98 proteins in *E. coli*, which exceeded the number of HA-yne-modified proteins by far. They synthesized a hydroxylamine probe, that already contained a desthiobiotin group (DBHA) and thereby enabled a workflow omitting the click-reaction (Figure 6b). However, their analogous binding site-ID approach enabled the detection of only two RRs (ompR and basR). Still, this finding is striking, since DBHA-labeling experiments were performed at pH = 6.5-7.0. Without precluding pAsp trapping at neutral pH for other proteins, here, initial pAsp trapping experiments with PhoB (Figure 5b, Figure 7, Figure S2) suggested an exclusive turnover at acidic pH. Therefore, the proof of pAsp trapping at neutral pH by Chang *et al.* confirms the aforementioned possibility, that protein environment affects its reactivity toward hydroxylamines.

To resume the enrichment method aspect, Chang *et al.* performed a different approach by digesting the proteins prior to enrichment on streptavidin beads (peptide enrichment).[79] Compared to common protein enrichment, this reverse order potentially facilitates the accessibility of desthiobiotin tags for the streptavidin beads, although precluding the target-ID approach. Interestingly, peptide enrichment was shown to be beneficial for the number of identifiable sites in a recent comparative study.[131] Moreover, additional key differences in the study by Chang *et al.* are represented by the timing of pAsp trapping, protein concentration and temperature while labeling as well as the proteome amount for enrichment.[79] To improve the rp-ABPP workflow, the recently introduced DBHA probe[79] was re-synthesized as published and compared to HA-yne by western blot analysis while concurrently assessing the aforementioned parameters, before repeating the binding site-ID experiments with the peptide enrichment approach.

2.2.4. Western Blot Analysis (HA-yne vs. DBHA)

In general, the key advantages of both methods should be utilized. Regarding the labeling conditions, pAsp trapping seemed to be most promising by immediate nucleophile presence upon cell lysis because of the hydrolytic instability of pAsp . Relying on the established IPMS assays with PhoB, pH = 4 was chosen. Therefore, *B. subtilis* cells were grown and harvested, followed by lysis and labeling for 1 h in a buffer containing either DMSO as control or 125 mM probe (HA-yne vs. DBHA) in 20 mM HEPES with 1% (w/v) LDAO. Afterwards, the soluble and insoluble fractions were separated and washed to remove excess probe. In order to allow a comparison between both probes, HA-yne- and a DMSO-treated samples were clicked to desthiobiotin azide before performing western blot analysis by SDS-PAGE, followed by streptavidin-linked horseradish peroxidase (HRP) and subsequent enhanced chemiluminescence (ECL) substrate treatment. Finally, the western blots were read out by fluorescence scanning with subsequent Ponceau S staining for protein loading control (Figure 11).

First, labeling was conducted at either 4 °C, 25 °C or 37 °C (Chang *et al.*),[79] which revealed the strongest labeling at 37 °C in both the insoluble and the soluble fractions of HA-yne and DBHA labeled proteomes (data not shown). Therefore, labeling at 37 °C was chosen for the next variable parameter, the protein concentration while labeling. Since labeling at OD_{600} = 40 resulted in overall protein concentrations of slightly more than 1 mg/mL protein in the same volume as in rp-ABPP experiments with HA-yne, this was roughly half the protein concentration during labeling compared to 2.5 mg/mL in the study by Chang *et al.*[79] Therefore labeling was compared between OD_{600} = 40 and OD_{600} = 80 at 37 °C. Regarding Ponceau S staining, the majority of the proteins were in the insoluble fraction (Figure 11b). Interestingly, the least difference between soluble and insoluble fractions was observed with HA-yne at OD = 40, which allows separate analysis of the binding site-ID of both fractions. In the fluorescence gel, it was notable that bands appeared in the DMSO-treated insoluble fraction. This indicates that some proteins in the lysate are biotinylated, which is known to occur on individual proteins and therein primarily on lysine residues. Indeed, the band at 36 and particularly 127 kDa would be indicative of the known biotinylated proteins BirA and Pyc, respectively.

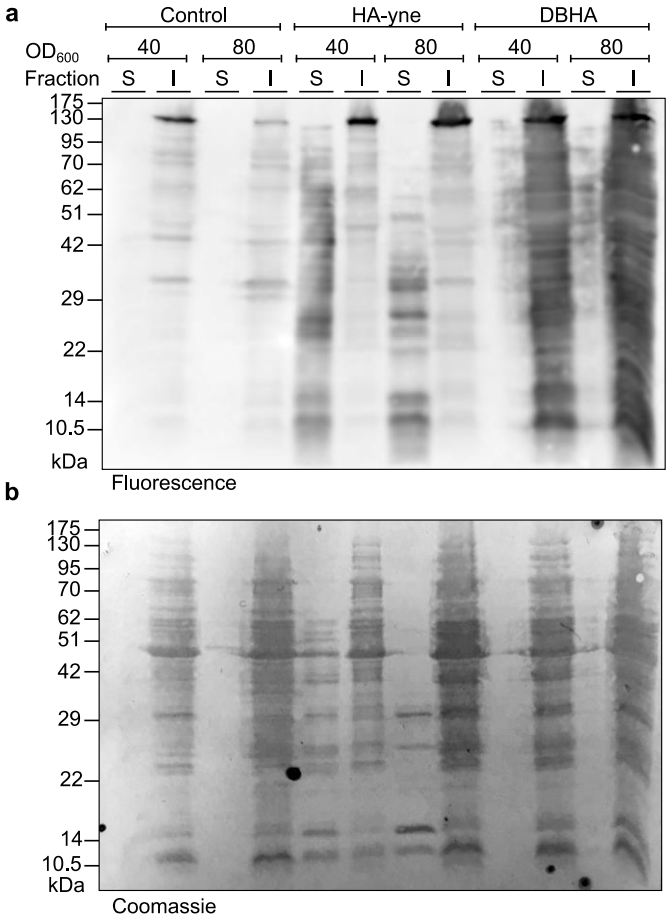

Figure 11: Comparison of HA-yne and DBHA labeling by western blotting. *B. subtilis* cells were grown to exponential phase, adjusted to either OD_{600} = 40 or 80 and lysed in a buffer containing the nucleophilic HA-yne probe (125 mM) or DBHA at pH = 4 or DMSO as control. The soluble (S) and insoluble (I) fractions were separated and washed to remove excess probe. HA-yne labeled or DMSO-treated proteins were reacted with desthiobiotin azide and was not necessary for DBHA. HA-yne, DBHA and control samples were subjected to SDS-PAGE and western blot analysis and conjugated to streptavidin-horseradish peroxidase, followed by incubation with enhanced chemiluminescence (CL) substrate. Labeled proteins were analyzed by in-gel fluorescence scanning (a) and Ponceau S staining for loading control (b).

Remarkably, DBHA showed very strong labeling over the complete range with a slight shadow (Figure 11a), which is consistent with published western blots.[79] Since most of the proteome was in the insoluble fraction, the faint labeling in the soluble fraction was not surprising. However, this behavior was not apparent for HA-yne labeling, which was markedly different. Curiously, labeling was most evident in the soluble fraction, although more protein was present in the insoluble fraction. In addition, the labeling pattern differed significantly in the respective fractions. While the soluble fraction contained

bands over the complete range at OD_{600} = 40, the insoluble fraction showed mainly bands in the higher molecular weight range.

This confirms the plan to examine both fractions separately in binding site-ID experiments. Because of these favorable characteristics, labeling with HA-yne at OD_{600} = 40 and 37 °C was chosen for the following binding site-ID experiments. Nonetheless, utilization of the insoluble fraction of the proteome labeled at pH = 4 with DBHA might have provided interesting insights into DBHA binding behavior.

2.3. Binding Site Identification in *B. subtilis* and *P. aeruginosa*

2.3.1. Binding Site-ID Analysis for Asp-Modified Sites

To analyze HA-yne-modified sites in complete proteomes of *B. subtilis* and *P. aeruginosa*, the established and improved rp-ABPP methodology was performed in combination with promising peptide enrichment. In brief, bacteria were grown to exponential phase, harvested and adjusted to OD_{600} = 40, followed by lysis in a buffer containing 125 mM HA-yne, 20 mM HEPES and 1% (w/v) LDAO at pH = 4. Upon 1h labeling at 37 °C, fractions were separated, washed and clicked to desthiobiotin azide or to rhodamine azide as control. Proteomes were tryptically digested and labeled peptides were enriched, eluted from the beads and finally subjected to LC-MS/MS analysis (Figure 12).

Regarding the gel-based labeling, remarkably, HA-yne labeling showed intense and distinct labeling patterns in both fractions in *B. subtilis* and *P. aeruginosa*, respectively (Figure 13b). Interestingly, while labeling in the soluble fraction occurred more in the low molecular weight range, labeling in the insoluble fraction is observed in the higher molecular weight region. Altogether, both fractions nicely cover the complete range, which supports the decision for this split fraction strategy.

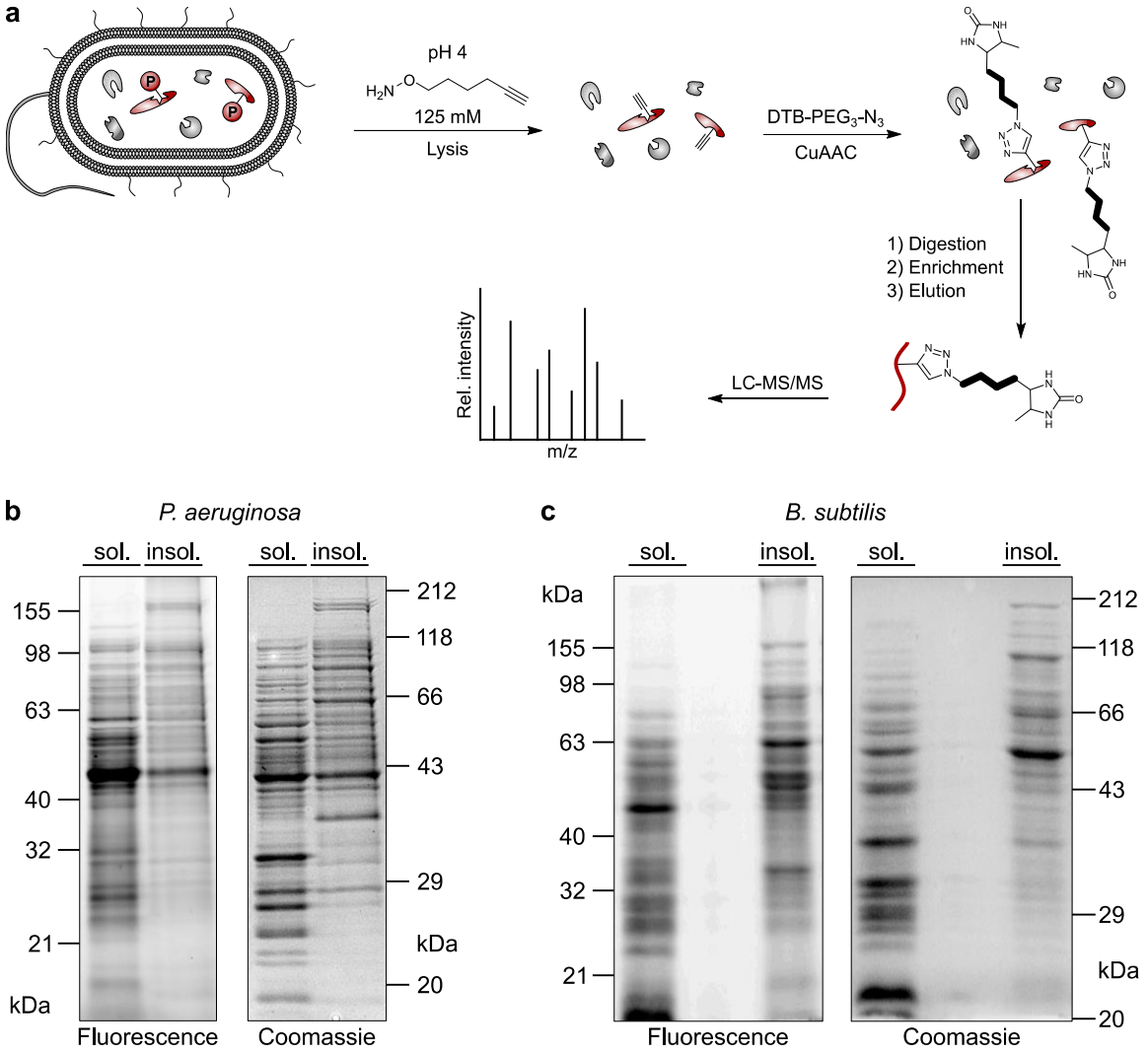

Figure 12: rp-ABPP workflow and SDS-PAGE. Bacterial cells of *P. aeruginosa* and *B. subtilis* were grown to exponential phase and lysed in a buffer containing the nucleophilic HA-yne probe (125 mM) at pH = 4 and clicked to either desthiobiotin-azide (DTB-PEG3-N_3) (a) or rhodamine azide (b,c). Modified proteins were tryptically digested, enriched on streptavidin beads, eluted from the beads and subjected to LC-MS/MS analysis (a). Labeling of bacterial lysates under optimized conditions. Exponentially growing *P. aeruginosa* (a) and *B. subtilis*. (b,c) SDS-PAGE analysis labeled and rhodamine azide conjugated proteins was performed by in-gel fluorescence scanning and Coomassie staining. Adapted from Allihn *et al.*[55]

Continuing with the MS-based binding site-ID results, the adapted methodology successfully revealed the detection of 141 and 198 HA-yne-modified Asp sites with high confidence in *B. subtilis* and *P. aeruginosa*, respectively. Remarkably, many known pAsp sites of RRs from UniProt[132] were found to be HA-yne-modified, 15% (6/41) in *B. subtilis* and 19% (18/93) in *P. aeruginosa* (Figure 13a,c). This finding is striking, since RRs are

usually not highly expressed and only phosphorylated to some degree, which is the reason they easily escape detection in traditional proteomics. [133, 134] Additionally, it is interesting to note that cognate phosphorylated HKs are estimated to account for only <1% of the total HK population.[53] Further illustrating the selectivity of the method, postulated pAsp

a *P. aeruginosa*

Gene	Ann. Site	Fd. Site	TCS	Implication
AlgB	D59	D59	AlgB/KinB	Alginate biosynthesis, virulence, acute/chronic infection
AmgR	D61	D61	AmgR/AmgS	Aminoglycoside resistance, stress response
BfiR	D57	D57	BfiR/BfiS	Biofilm formation
CbrB	D52	D52	CbrA/CbrB	Cytotoxicity, virulence, swarming motility
ChpA	D2401	D2401	ChpA/PilG/PilH/ChpB	Virulence, biofilm formation, twitching motility
GacA	D54	D54	GacA/GacS	Virulence, quorum sensing, biofilm formation, antibiotic resistance, swarming motility
GacS	D715	D715		
MifR	D53	D53	MifR/MifS	Acute/chronic infection, biofilm formation
NarL	D64	D64	NarX/narL	Nitrate sensing and respiration, biofilm formation, swarming motility
NtrC	D55	D55	NtrB/NtrC	Cellular response to nitrogen levels
PhoP	D51	D51, D86	PhoP/PhoQ	Antimicrobial peptide resistance, virulence, biofilm formation, swarming motility
PilG	D58	D58	ChpA/PilG/PilH/ChpB	Virulence, biofilm formation, twitching motility
PilR	D11, D54	D54	PilR/PilS	Biofilm formation, twitching and swarming motility
RetS	D713, D858	D713	PA1611/RetS	Virulence, biofilm formation
RoxR	D63	D63	RoxR/RoxS	Cyanide tolerance, neutrophil transmigration response
PA1243	D793	D793	Unknown	Unknown (Probable sensor/RR hybrid)
PA2798	D56	D56	Unknown	Unknown (Probable TCS regulator)
PA4112	D1064, D1210	D1064	Unknown	Unknown (Probable sensor/RR hybrid)

b

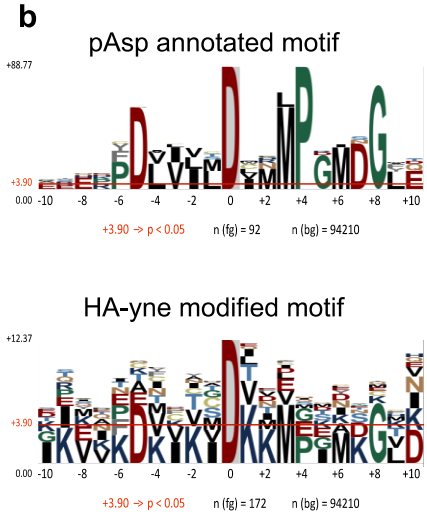

c *B. subtilis*

Gene	Ann. Site	Fd. Site	TCS	Implication
ComA	D55	D55	ComA/ComP	Regulation of genetic competence and quorum sensing
PhoP	D53	D53	PhoP/PhoR	Regulation of phosphate metabolism
ResD	D57	D57	ResD/ResE	Aerobic and anaerobic respiration
Spo0F	D54	D54	Spo0F/KinB	Sporulation initiation
YvrH	D55	D55	YvrH/YvrG	Regulation of cell surface maintenance
ZosA	D337	D337	no TCS	Oxidative stress protection

d

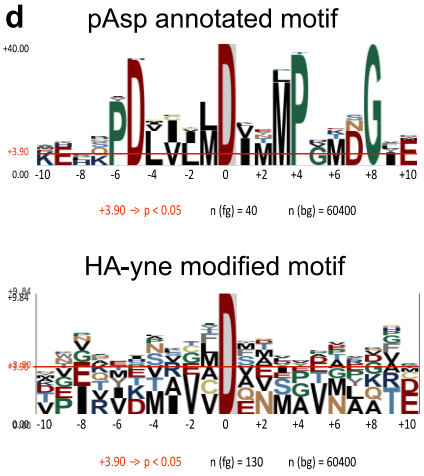

Figure 13: Binding site analysis in *P. aeruginosa* and *B. subtilis*. (a and c) Table of HA-yne-modified sites in *P. aeruginosa* and *B. subtilis*, that also have UniProt annotated pAsp sites. Moreover, the corresponding genes, TCSs and their implications are listed. (b and d) Comparison of pAsp annotated and HA-yne-modified sequence motifs in *P. aeruginosa* and *B. subtilis* using pLogo.[135] Residues ranging from positions -10 to +10 next to the modification site were included in the analysis. pAsp annotated and HA-yne-modified sequences (fg) were compared with the complete proteomic background (bg) in *P. aeruginosa* or *B. subtilis* from the UniProt database. Red horizontal bars indicate the Bonferroni-corrected statistical significance (p = 0.05).

residues were HA-yne-modified almost exclusively within the pAsp annotated proteins of both analyzed organisms (24/25) (Figure 13a,c). However, it cannot be excluded that the additional unannotated site was also pAsp-modified. In this context, many of the postulated pAsp sites are annotated as such based on sequence similarity and have never been experimentally verified to this point. Although other modifications are possible, the applied method strongly supports their correct pAsp annotation and can therefore serve as complementary strategy to sequence homology for pAsp annotation. For instance, annotated pAsp sites were confirmed for hitherto only poorly characterized proteins, such as probable response regulators PA1243, PA2798 and PA4112. Moreover, the results suggest the existence of many new potential pAsp sites.

In this sense, the modified sequences were superimposed to discover a possible general sequence dependence in addition to the known one (Fig 13b,d).[132] In *B. subtilis*, there was only little sequence similarity within the modified peptides (Figure 13d). This implies the trapping of other electrophilic modifications or new pAsp sites without a distinct sequence dependence. The absence of pAsp sequence homology is also consistent with the results by Chang *et al.*[79] In contrast, distinct similarities with the known pAsp motif were evident in *P. aeruginosa,* particularly at positions -5 (D), -3 (I/V), +3 M, +4 (P), +6 (M) and +8 (G) (Figure 13b), which is probably due to the enhanced number of identified pAsp annotated sites. Additionally, GO-term enrichment analysis disclosed “signal transduction RR REC domain” as the highest enriched protein domain.

2.3.2. Binding Site-ID Analysis for Glu-Modified Sites

The standard setting for binding site-ID analyses with MaxQuant in this study also included possible modifications other than phosphorylation on glutamic acid (DE-search), since trapping of other possible electrophilic modifications like glutamate methylation and ADP-ribosylation could not be exluded.[125, 126] For instance, hydroxamate formation by reaction of hydroxylamine with several small molecule methylesters like acetylcholine is known to occur at neutral and acidic pH.[136] Remarkably, binding site-ID additionally uncovered the detection of 600 and 451 HA-yne-modified Glu sites with the standard MaxQuant localization probability cut-off of >75% in *B. subtilis* and *P. aeruginosa*, respectively. Among the known Glu methylated proteins, for which only a few sites are experimentally

verified so far, CheR and Aer2 were found in *B. subtilis* and *P. aeruginosa*, respectively. However, they were not HA-yne-modified at the annotated site. Interestingly, an overlay of Glu-modified sequences displayed explicit preferences for positions -1 (V), +1 (V) and +2 (D) in both organisms (Figure S9). Furthermore, lysine residues are significantly enriched within this sequence in *P. aeruginosa.*

Notably, the binding site-ID analysis conducted by Chang *et al.* did not account for Glu modifications and therefore might contain several incorrect modifications at Asp instead of Glu.[79] To exemplify this issue, binding site-ID analysis was also performed for HA-yne modifications solely at Asp (D-search). Here, the response regulator was falsely detected at Asp24, since no modification was allowed on Glu within this peptide. In contrast, allowing HA-yne modifications on Glu as well (DE-search) exposed <1% localization probability for modification of Asp24 and instead, Glu30 was detected with >95% localization probability. Furthermore, D-search resulted in 367 and 360 HA-yne-modified pAsp sites in *B. subtilis* and *P. aeruginosa*, respectively. Although some of these sites were presumably not true, they exceeded the ones of Chang *et al.* even with a more stringent cut of >99% localization probability.[79] On the other side, the number of Asp sites was drastically reduced, when HA-yne modification was allowed *e.g.* on all possibly nucleophilic residues, namely cysteine, aspartic and glutamic acid, histidine, lysine, asparagine, glutamine, arginine, serine, threonine, and tyrosine (CDEHKNQRSTY). This observation is due to statistical reasons, since the indicated mass of modification is theoretically impossible for residues other than Asp and Glu. Hence, the settings in the respective search engine must be chosen carefully and are of the utmost importance for correct identification.

2.3.3. Binding Site-ID Analysis for Asn and Gln-Modified Sites

In order to identify all HA-yne-modified peptides correctly, further possibly modified residues were reconsidered. Asparagine (Asn) and glutamine (Gln) residues can be potentially HA-yne-modified in several ways. They could react with HA-yne directly as unmodified or methylated amino acid, during deamidation as cyclic intermediate or after deamidation and subsequent methylation.[137-141] In either way, a hydroxamic acid is formed. However, in order to perform binding site-ID for HA-yne-modified Asn and Gln

residues, a separate MaxQuant search (NQ-search) compared to the standard DE-search is required. This is because the resulting mass difference between the HA-yne-modified Asn/Gln and the unmodified residue is 0.98 Da higher (510.31 Da) than the one between the corresponding modified and unmodified Asp/Glu residue (509.33 Da).

Before performing NQ-searches, the existence of other potential mass shifts was investigated to infer additional modifications. Therefore, an open search was conducted using MSFragger, which can give information about the occurring mass shifts between modified and unmodified peptides and about the quantity of PSMs that contain these mass shifts.[98] Though, no other frequently appearing mass shifts were found. Instead, the prevalence of PSMs with a mass shift corresponding to HA-yne modification at Asn/Gln residues was sixfold higher than the one at Asp/Glu residues in both organisms. Following up on these surprising results, subsequent NQ-search using MaxQuant revealed the detection of 1762 and 1531 HA-yne-modified Asn sites in addition to 4834 and 4172 HA-yne-modified Gln sites in *B. subtilis* and *P. aeruginosa*, respectively (Figure 14). These numbers seemed very high, and therefore the underlying causes were investigated.

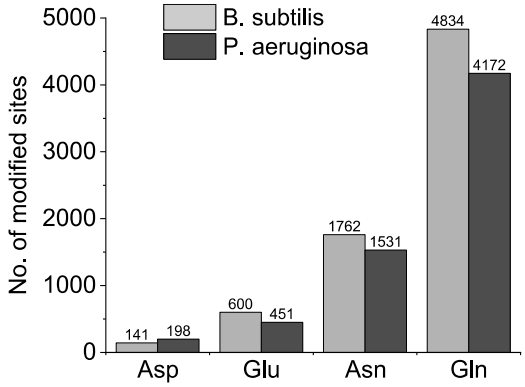

Figure 14: Distribution of HA-yne-modified residues. The binding sites were identified by specifying variable modification on either Asp/Glu (+ 509.33 Da) or Asn/Gln (+ 510.32 Da) residues in MaxQuant.[97]

Regarding the sequence motif in *P. aeruginosa*, significant preferences for lysine residues were observed around Asn- and Gln-modified sites (Figure S10). Moreover, being more distinct in *B. subtilis,* acidic residues were highly enriched. Yet, these preferences did not allow any conclusion to be drawn about the existence of a possible modification. The fact

that mainly ribosomal proteins were HA-yne-modified at Asn and Gln residues, suggests a general background reactivity, since proteins involved in translational processes belong to the highest abundant proteins in bacterial cells.[129] Therefore, possible reactions at Asn and Gln were considered before investigating the applied labeling conditions to determine whether they could be responsible for this effect.

As mentioned above, there are several conceivable opportunities of Asn and Gln conversion with HA-yne. The first one implies hydroxamate formation without any influence of posttranslational modifications. It has been shown that amides can react directly with amides at 37 °C with and without the aid of enzymes, having a maximum turnover at pH = 6. [137, 138] Therein, hydroxylamine can additionally function as catalyst. However, the conversion is only marginal, whereas it is significantly higher at elevated temperatures or when suitable enzymes are used. Moreover, direct reactivity could be explained by possible deamidation, since Asn and Gln residues are known to form succinimide and glutarimide intermediates within peptides.[140, 142]

In turn, these activated cyclic species can be attacked at two electrophilic positions by hydroxylamines under ring opening and hydroxamic acid formation (Figure 15).[143] In addition, although favored at alkaline pH and therefore not very likely, methylesters could be converted with HA-yne.[139] Notably, release factors 1 and 2 are methylated at Gln, containing a conserved GGQ motif.[144] Although these proteins were HA-yne-modified on Gln residues both in *B. subtilis* and *P. aeruginosa*, the annotated sites were not detected. Furthermore, other proteins containing a GGQ motif were modified at the exact Gln residue, which could potentially point toward their methylation. In addition, there are 26 chemoreceptors in *P. aeruginosa* that are regulated by Glu and Gln methylation and demethylation using the methyltransferase CheR and the methylesterase CheB.[125] Interestingly, 16 of these chemoreceptors were modified on Asn and Gln, although only partially revealing reactivity at annotated methylation sites. Nonetheless, a few Gln sites were found to be at the interaction site with the adaptor protein CheW. Another option for HA-yne labeling at Gln could be caused by Gln deamidation and subsequent Glu methylation.[141]

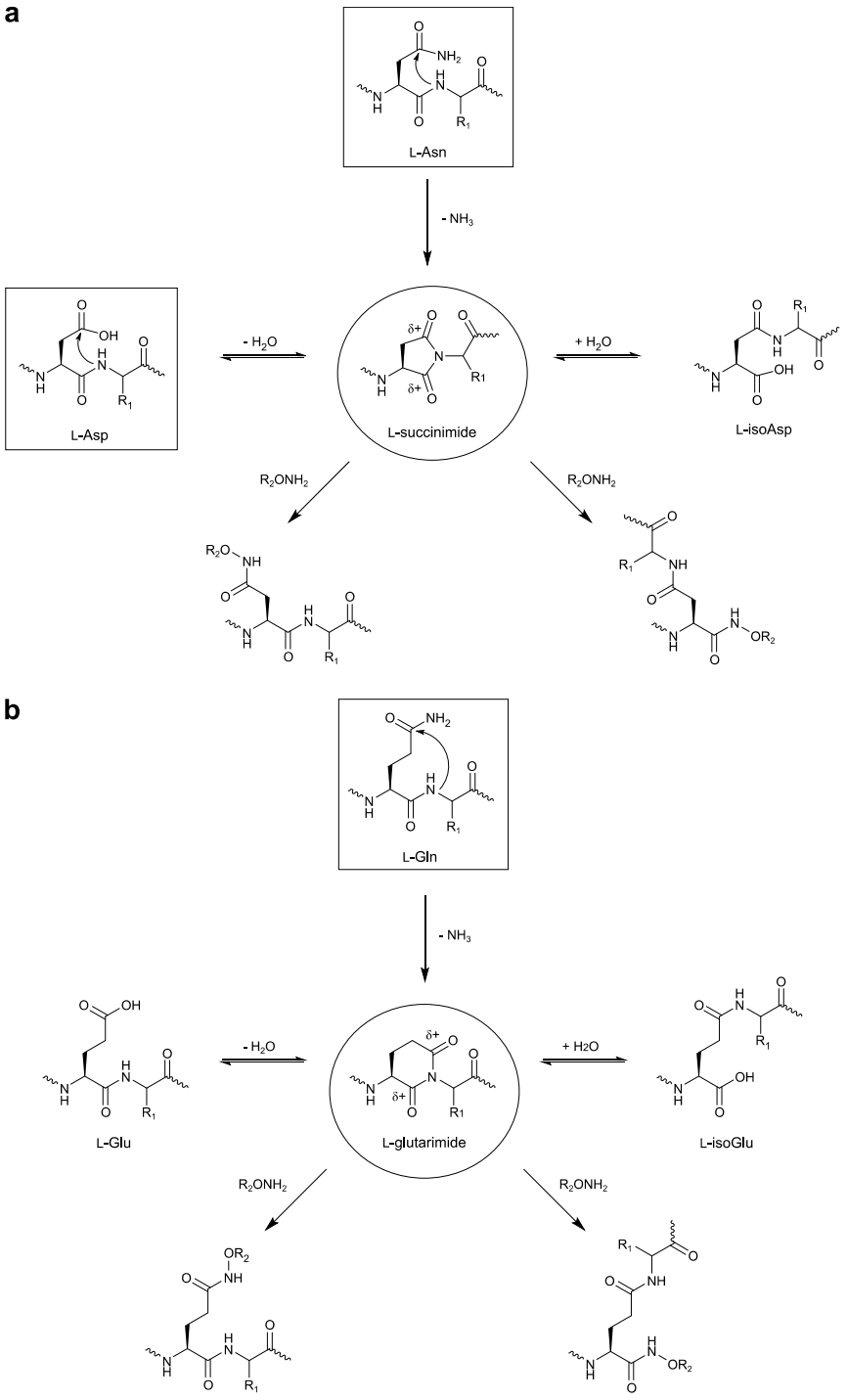

Figure 15: Isomerization of Asn/Asp and Gln/Glu residues. The intermediates L-succinimide (a) and L-glutarimide are formed by intramolecular cyclization of Asn and Glu under ammonia loss, respectively. The cyclic intermediates can be converted with hydroxylamines. Adapted from Geiger and Clarke.[140]

Regarding methylated residues, the results might even hint towards a reduced reactivity of Asn and Gln methylated proteins toward HA-yne, since many known methylated

proteins were found, however not at the postulated sites. The reason for this could be its reduced tendency to form cyclic indermediates.[145] In summary, however, the results suggest direct reactivity between HA-yne and Asn/Gln residues, presumably via their cyclic intermediates, since the sum of Asn and Gln sites is vast and many sites were detected even within one protein.

Consequently, the applied labeling conditions were investigated by analysis of the test proteins α-casein, BSA and phosphorylated PhoB. All proteins were treated under standard HA-yne labeling conditions prior to examination of formed adducts by MS (Figure S11). However, only the share of phosphorylated PhoB was labeled quantitatively, whereas unphosphorylated proteins showed no detectable characteristic mass shifts. Hence, on the one hand, high reactivity at Asn and Gln residues might be caused by posttranslational modifications during diverse processes in the cell, although these cannot be proven at this stage. On the other hand, the background reactivity by the mentioned mechanisms could occur at a very low level that would still be detectable via MS. The latter is further supported by the fact that mainly high abundance proteins are detected (Figure S12). However, since RRs of low abundance were detected solely at Asp sites and because RRs were exclusively identified at the annotated pAsp site, the rp-ABPP method can be used for the initial goal, the detection of Asp phosphorylation.[129]

2.3.4. Optimization Possibilities for rp-ABPP Data Acquisition and Analysis

Although leading to successful identification of numerous modified sites, the applied rp-ABPP method represents a special case, because the corresponding peptides bear high molecular weight modifications. Therefore, there is an increased chance of insufficient modification localization or even failure of peptide fragmentation in the first place. This issue could be addressed by optimizing data acquisition and search engine settings.

In terms of data acquisition, altering the scan range and the MaxQuant.Live software framework initially appeared to be promising options for improving data acquisition. An extension of the scan range could allow the measurement of lower charged precursors, which might occur with higher intensity. For instance, extending the scan range from 300-1500 m/z up to 2000 m/z could allow identification of a +3 charged precursor of <6000 Da

molecular mass. However, a detailed analysis revealed that longer peptides exhibited higher intensity at larger charge states in most cases. Therefore, a change of the default scan range in XCalibur was not needed for HA-yne-modified peptides. Another interesting possibility to improve precursor selection is the software framework MaxQuant.Live, which can monitor MS data in real time and control data acquisition on Q Exactive and Orbitrap Exploris mass spectrometers.[146] Among other things, unlike XCalibur, it is able to select precursors with a minimum mass for fragmentation. Interestingly, this feature was recently exploited by Hendriks *et al.* to increase the identification of SUMO- and ubiquitin-modified peptides.[147] To implement MaxQuant.Live also for the rp-ABPP method, a minimum precursor mass of 1200 Da should be chosen, representing the sum of the smallest identifiable peptide mass of about 700 Da and the HA-yne modification of 509 Da (Asp/Glu) and 510 Da (Asn/Gln), respectively. In principle, application of data-independent acquisition (DIA) would also be conceivable to better detect low abundance proteins such as RRs.[148, 149] In contrast to data-dependent acquisition (DDA), precursors are split into small m/z windows and fragmented regardless of their abundance. Since this requires libraries of identified peptides, it is extremely difficult to realize for modified peptides. However, a method has recently been developed, direct DIA, which no longer requires libraries.[150, 151]

Especially in the case of large peptides, localization of PTMs is often challenging. The longer the peptide of interest and the further the modified amino acid is located within the peptide, the less likely the modified fragment will be identified. This becomes even more problematic when the modifiable amino acid occurs more than once. For instance, the *P. aeruginosa* RRs PA3349 and RetS were both HA-yne-modified at the correct site, though with <75% localization probability. That is because PA3349 and RetS have a length of 28 and 26 amino acids, respectively, and both contain an Asp and a Glu residue in the middle of the peptide. Yet, neither the y-ion series nor the b-ion series included the binding-site containing fragments, due to their respective sizes. In both cases, the D-search finds only the pAsp annotated sites, since modification on Glu would be excluded. However, the D-search is not helpful, if both modifiable residues were Asp. Therefore, the correct identification and localization of HA-yne-modified peptides relies also on the

properties of the modified tryptic peptides. One way to address this issue in the data acquisition process is to adjust fragmentation energy. This allows fragments of appropriate size to be obtained to give the best possible peptide identification, which is crucial for the correct localization of PTMs.[146, 152] The more energy applied, the more fragmentation takes place, resulting in smaller fragments that are detrimental to identifying large modifications.[152] Furthermore, different fragmentation methods could be applied, if available. In the field of PTM detection, electron transfer dissociation (ETD) is a popular methodology, as often labile PTMs remain intact.[153] Although it would be interesting for HA-yne-modified peptides, an improvement is unlikely because both desthiobiotin azide and the later used isoDTB tags have similar fragmentation properties as the peptides under investigation due to the peptide bonds contained within them.

To account for the size of the modified peptides in MaxQuant, the maximum peptide mass can be increased. By calculating the expected mass of pAsp-modified tryptic peptides, the value can be reasonably determined. For instance, here it was shown that by increasing the default value from 4600 Da to 5600 Da, the HA-yne-modified and pAsp annotated site of the known RR CheY was successfully found. Moreover, it is possible to increase the quality of identification, provided that known fragmentation patterns of its modification have been detected. By specifying these as possible diagnostic peaks in MaxQuant, the complexity of the MS/MS spectra for the Andromeda search engine can be reduced. This in turn is reflected by a higher Andromeda Score, which is a measure of the quality of peptide identification. This aspect will be discussed in the following section.

2.3.5. DTB-Tag Fragmentation

Analysis of HA-yne-modified sites at Asp, Glu, Asn and Gln residues, using the MS/MS spectra of rp-ABPP experiments, revealed the recurrent appearance of specific fragment ions with high intensity, which could originate from the modification of the peptides. These were investigated in more detail, because fragment characteristics of a particular modification can be specified in MaxQuant as diagnostic peaks for the Andromeda search engine to increase the quality of peptide identification.

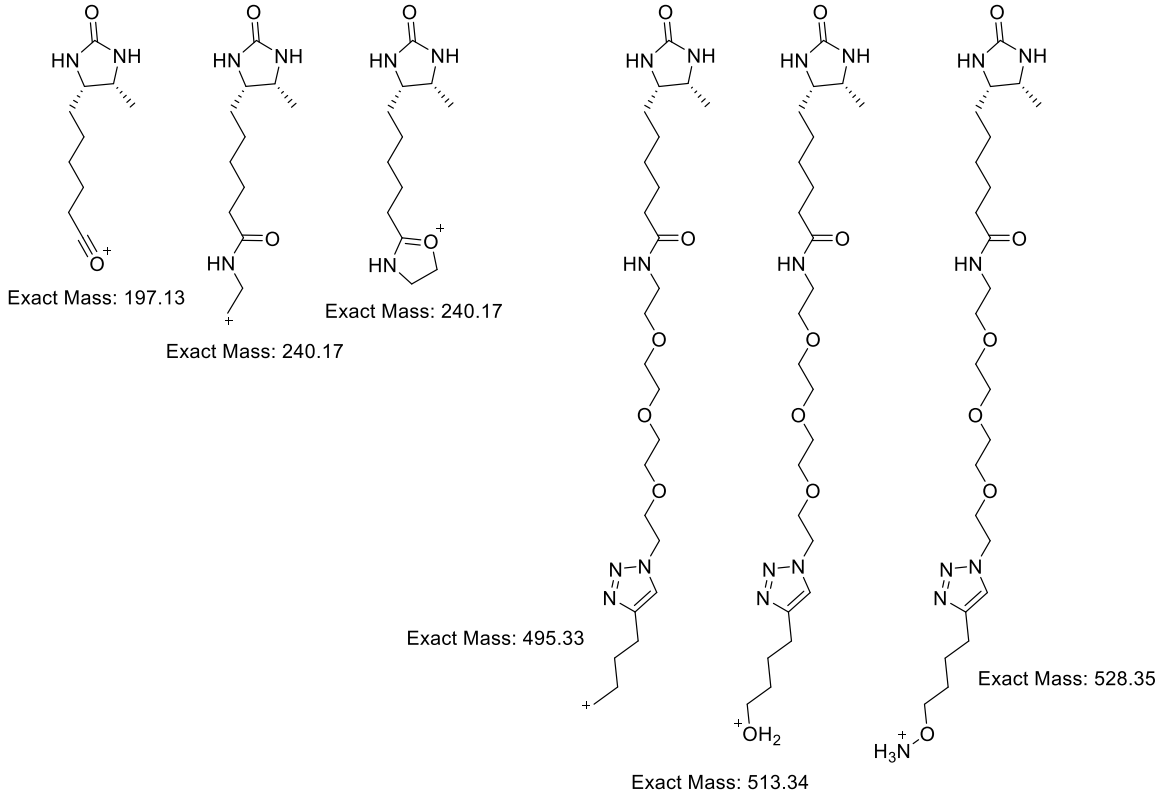

Figure 16: Overview of signature fragments of HA-yne modified peptides either originating from within the DTB-tag (tag-specific) or from the hydroxamate (probe-specific).

Performing an in-depth inspection of MS/MS spectra, in particular ions *m*/*z* 240.17, *m*/*z* 528.35, *m*/*z* 513.34, *m*/*z,* 495.33 and *m*/*z* 197.13 showed the highest signals in decreasing order (Figure 16, Figure S13). Interestingly, all of these signals correspond to fragments harboring desthiobiotin and can be categorized in two groups. The ions *m*/*z* 197.13 and *m*/*z* 240.17 originate from internal fragmentation within the desthiobiotin azide tag (tag-specific), whereas ions *m*/*z,* 495.33, *m*/*z* 513.34 and *m*/*z* 528.35 derive from fragmentation at the HA-yne binding site, the hydroxamate (probe-specific). Displaying dehydro-desthiobiotin, the ion *m*/*z* 197.13 corresponds to the known analogous dehydrobiotin fragment explored in previous biotinylation fragmentation studies.[154, 155] This acylium ion is in equilibrium between the oxonium and carbenium species (Figure S14). The ion *m*/*z* 240.17 shows a carbenium ion, which might also be present as a cyclic oxonium species.[156] Furthermore, there appeared additional linear carbenium ions containing two or three PEG units, though with less intensity. Regarding the probe-specific

group, ion *m*/*z* 528.35 represents the complete modification as hydroxylammonium ion. The ions *m*/*z* 528.35 and *m*/*z* 513.34 stem from ammonia (NH_3) and subsequent water loss. In addition, there are several further fragments from both groups with lower intensity.

Consequently, these five signature fragments were specified as diagnostic peaks in MaxQuant and annotated pAsp levels were analyzed on the basis of the rp-ABPP data in *P. aeruginosa*, since this bacterium contains more than twice as many RRs and hence known pAsp sites compared to *B. subtilis*. Overall, the sum of the best scores of the shared high fidelity pAsp sites revealed a striking 45% increase of the median Andromeda score from 98 to 143. Even more important, the number of HA-yne-modified Asp sites increased from 198 to 324. This discloses a 64% boost and comes close to the number of sites (360), when exclusively allowing for modifications on Asp (D-search) instead of additionally Glu (DE-search). Notably, the number of Glu sites raised by 22% from 451 to 550. Assuming that these new results are true, the coverage of identified HA-yne-modified Asp and Glu sites improved drastically. However, regarding pAsp annotated sites, the number remained the same.

2.4. Dynorphin A Signaling in *P. aeruginosa*

2.4.1. RP-ABPP Experiments

With optimized rp-ABPP methodology and corresponding binding site-ID analysis for the detection of pAsp sites in RRs in hand, downstream dynorphin A signaling in *P. aeruginosa* was explored. As already described in section “Dynorphin A Signaling and Adaptive Resistance”, this human peptide hormone is sensed by the *P. aeruginosa* TCS ParRS, leading to antimicrobial response induced by the ArnBCADTEF system.[39, 42] Hence, rp-ABP was applied to investigate phosphorylation of presumably the RR ParR upon dynorphin treatment.

Accounting for the conditions applied for the target-ID of a dynorphin A photoprobe in the previous AfBPP method by Wright *et al.*,[39] cells were treated with either dynorphin A or DMSO for 1, 5, or 15 minutes in 3-(*N*-morpholino)propanesulfonic acid (MOPS) buffer. In order to allow detection of transient pAsp modifications mediated by rapid dynorphin A

induced signaling events, these shorter treatment durations were initially chosen compared to the former proteomic study (30 min). Then, the proteomes were prepared and analyzed as described in section "Binding Site Identification in *B. subtilis* and *P. aeruginosa*." In brief, harvested cells were HA-yne-treated during lysis, labeled proteomes were clicked to desthiobiotin azide and digested, followed by enrichment of the labeled peptides and LC-MS/MS analysis.

Binding site-ID analysis revealed the detection of 103 and 113 HA-yne-modified Asp sites in dynorphin A-treated and DMSO-treated samples, respectively. Remarkably, 24 and 23 annotated pAsp sites of RRs were found to be modified upon dynorphin A or DMSO treatment, respectively, without a single Asp site at a position other than the pAsp annotated one. Interestingly, both annotated pAsp sites of the RR RetS (Asp713 and Asp858) were detected at the same time. But most importantly, representing the only RR present in dynorphin A-treated samples, not ParR but the cationic peptide resistance regulator (CprR) was identified at all treatment durations. Although direct Asp phosphorylation cannot be proven by the rp-ABPP method, initial phosphorylation of Asp53 is nevertheless very likely, because the annotated site has been identified and is located within the well-known RR motif. Like ParRS, CprR and its corresponding HK CprS belong to a family of TCSs that can sense cationic antimicrobial peptides such as the antibiotic polymyxin B and trigger adaptive resistance.[44] For this purpose, these TCSs activate the ArnBCADTEF operon, which in turn conveys the addition of positively charged 4-aminoarabinose to the lipid A moiety of lipopolysaccharides (LPS) (Figure 17).[42, 43] Thereby, the negative charge of the LPS is masked, which is responsible for the binding and uptake of cationic antimicrobial peptides. Accordingly, the interaction of dynorphin A, bearing five positive charges, with CprS is plausible, since CprS is the HK with the greatest negative net charge of -18 in its periplasmic loop.[44]

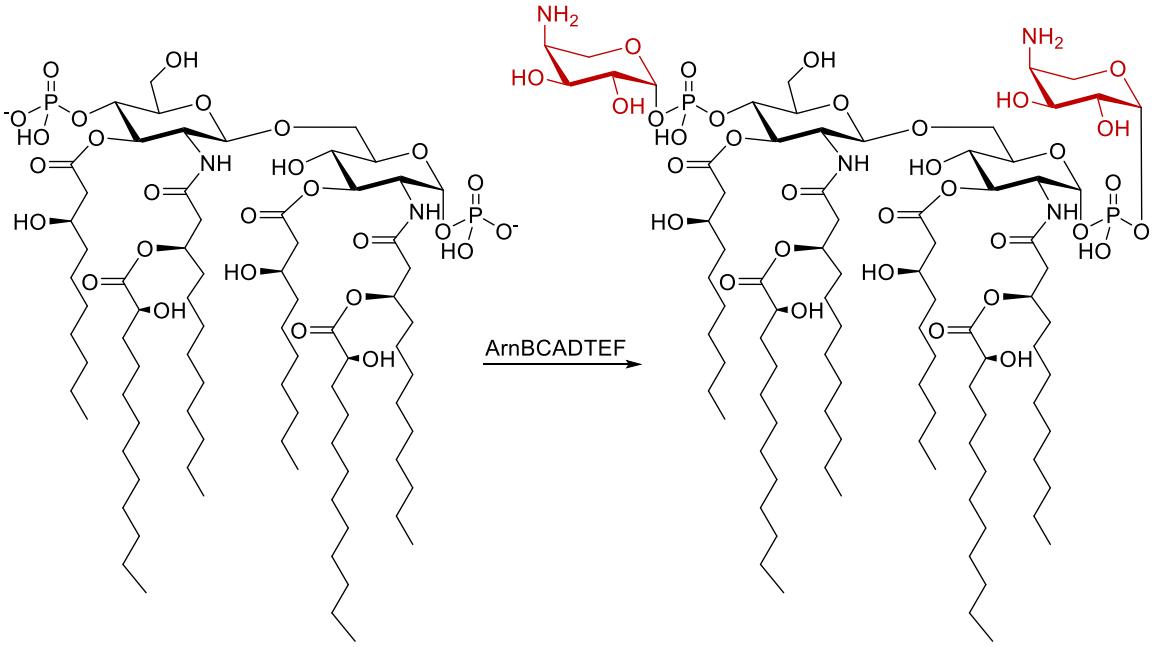

Figure 17: Lipid A modification**.** In the course of adaptive resistance, TCSs activate the ArnBCADTEF operon to mediate addition of 4-aminoarabinose (red) to the lipid A moiety of LPS**.** Thereby, the negative charge is masked and interaction with cationic antimicrobial peptides can be prevented.

2.4.2. isoDTB-ABPP Experiments

To confirm that CprR is the only RR that is phosphorylated solely when exposed to dynorphin A, the recently developed isoDTB tags were used, enabling the simultaneous detection and quantitative comparison of HA-yne-modified Asp sites under two different conditions (Figure 18). This time, besides 1 min dynorphin A vs. DMSO treatment, the cells were also treated for 30 min to allow a comparison to the previous study.[39] To implement the isoDTB methodology in the rp-ABPP workflow, differently treated (1 min or 30 min dynorphin A vs. DMSO) and HA-yne labeled proteomes were clicked to either the light (dynorphin A) or the heavy (DMSO) isoDTBtag. The proteomes were pooled and digested, followed by enrichment of the labeled peptides and LC-MS/MS analysis.

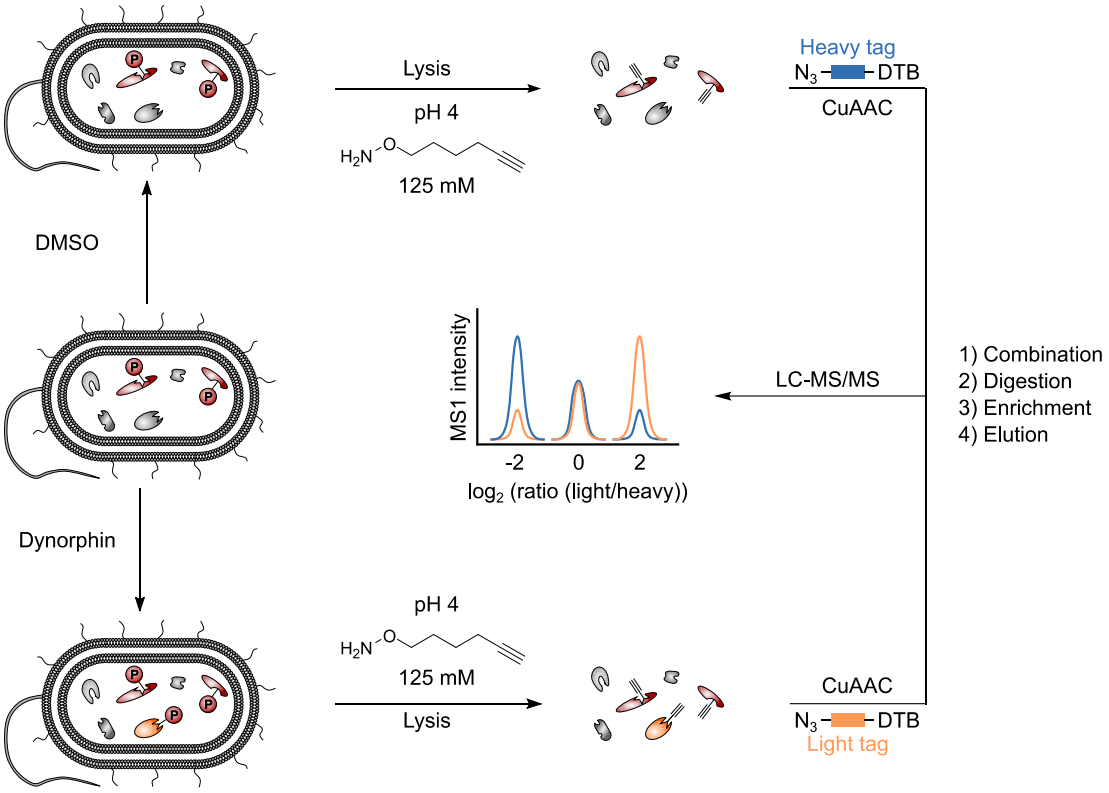

Figure 18: rp-isoDTB workflow for quantitative MS1 binding site analysis. *P. aeruginosa* was grown to exponential growth and treated with either DMSO or 10 µM dynorphin A (Dyn). Cells were lysed in a buffer containing the nucleophilic HA-yne probe (125 mM) at pH 4 and proteomes were clicked to the isoDTB tags. The peptidic samples were combined, tryptically digested, enriched on streptavidin beads, eluted from the beads and subjected to LC-MS/MS analysis. Adapted from Allihn *et al.*[55]

Remarkably, substantiating the previous results, the isoDTB-ABPP experiment uncovered the peptide, containing the pAsp annotated site (Asp53) of CprR, with an intensity ratio of 16.2 between dynorphin A- and DMSO-treated samples (1 min treatment). Importantly, this depicts by far the highest intensity ratio among all HA-yne-modified sites (Figure 19). To account for the conditions of the previously applied AfBPP method,[39] treatment for 30 min revealed a similar ratio of 12.0 (Figure S15a,b). Notably, further confirming the previous results, the isoDTB method disclosed the identification of 24 HA-yne-modified Asp sites exclusively localized at the pAsp annotated site.

Since the previous study by Wright *et al.* identified the HK ParS as dynorphin A sensor, the existence of the HA-yne-modified pAsp annotated site of its cognate ParR was investigated. Interestingly, binding site-ID analysis of the isoDTB-ABPP experiments with

treatment duration of 1 min showed, that the pAsp annotated site (Asp57) was identified in one out of eight samples with a localization probability of 50%, which is below the cut-off for high fidelity sites (>75%). The reason for the low localization probability is the insufficient quality of the corresponding MS2 spectra, which make it impossible for the MaxQuant software to unequivocally identify the modification at one of the two possible Asp residues within the ParR peptide. Moreover, the insufficient quality is related to the inherent properties of the peptide. Since both aspartates (Asp48 and Asp57) are far within the 32 amino acid long peptide (at position 10 and 19), the corresponding fragments b10 and presumably modified y14 are probably too low abundant.

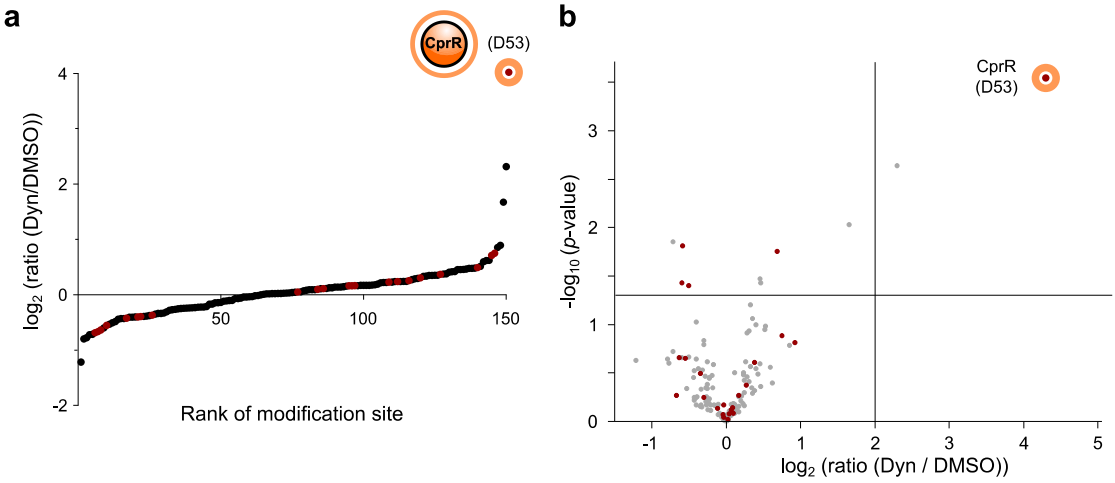

Figure 19: MS1 quantification results of isoDTB-ABPP experiments. (a) Waterfall plot representing the ratio between dynorphin A (light) and DMSO (heavy) treated HA-yne modified Asp and Glu residues (b) Volcano plot, displaying the statistical significance of peptide enrichment as function of the logarithmic ratio of peptide enrichment from dynorphin A-treated and control cells (DMSO). Red dots indicate sites, that are also annotated as pAsp sites in UniProt. Adapted from Allihn *et al.*[55]

Although HCD fragmentation usually generates a significantly less intense b-ion series compared to the y-ion series,[146] the unmodified fragment b10 should be detectable with sufficient MS1 precursor ions. Remarkably, analysis of the samples with 30 min dynorphin A treatment allowed the detection and high fidelity localization (99%) of the pAsp annotated site (Asp57) of ParR in one treated sample, since position 48 could be excluded with the respective unmodified b10 fragment. Consequently, if the modified Asp site is solely present in one sample, no ratio can be obtained. Actually, the ideal case is

represented, when phosphorylation occurs only under one condition. However, since the ParR peptide was not reliable detected in many samples, it might be at the limit of detection. Therefore, a more sensitive method and targeted proteomics method was applied - parallel reaction monitoring (PRM).

2.4.3. PRM Analysis of isoDTB-ABPP Experiments

To further investigate, whether ParR phosphorylation, in addition to CprR, is also upregulated under dynorphin A exposure, PRM analysis of the isoDTB-ABPP experiments was conducted. As previously described in section "Quantification of Identified Binding Sites", PRM is not data dependent. Instead, selected precursors are fragmented either during the whole chromatographic run (unscheduled) or during defined retention time windows (scheduled).

Here, the most interesting precursors, light and heavy Asp-modified peptides of CprR and ParR, were selected for an unscheduled PRM measurement. In addition, the RRs GacA and PhoP were also picked as positive controls for ratios of roughly one. In order to find suitable precursors for fragmentation, MS1 Filtering was performed using Skyline.[157] Analyzing the data from the corresponding DDA experiments, the precursors were selected based on their most intense charge state. Furthermore, 40 PROCAL retention time peptides were spiked in the samples to allow retention time comparison between the LC-MS/MS runs. Then, apart from precursor selection, PRM measurements were conducted with otherwise identical LC-MS/MS settings. For PRM data analysis, MS2 quantification was performed based on the 6 most intense fragment ions of each precursor using Skyline.

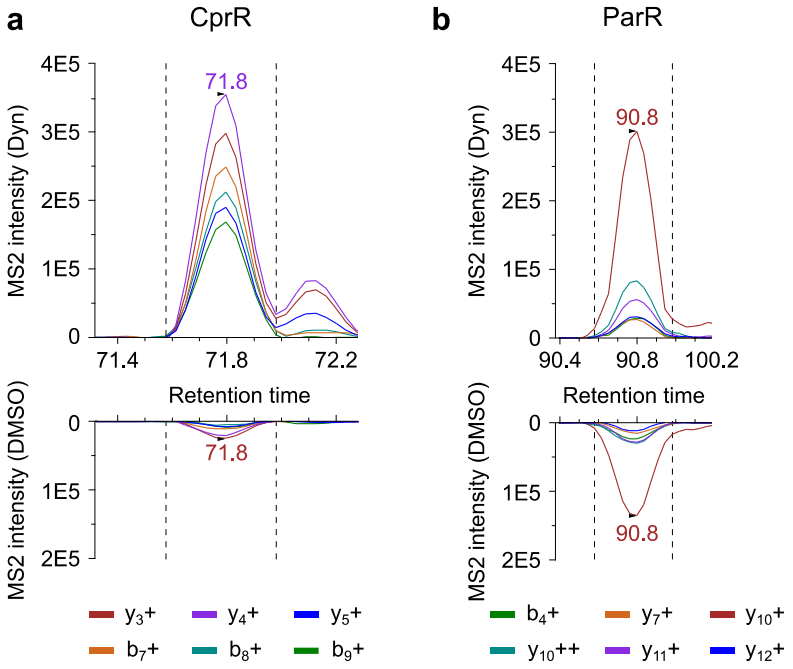

Figure 20: PRM analysis (MS2) of isoDTB-ABPP results. PRM transitions (Dyn/light vs. DMSO/heavy) of pAsp annotated and HA-yne modified peptides of response regulators CprR and ParR. Data was analyzed using the Skyline software[157] and revealed MS2 ratios of 20.8 and 2.0 for CprR and ParR, respectively, disclosing CprR as the only protein with highly enhanced modification. Adapted from Allihn *et al.*[55]

Overall, PRM analysis enabled the successful identification of all 40 PROCAL peptides and all selected light and heavy precursors. Importantly, while the control (GacA) showed an expected ratio of 1.0, MS2 quantification uncovered a ratio of 2.0 for ParR and a considerably higher ratio of 20.8 for CprR (Figure 20). These results were further substantiated by the analogous experiment with 30 min dynorphin A treatment, which resulted in similar ratios of 2.8 and 19.4 for ParR and CprR, respectively (Figure S15c). As a result, while the effect on ParR was modest, PRM analyses confirmed a striking upregulation of Asp phosphorylation of CprR after dynorphin A exposure under the given conditions. Thus, the developed rp-ABPP methodology turned out to be a valuable strategy for studying signaling in bacteria.

2.4.4. isoDTB Tag Fragmentation

To follow up on the evaluation from section “DTB Tag Fragmentation”, the analogous analysis was performed for the isoDTB tags. In general, the isoDTB tag analysis has the

advantage that the internal tag-specific fragments can be assigned with great certainty because of the isotopic labeling.

This time, analysis of MS/MS spectra revealed the recurrent appearance of high intensity ions shown in Table 1 (Figure 21, Figure S16-18). Again, they were grouped in tag-specific fragments, which are independent of the alkyne probe used, and probe-specific fragments.

Table 1: Diagnostic peaks in isoDTB experiments.

tag-specific fragments [m/z]				probe-specific fragments [m/z]			
no.	light	heavy	diff.	no.	light	heavy	diff
1	197.13	197.13	0	7	562.35	568.35	6
2	226.16	228.16	2	8	578.34	584.35	6
3	254.15	257.15	3	9	580.36	586.36	6
4	283.17	288.18	5	10	595.37	601.37	6
5	311.17	317.18	6				
6	328.20	334.20	6				

First of all, identical to the DTB tag fragmentation analysis, dehydro-desthiobiotin (m/z 197.13) was detected. It represented the only fragment present in both light and heavy samples, whereas all other fragments were related to light or heavy samples. Displaying a mass differences of 2 Da (226.16/228.16) and 5 Da (283.17/288.18), respectively, light and heavy iminium ion fragments were identified resulting from α-cleavage, which are in balance with the corresponding carbenium ion. Similar to dehydro-desthiobiotin, also acylium ions with a mass difference of 3 Da (254.15/257.15) and 6 Da (311.17/317.18) were detected. Here, the oxonium and carbenium species are in equilibrium, too.

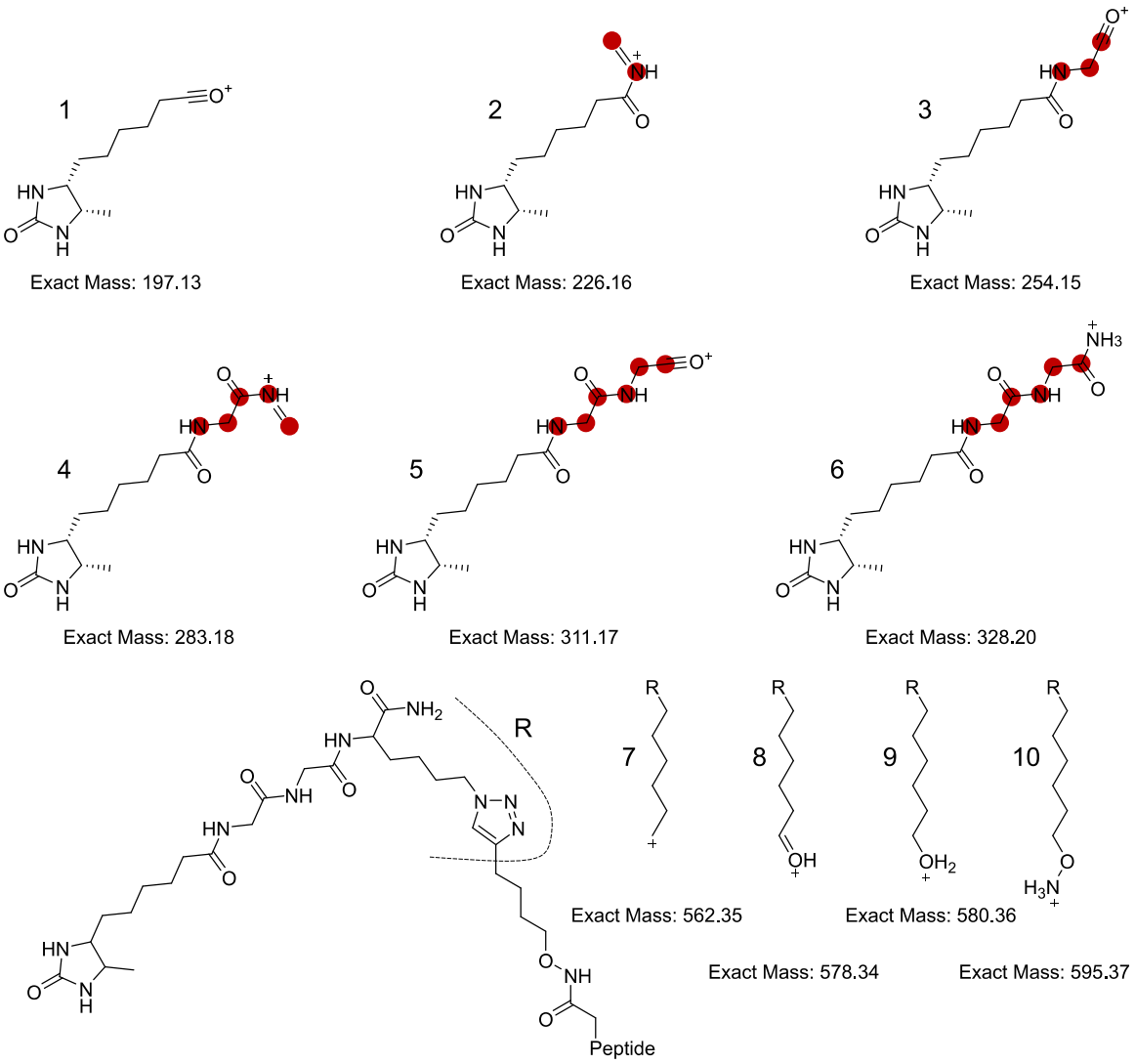

Figure 21: Structures of diagnostic peaks of isoDTB experiments. Fragments 1-6 are tag-specific and fragments 7-10 probe-specific. All fragments were specified in search engines for advanced data analysis.

In addition, displaying moderate ion intensity, another fragment with 6 Da difference (328.20/334.20) was found. Moreover, further less intense tag-specific fragments were identified with 6 Da difference (482.31/488.31, 517.32/523.33, 535.33/541.34, 545.32/551.32). Related to the probe-specific group, a strong analogy to DTB fragments was recognized. To begin with, the hydroxylammonium ion (595.37/601.37) represents the complete modification. Also, the fragments resulting from ammonia (580.36/586.36) and subsequent water loss (562.35/568.35) were found again. Furthermore, another

quite intense fragment was detected (578.34/584.35), which displays presumably a carbenium ion.

Overall, the isoDTB tags allowed accurate identification of the individual fragments, which were later used as diagnostic peaks. However, the emergence of so many fragmentations is actually not favored, since it might prevent correct HA-yne localization and also cause false positives, if these fragments are not specified as diagnostic peaks. In addition, another significant drawback emerged surprisingly. Especially for higher charged precursors, fragments of both light and heavy isoDTB tags were detected in single MS/MS spectra. This means, co-fragmentation of the isoDTB-labeled peptides took place, which is due to the low delta mass of 6 Da. Although, this seems surprising, since the isolation window of 1.6 m/z should be small enough to prevent co-fragmentation of fragments with common charge states.

Analogous to the DTB tag fragmentation analysis, the signature fragments were specified as diagnostic peaks in MaxQuant and annotated pAsp levels were analyzed on the basis of the rp-ABPP data in *P. aeruginosa*. Altogether, the shared dehydro-desthiobiotin fragment plus nine fragments each (light vs. heavy fragments) were enrolled. As a result, the sum of the best scores of the shared high fidelity pAsp sites bearing light or heavy labeled tags showed an increase of the median Andromeda score from 131 to 176 and from 124 to 165, respectively. This equals a gain of 34% and 33% for the light and heavy sites, respectively. Furthermore, the number of HA-yne-modified Asp sites increased by 44 and 63%. Notably, the number of Glu sites raised also 70% and 63% for light and heavy tags, respectively. Hence, the coverage of identified HA-yne-modified Asp and Glu sites improved significantly using the discovered signature fragments as diagnostic peaks. However, regarding pAsp annotated sites, the number remained unchanged just as in the DTB tag analysis.

2.5. Steroid Signaling in *P. aeruginosa*

As discussed in section “The Cystic Fibrosis Gender Gap”, there is a gender gap in cystic fibrosis for which bacteria might be responsible, as there is a known correlation between pulmonary exacerbations and the estrogen concentration during the menstrual cycle and

because the presence of an estrogen binding protein was postulated.[36, 158, 159] Therefore, the impact of the steroid hormones estradiol (E2) and testosterone (TT) on *P. aeruginosa* was investigated. Here, changes in the Asp phosphorylation level of RRs were monitored, since these might give important information about receptor binding, signal transduction processes and possibly subsequent virulence factor expression. Hence, the rp-ABPP workflow was performed analogously to section "isoDTB-ABPP Experiments" by treating *P. aeruginosa* for 2 min in MOPS2-buffer[39] with either steroid hormones at their physiological concentration (10 nm E2/TT) or EtOH. The short treatment duration was again chosen in order to enable capturing of anticipated fast signaling events and because these conditions mediated a strong response upon dynorphin A treatment in as previously described in section "Dynorphin A Signaling in *P. aeruginosa*."

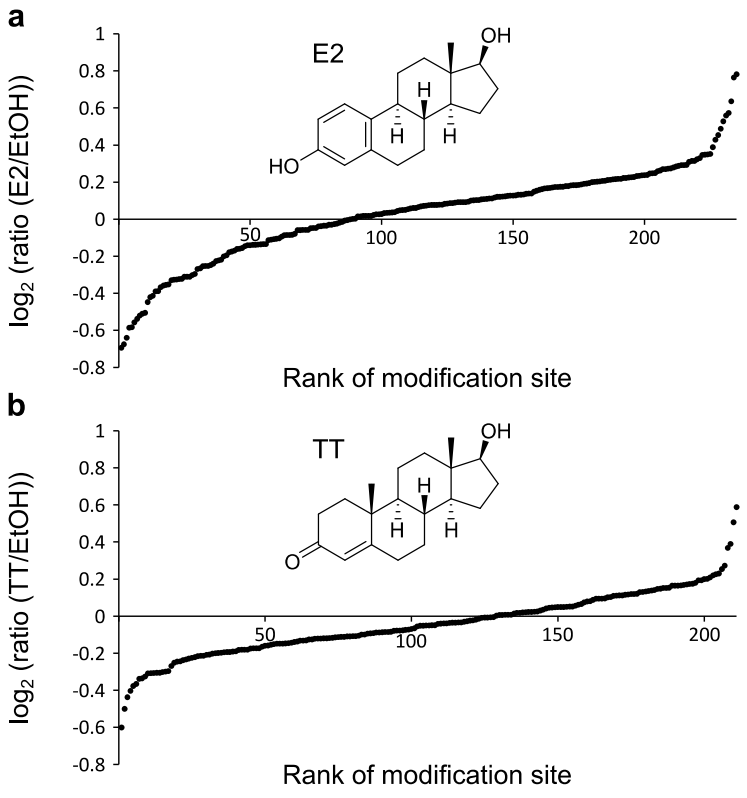

Figure 22: isoDTB MS1 quantification results of isoDTB-ABPP experiments. (a) Waterfall plot representing the ratio between estradiol/ testosterone (10 nM) (light) and EtOH (heavy) treated HA-yne modified Asp and Glu residues. No significant upregulation under both treatment was detected.

However, both treatments resulted in no significant ratios for hormone-treated vs. untreated *P. aeruginosa* (Figure 22). There are several possible reasons for the absence of an effect on pAsp level. First, it is possible that there is no TCS response to steroid hormone treatment, since these hormones display no danger nor inhibit bacterial growth. Conversely, the treatment duration might have been too short for the uptake of estrogen or a bacterial response. Although bacteria are known to respond to environmental changes in a split second during chemotaxis, signaling of transcription regulating RRs occurs more slowly.[160-162] On the other side, it seems reasonable that possible RR phosphorylation has already decayed, since it takes around 40 minutes after initial hormone exposure, due to sample processing reasons, until the pAsp modification can be captured by the nucleophilic probe. However, the time factor could only be countered by in situ labeling, which in turn is not convenient, because no acidic pH inside the cells would be accomplished for HA-yne labeling. Another reason for missing pAsp changes might be the choice of medium. Here, a *P. aeruginosa* minmal medium (MOPS2-buffer)[39] was used. However, since it has been shown that virulence expression is dependent on the medium, the bacterial cells might require a different medium that better reflects the physiological environment of the CF lung in order to respond particularly to estradiol. These conditions could potentially be reflected by the use of bronchial epithelial cell growth medium.[27] Furthermore, the choice and state of the utilized *P. aeruginosa* strain might play an essential role. Yet, it has been shown that *P. aeruginosa* characteristics such as mucoidy and virulence factor expression vary widely among clinical cystic fibrosis isolates, making their investigation complex.[159]

Another important issue will be the identification of the bacterial target of sex hormones by using AfBPP as in the study by Wright *et al.*,[39] which addressed the target-ID of the hormone dynorphin A. However, the question is if there is a bacterial target and if yes,[158] which readout or virulence factor the most suitable for *P. aeruginosa* virulence that could be used to validate the activity of a potential AfBPP probe. Hence, there are a lot of important factors that have to be taken into account to elucidate the bacterial role in the CF gender gap. Whether TCS signaling is responsible for the CF gender gap remains to be elucidated. Here, the initial rp-ABPP attempt showed no effect of the hormones on RR

pAsp level. However, once a model and conditions are appropriately set up, the rp-ABPP approach using the isoDTB methodology displays a valuable strategy for further studies.

3 Summary and Outlook

This thesis describes the development of a chemical proteomic strategy to analyze the transient posttranslational modification (PTM) of aspartate phosphorylation in bacteria and decipher its role in in interkingdom signaling in *P. aeruginosa*.

Two-component systems are vital for the survival and pathogenicity of bacteria, as they can perceive a multitude of environmental changes like the existence antibiotics and respond by triggering adaptive resistance. They consist of a histidine kinase and a response regulator that contains a conserved site for aspartate phosphorylation. Phosphoaspartate (pAsp) is a key intermediate in these multifaceted signal transduction systems. However, it is hydrolytically unstable under neutral, acidic and alkaline conditions, impeding its detection via common analytical methods.

To enable the analysis of this short-lived PTM, a chemical proteomic methodology was used to capture the electrophilically activated state by turnover with an α-effect nucleophile. Initially, pAsp trapping was optimized using the model response regulator PhoB from *E. coli* by IPMS assays. This revealed the requirement of an acidic pH for conversion with hydroxylamine and a synthesized hydroxylamine-based alkyne probe (HA-yne). Subsequently, applying gel-based activity-based protein profiling (ABPP) in *B. subtilis*, the method was subsequently adapted to allow for its utilization in bacterial proteomes. Using the refined reverse-polarity ABPP methodology, proteomes of *B. subtilis* and *P. aeruginosa* were analyzed for the presence of pAsp sites by mass spectrometry. Binding site-ID analysis revealed many annotated pAsp sites and further putative pAsp sites. Noteably, also numerous probe modifications were found on glutamate, asparagine and glutamine residues. However, it has not yet been proven whether background-labeling, other PTMs or processes such deamidation are the cause and is subject to further investigations. Nevertheless, only the annotated pAsp site was detected within the response regulators, demonstrating the proof-of-concept.

Consequently, interkingdom signaling in *P. aeruginosa* was examined at the pAsp level. For this purpose, the validated strategy was extended by utilizing the recently developed isoDTB tags to allow evaluation of pAsp levels under different conditions simultaneously and with highest possible quantification accuracy. Since it was shown in a previous study

that the human peptide stress hormone dynorphin A is sensed by the histidine kinase ParS, the influence of the hormone was additionally assessed at the pAsp level. Surprisingly, it was shown that a similar, but not the expected, response regulator was very strongly upregulated at the pAsp level and thus had to be responsible for interkingdom signaling under the applied conditions. Surprisingly, binding site-ID analysis disclosed that a similar (CprR), but not the expected (ParR) RR was strongly upregulated on pAsp level and thus had to be responsible for interkingdom signaling under the applied conditions. Importantly, different treatment durations and targeted proteomics experiments supported CprR as the major and only protein showing highly upregulation of pAsp.

P. aeruginosa is the major pathogen in patients affected by cystic fibrosis (CF), a genetic disorder leading to premature mortality, which is more pronounced in women. To investigate reasons for this CF gender gap, the influence of the sex hormones estradiol and testosterone on *P. aeruginosa* was also studied by rp-ABPP. However, in contrast to the experiments with dynorphin A, there was no significant upregulation of Asp phosphorylation of a RR. This may be due to many reasons, such as choice of incubation period, medium, or strain, and will be determined in future studies.

Interestingly, in-depth MS analysis of probe-modified sites in rp-ABPP experiments disclosed recurrent patterns in the MS2 spectra resulting from fragmentation of the commercial DTB as well as the isoDTB tags. The fragments were accurately assigned and then used for specification as diagnostic peaks in the search engine, resulting in significantly increased coverage of the pAsp sites found.

Overall, the established rp-ABPP platform allows the exploration of all processes in which pAsp is involved or expected to be. Focusing on pathogenic bacterial strains, the impact of pAsp on resistance development can be studied analogously. Interestingly, since activity of both ParR and CprR is suspected for the development of resistance of *P. aeruginosa* toward polymyxin B, rp-ABPP could provide evidence.[44] In addition, the method could be employed to explore the influence of pAsp in human cells. For example, it is known that the activity of P-type ATPases depends on Asp phosphorylation.[63-65, 163] As

these enzymes, similar to TCSs, have a conserved sequence motif (DKTGT), they can be used as a positive control.[164] Moreover, since these P-type ATPases also have a conserved dephosphorylation motif (TGES), within which the Glu residue was shown to be essential, this might give a hint towards the phosphorylation of a Glu.[165] Therefore, rp-ABPP seems valuable for studying P-type ATPase ion channels. Furthermore, it can be investigated whether the postulated Asp phosphorylation in prostate cancer cells can be proven.[166] However, ADP ribosylation can also take place on Asp and Glu residues in human cells and is known to be convertible with hydroxylamine at neutral pH.[167] Therefore, rp-ABPP in humans might be less selective, though very promising with regard to P-type ATPases.

4 Experimental Procedures

Contributions:

See “introductory remarks.”

The majority of experimental procedures were adapted from Allihn *et al.*[55]

4.1. General Remarks

All reactions sensitive to air and moisture were carried out under argon atmosphere in oven-dried flasks. Chemicals were purchased from *Acros Organics*, *Alfa Aesar*, *Fisher Chemical* and *Sigma-Aldrich* and were used without further purification. Solvents for column chromatography were distilled prior to use. Analytical thin layer chromatography was carried out on silica-coated aluminum plates (Silica gel 60 F_{254}, *Merck*) with detection by UV-absorption (λ = 254 and/or 366 nm) and/or by coloration using a potassium permanganate ($KMnO_4$) staining solution with subsequent heat treatment. Flash column chromatography was performed on silica gel (40-63 µM, *VWR*) with solvent compositions reported as volume/volume (v/v) ratios. ^{1}H- and ^{13}C-NMR spectra were recorded on *Bruker* Avance III HD (400 MHz and 500 MHz) instruments and referenced to the residual solvent signal (δ_H = 7.26 ppm and δ_C = 77.16 ppm for $CDCl_3$; δ_H = 2.50 ppm and δ_C = 39.52 ppm for DMSO-d_6). Signal assignment was reported using following abbreviations: s - singlet, d - doublet, t - triplet, q - quartet, m - multiplet. High-resolution mass spectrometry (HR-MS) spectra were recorded in the ESI mode on an LTQ-FT Ultra (*Thermo Fisher Scientific*) coupled to an UltiMate 3000 HPLC system (*Thermo Fisher Scientific*). DNA and Protein concentrations were determined in duplicates with a NanoQuant plate on an Infinite F200 PRO reader (*Tecan*) by measuring the absorbance at λ = 260 nm or 280 nm, respectively. Primers were purchased as custom synthesized and lyophilized solids (*Eurofins*). Dynorphin A (1-13) was obtained from *Bachem*.

4.2. Synthetic Procedures

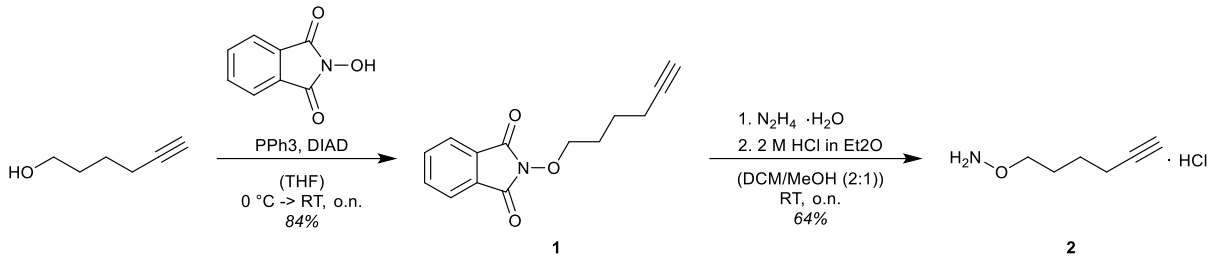

4.2.1. 2-(Hexyloxy)isoindoline-1,3-dione (1):

5-Hexyn-1-ol (3.07 g, 30.0 mmol, 1.00 eq.) was dissolved in dry THF (120 mL) and *N*-hydroxyphthalimide (6.36 g, 39.0 mmol, 1.30 eq.) and triphenylphosphine (PPh_3) (11.8 g, 45.0 mmol, 1.50 eq.) were added. Upon cooling to 0 °C, a solution of diisopropyl azodicarboxylate (DIAD) (8.83 mL, 45.0 mmol, 1.50 eq.) in dry THF (30 mL) was added over 30 min at 0 °C. The mixture was stirred overnight at room temperature. After all volatiles were removed under reduced pressure, the residue was filtered and washed with hexane (3 × 15 mL). Purification by column chromatography (dry loading) (hexane/EtOAc 4:1) yielded **1** as a white solid (6.23 g, 25.2 mmol, 84%).

^{1}H-NMR (400 MHz, $CDCl_3$, 298 K): δ [ppm] = 7.86-7.79 (m, 2H, H_{Ar}), 7.77-7.70 (m, 2H, H_{Ar}), 4.22 (t, ^3J = 6.3 Hz, 2H, OCH_2), 2.37-2.22 (m, 2H, CCH_2), 1.95 (t, ^4J = 2.7 Hz, 1H, CH), 1.94-1.86 (m, 2H, $OCH_2\underline{CH_2}$), 1.84-1.67 (m, 2H, $CCH_2\underline{CH_2}$).

^{13}C-NMR (101 MHz, $CDCl_3$, 300 K): δ [ppm] = 163.73 (s, 2C), 134.58 (s, 2C), 129.09 (s, 2C), 123.62 (s, 2C), 83.97 (s, 1C), 77.94 (s, 1C), 68.93 (s, 1C), 27.24 (s, 1C), 24.62 (s, 1C), 18.12 (s, 1C).

The analytical data obtained are in agreement with those reported in the literature.[168]

4.2.2. *O*-(Hex-5-yn-1-yl)hydroxylamine (2):

1 (2.47 g, 10.0 mmol, 1.00 eq.) was dissolved in DCM/MeOH (2:1) and hydrazine monohydrate (509 µL, 10.5 mmol, 1.05 eq.) was added dropwise. The solution was stirred overnight at room temperature and completion was indicated by TLC. After solvent removal under reduced pressure, the residue was resuspended in H_2O and the pH

adjusted to 12. The mixture was extracted with DCM (3 × 20 mL) and the combined organic layers were washed with brine (20 mL), dried over Na_2SO_4 and filtered. The solvent was removed under reduced pressure and the residue was dissolved in Et_2O, followed by addition of HCl in Et_2O (2 M). The formed precipitate was cooled to -20 °C overnight, filtered and dried under high vacuum to yield **2** as a light yellowish solid (962 mg, 6.43 mmol, 64%).

^{1}H-NMR (500 MHz, DMSO-d_6, 298 K): δ [ppm] = 10.84 (s, 3H, NH_3), 3.99 (t, ^3J = 6.3 Hz, 2H, OCH_2), 2.80 (t, ^4J = 2.7 Hz, 1H, CH), 2.20 (td, ^3J = 7.1, ^4J = 2.6 Hz, 2H, CCH_2), 1.71-1.61 (m, 2H, $OCH_2\underline{CH_2}$), 1.54-1.45 (m, 2H, $CCH_2\underline{CH_2}$).

^{13}C-NMR (101 MHz, DMSO-d_6, 300 K): δ [ppm] = 84.09 (s, 1C), 73.41 (s, 1C), 71.55 (s, 1C), 26.23 (s, 1C), 24.24 (s, 1C), 17.27 (s, 1C).

HRMS-ESI (m/z): calc. ($C_6H_{12}NO$ $[M+H]^+$): 114.0919; found: 114.0914.

4.4. Biochemical Procedures

4.4.1. Bacterial Strains and Media

Unless stated otherwise, *E. coli* BL21 (DE3), *B. subtilis 168* and *P. aeruginosa (PAO1)* were cultivated in LB medium (10 g/L peptone, 5 g/L NaCl, 5 g/L yeast extract, pH 7.5). For the growth of *E. coli* BL21 (DE3) bearing the pET300 expression vector, LB medium was supplemented with ampicillin (100 mg/L). Overnight cultures of bacteria were inoculated with a pipette tip of the corresponding glycerol stock in 5 mL of the corresponding medium and cells were grown overnight at 37 °C with shaking at 220 rpm.

4.4.2. Cloning, Protein Overexpression and Purification

N-terminal His_6-tagged *E. coli* PhoB with a TEV-cleavage site between the His_6-tag and the protein sequence was cloned in a pET300 vector in *E. coli* BL21 (DE3) competent cells via Gateway cloning (*Life Technologies*). For PhoB expression, LB medium was inoculated (1:100) with *E. coli* overnight cultures (37 °C, 220 rpm) and incubated at 37 °C, 220 rpm. After induction at OD_{600} = 0.6 with 0.5 mM IPTG, PhoB was expressed overnight at 25 °C with shaking at 220 rpm. Cells were harvested by centrifugation (6,000 g, 4 °C, 10 min), washed with PBS, resuspended in lysis buffer (20 mM Trizma, pH 8.0, 150 mM NaCl, 2 mM β-mercaptoethanol, 10 mM imidazole, 0.4% (v/v) NP-40) and lysed by sonication (2 x (7 min, 30% int.; 3 min, 80% int.); *Bandelin* Sonopuls HD 2070) under constant cooling with ice. The lysate was centrifugued (38,000 g, 4 °C, 30 min) to remove cellular debris and by using an ÄKTA Purifier 10 system (*GE Healthcare*), the supernatant was loaded on a 5 mL HisTrap HP column (*GE Healthcare*) equilibrated with wash buffer 1 (20 mM Trizma, pH 8.0, 150 mM NaCl, 2 mM β-mercaptoethanol, 10 mM imidazole). The column was washed with wash buffer 1 (8 CV), wash buffer 2 (20 mM Trizma, pH 8.0, 1 M NaCl, 2 mM β-mercaptoethanol, 10 mM imidazole; 8 CV) and wash buffer 3 (20 mM Trizma, pH 8.0, 150 mM NaCl, 2 mM β-mercaptoethanol, 40 mM imidazole; 8 CV). Elution was performed with elution buffer (20 mM Trizma, pH 8.0, 1 M NaCl, 2 mM β-mercaptoethanol, 500 mM imidazole; 4 CV) and PhoB containing fractions were pooled, concentrated using a 50 kDa MWCO centrifugal filter (Merck) and purified by size-exclusion chromatography with a HiLoad 16/60 Superdex 76 pg column (*GE Healthcare*)

equilibrated in PhoB storage buffer (20 mM HEPES, pH 7.0, 150 mM NaCl, 0.1 mM EDTA, 0.1 mM DTT). Fractions containing PhoB were pooled, concentrated and stored at -80 °C after addition of 10% (v/v) glycerol. Purity of the protein was verified by SDS-PAGE and intact-protein mass spectrometry (IPMS).

A point mutant of PhoB (D53N) was generated using the Quikchange Site-Directed Mutagenesis Kit (*Stratagene*) with the pET300 PhoB expression vector as template. Sequences of PhoB and the D53N point mutant were verified by Sanger sequencing (*GATC Biotech AG*). Expression and purification of the mutant was performed as described above.

Unless stated otherwise, tagged PhoB was used for further experiments since it behaved identical to tag-free PhoB. For the generation of tag-free PhoB, the protein was dialysed after His-affinity purification in PhoB storage buffer at 4 °C overnight. PhoB was incubated with 1:3 (w/w) TEV protease at 10 °C overnight without shaking and complete cleavage was verified by IPMS. Tag-free PhoB was concentrated and purified by size-exclusion chromatography as described above.

4.5. Proteomics Experiments

4.5.1. Intact Protein Mass Spectrometry

High-resolution IPMS measurements were performed on an UltiMate 3000 HPLC system (*Thermo Fisher Scientific*) coupled to an LTQ-FT Ultra (*Thermo Fisher Scientific*) mass spectrometer with an electrospray ionization source (spray voltage 4.0 kV, tube lens 110 V, capillary voltage 48 V, sheath gas 60 a.u., aux gas 10 a.u., sweep gas 0.2 a.u.). Protein samples (1-10 pmol) were desalted on-line with a Massprep desalting cartridge (*Waters*) prior to measurement. The mass spectrometer was operated in positive ion mode and full scans were recorded at high resolution (200,000) in a range of m/z = 600-2000 Th. Protein spectra were deconvoluted using the Xcalibur Xtract algorithm (*Thermo Fisher Scientific*).

4.5.2. *In vitro* phosphorylation and phosphoaspartate conversion of PhoB

In vitro phosphorylation of PhoB was initiated by addition of $MgCl_2$ and lithium potassium acetyl phosphate to PhoB in reaction buffer (20 mM HEPES, pH 7.0, 0.1 mM DTT; final

concentrations: 12.5 µM PhoB, 10 µM $MgCl_2$ and 20 µM lithium potassium acetyl phosphate). The reaction mixture was incubated for 1 h at 37 °C without shaking. Meanwhile, Bio-Spin 6 Columns (*Bio-Rad*) for gel filtration were equilibrated four times by addition of 500 µL reaction buffer, centrifugation (1,000 g, 1 min, 4 °C) and removal of the supernatant. Acetyl phosphate was then removed from the sample by application of the sample to the column and centrifugation (1,000 g, 4 min, 4 °C). An aliquot of the sample was taken and 1-10 pmol protein were subjected to IPMS analysis to assess the degree of phosphorylation. The remaining sample was treated with either hydroxylamine or HA-yne at the indicated concentrations. Both preceding steps (IPMS and nucleophile addition) were conducted immediately in order to minimize loss of phosphorylation. Unless stated otherwise, the reaction proceeded at pH = 4 and was checked with pH-indicator strips (*Merck*). The reaction was allowed to stand at room temperature for 1 h before IPMS measurement and assessment of phosphoaspartate conversion. For time-course experiments, aliquots of the samples were subjected to IPMS analysis at the indicated time points and performed in triplicates.

Several control experiments were conducted in order to prove the selectivity of the conversion with hydroxylamine and HA-yne at the optimized conditions with exclusively phosphoaspartate modified proteins. Control experiments were conducted analogously to the procedure described above. For reactions at different pH values, the pH value of the solution containing the nucleophile was adjusted with 0.5 M KOH or HCl prior to the reaction with the indicated protein. Proteins α-Casein and BSA were used as 200 µg/mL solutions and treated with HA-yne without prior phosphorylation.

4.5.3. Gel-Based RP-ABPP Experiments for HA-yne Labeling Optimization

For the development of an RP-ABPP workflow, exponentially growing *B. subtilis* were labeled with HA-yne on analytical scale. LB medium was inoculated (1:100) with *B. subtilis* overnight cultures (37 °C, 220 rpm) and incubated at 37 °C with shaking at 220 rpm. At OD_{600} = 0.5-0.6, cells were harvested by centrifugation (6,000 g, 4 °C, 10 min), washed with ice-cold PBS and resuspended to OD_{600} = 40 in 100 µL lysis buffer (basis: 20 mM HEPES, pH 7.0, HA-yne or DBHA at the indicated concentrations or DMSO; pH value, detergent content and HA-yne were adjusted as indicated) for each condition to be tested.

Cells were lysed by sonication (3 x 15 s, 80% int.) under constant cooling with ice and fractions were separated by centrifugation (21,000 g, 4 °C, 30 min). The insoluble fraction was washed twice with 100 µL ice-cold PBS and stored at -20 °C until subjection to click chemistry. To remove excess HA-yne, the soluble fraction was precipitated in 400 µL of cold acetone (-80 °C) and stored overnight at -20 °C. The precipitate was centrifuged (9,000 g, 4 °C, 10 min) and washed twice by respuspension in 100 µL MeOH (-80 °C) by sonication (10 s, 10% int.), centrifugation (9,000 g, 4 °C, 10 min) and removal of the supernatant.

Soluble and insoluble fractions were resuspended in 100 µL 0.8% SDS in PBS by sonication (10 s, 10% int.) and clicked to rhodamine azide by addition of 6 µL TBTA ligand (0.9 mg/mL in 4:1 *t*BuOH/DMSO), 2 µL rhodamine azide (5 mM stock in DMSO; final concentration: 100 µM), 2 µL TCEP (13 mg/mL in water) and 2 µL $CuSO_4$ (12.5 mg/mL in water). The click reaction was incubated for 1 h at room temperature in the dark, quenched by addition of 112 µL 2× Laemmli buffer and analyzed by SDS-PAGE. Rhodamine azide modified proteins were detected by in-gel fluorescence scanning and protein loading was visualized by Coomassie Brilliant Blue staining.

4.5.4. Western Blot Analysis

Samples were prepared as described in the previous section and soluble and insoluble fractions were resuspended in 100 µL 0.8% SDS in PBS by sonication (10 s, 10% int.). In order to allow a comparison between DBHA, HA-yne and DMSO, HA-yne- and DMSO-treated samples were clicked to 2 µL desthiobiotin azide (5 mM stock in DMSO) by addition of 6 µL TBTA ligand (0.9 mg/mL in 4:1 *t*BuOH/DMSO), 2 µL TCEP (13 mg/mL in water) and 2 µL $CuSO_4$ (12.5 mg/mL in water). The click reaction was incubated for 1 h at room temperature in the dark, quenched by addition of 112 µL 2× Laemmli buffer and analyzed by SDS-PAGE. Bands were transferred onto a membrane (Roti®-PVDF 2.0 pore size 0.2 µm; *Carl Roth*) with blotting buffer (48 mM Tris base, 39 mM glycine, 20% (v/v) MeOH, H_2O) in a Semi-Dry Transfer cell (Trans-Blot® SD; *Bio-Rad*) for 70 min at 20 V. Blocking was performed in blocking solution (1% BSA) in PBS-T (PBS buffer with 0.05% Tween-20®, pH = 7.4) for 1 h. Membranes were washed with PBS-T (2 x 5 min) and incubated with streptavidin-horseradish peroxidase (HRP) polymer conjugate (1:1000 in

PBS-T) at rt for 1 h. Membranes were washed with PBS-T (6 x 5 min) and subsequently incubated with enhanced chemiluminescence (ECL) substrate and peroxide solution (Clarity TM Western ECL Substrate, *Bio-Rad*,). Modified proteins were visualized by in-gel fluorescence scanning (LAS 4000 luminescent image analyzer, *Fujifilm*) in chemiluminescence mode. Protein loading control was performed by subsequent Ponceau S staining.

4.5.5. Target-ID in *B. subtilis*

LB medium was inoculated (1:100) with a *B. subtilis* overnight culture (37 °C, 220 rpm) and incubated at 37 °C with shaking at 220 rpm. At OD_{600} = 0.5-0.6, cells were harvested by centrifugation (6,000 g, 4 °C, 10 min), washed with ice-cold PBS and resuspended to OD_{600} = 40 in 1 mL of HA-yne buffer (20 mM HEPES, pH 4.0, 125 mM HA-yne, 1% (w/v) LDAO). Cells were lysed by sonication (4 x 15 s, 80% int.) under constant cooling with ice. The reaction proceeded for 1 h at 37 °C without shaking. Fractions were separated by centrifugation (21,000 g, 4 °C, 30 min). The insoluble fraction was washed twice with 1 mL ice-cold PBS and stored at -20 °C until subjection to click chemistry. The soluble fraction was precipitated in 4 mL of cold acetone (-80 °C) and incubated overnight at -20 °C. The precipitate was centrifuged (9,000 g, 4 °C, 10 min) and washed twice by resuspension in 1 mL MeOH (-80 °C) by sonication (10 s, 10% int.), centrifugation (9,000 g, 4 °C, 10 min) and removal of the supernatant. The soluble and insoluble fraction were resuspended in 0.8% SDS in PBS by sonication (10 s, 10% int.) and combined (final volume: 1 mL). 800 µL of each sample was clicked to 20 µL biotin azide (10 mM stock in DMSO) by addition of 30 µL TBTA ligand (0.9 mg/mL in 4:1 tBuOH/DMSO), 10 µL TCEP (13 mg/mL in water) and 10 µL CuSO4 (12.5 mg/mL in water). The click reaction was incubated for 1 h at room temperature and quenched by addition of 4 mL of cold acetone (-80 °C) and stored overnight at -20 °C. Precipitates were centrifuged (9,000 g, 4 °C, 10 min) and washed twice by respuspension in 1 mL MeOH (-80 °C) by sonication (10 s, 10% int.), centrifugation (9,000 g, 4 °C, 10 min) and removal of the supernatant. Pellets were resuspended in 500 µL 0.4% SDS in PBS by sonication (10 s, 10% int.). Per sample, 50 µL of avidin-agarose beads were washed with 0.4% SDS in PBS (3 × 1 mL). Samples were added to the beads and incubated by rotation at room temperature for 1 h. The beads were washed by

addition of 0.4% SDS in PBS (3 × 1 mL) and PBS (3 × 1 mL), followed by resuspension in 200 µL digestion buffer (7 M urea, 2 M thiourea in 20 mM HEPES, pH = 7.5). After reduction of disulfides with 2 µL dithiothreitol (DTT; 1 M) and incubation at 37 °C with shaking at 850 rpm for 45 min, free thiols were alkylated by adding 2 µL iodoacetamide (IAA; 0.55 mM) and incubation in the dark at rt with shaking at 850 rpm for 30 min. Remaining IAA was quenched by addition of 0.8 µL DTT (1 M) and incubation at 25 °C with shaking at 850 rpm for 30 min. Proteins were digested with 1 µL LysC (0.5 mg/mL) by incubation at rt with shaking for 2 h. 600 µL 50 mM triethylammonium biocarbonate buffer (TEAB) were added and proteins digested by addition of 1.5 µL of sequencing grade modified trypsin (0.5 mg/mL; *Promega*) and shaking at 37 °C overnight at 220 rpm. Digestion was stopped by addition of 1% formic acid (FA; final pH <3) and samples were centrifuged (9,000 g, 3 min). Meanwhile, SepPak cartridges (50 mg) were equilibrated (1 mL ACN) and washed with elution buffer (80% ACN, 0.5% FA in H_2O) and wash buffer (3 × 1 mL 0.5% FA in H_2O). Peptides were loaded onto the cartridges, washed (3 × 1 mL wash buffer) and eluted (2 × 250 µL elution buffer). The solvent was removed using a vacuum centrifuge and samples were stored at -80°C until further processing. The samples were dissolved by addition of 30 µL 1% FA in H_2O and sonication for 3 min. The samples were filtered through pre-equilibrated 0.22 µm PVDF filters (UVC30GVNB, *Merck*) and transferred into MS vials for LC-MS/MS analysis.

4.5.6. *E. coli* PhoB Spike-in RP-ABPP Experiments in *B. subtilis*

For PhoB spike-in experiments, PhoB was phosphorylated and converted with 500 mM HA-yne as described in section “in vitro phosphorylation and phosphoaspartate conversion of PhoB.” 5 µg of HA-yne modified PhoB was precipitated in 400 µL of cold acetone (-80 °C) and stored at -20 °C until further processing.

LB medium was inoculated (1:100) with a *B. subtilis* overnight culture (37 °C, 220 rpm) and incubated at 37 °C with shaking at 220 rpm. At OD_{600} = 0.5-0.6, cells were harvested by centrifugation (6,000 g, 4 °C, 10 min), washed with ice-cold PBS and resuspended to OD_{600} = 40 in 1 mL of HA-yne buffer (20 mM HEPES, pH 4.0, 125 mM HA-yne, 1% (w/v) LDAO). Cells were lysed by sonication (4 x 15 s, 80% int.) under constant cooling with ice. The reaction proceeded for 1 h at 37 °C without shaking. Fractions were separated by

centrifugation (21,000 g, 4 °C, 30 min). The insoluble fraction was washed twice with 1 mL ice-cold PBS and stored at -20 °C until subjection to click chemistry. The soluble fraction was precipitated in 4 mL of cold acetone (-80 °C) and incubated overnight at -20 °C. The precipitate was centrifuged (9,000 g, 4 °C, 10 min) and washed twice by resuspension in 1 mL MeOH (-80 °C) by sonication (10 s, 10% int.), centrifugation (9,000 g, 4 °C, 10 min) and removal of the supernatant.

The pellet of PhoB, the soluble and insoluble fraction were resuspended in 0.8% SDS in PBS by sonication (10 s, 10% int.) and combined (final volume: 1 mL). 1 mL of each sample was clicked to desthiobiotin azide (*Jena Bioscience*) or isoDTB-tags (light/heavy) by addition of 60 µL TBTA ligand (0.9 mg/mL in 4:1 *t*BuOH/DMSO), 20 µL desthiobiotin azide/ isoDTB-tag (light/heavy) (5 mM stock in DMSO, final concentration: 100 µM), 20 µL TCEP (13 mg/mL in water) and 20 µL $CuSO_4$ (12.5 mg/mL in water). The click reaction was incubated for 1 h at room temperature and quenched by addition of 4 mL of cold acetone (-80 °C) and stored overnight at -20 °C. In experiments using the isoDTB-tags, both samples were pooled during the acetone precipitation step.

4.5.7. RP-ABPP Experiments in *B. subtilis* and *P. aeruginosa*

LB medium was inoculated (1:100) with *B. subtilis* or *P. aeruginosa* overnight cultures (37 °C, 220 rpm) and incubated at 37 °C with shaking at 220 rpm. At OD_{600} = 0.5-0.6, cells were harvested by centrifugation (6,000 g, 4 °C, 10 min), washed with ice-cold PBS and resuspended to OD_{600} = 40 in 1 mL of HA-yne buffer (20 mM HEPES, pH 4.0, 125 mM HA-yne, 1% (w/v) LDAO). Cells were lysed by sonication (4 x 15 s, 80% int.) under constant cooling with ice. The reaction proceeded for 1 h at 37 °C without shaking. Fractions were separated by centrifugation (21,000 g, 4 °C, 30 min). The insoluble fraction was washed twice with 1 mL ice-cold PBS and stored at -20 °C until subjection to click chemistry. The soluble fraction was precipitated in 4 mL of cold acetone (-80 °C) and incubated overnight at -20 °C. The precipitate was centrifuged (9,000 g, 4 °C, 10 min) and washed twice by respuspension in 1 mL MeOH (-80 °C) by sonication (10 s, 10% int.), centrifugation (9,000 g, 4 °C, 10 min) and removal of the supernatant. Soluble and insoluble fractions were resuspended in 1 mL 0.8% SDS in PBS by sonication (10 s, 10% int.) and protein concentration of both fractions was determined using a bicinchoninic acid (BCA) assay and

adjusted to 1 mg/mL with 0.8% SDS in PBS. 1 mL of each sample was clicked to desthiobiotin azide by addition of 60 µL TBTA ligand (0.9 mg/mL in 4:1 *t*BuOH/DMSO), 20 µL desthiobiotin azide (5 mM in DMSO), 20 µL TCEP (13 mg/mL in water) and 20 µL $CuSO_4$ (12.5 mg/mL in water). The click reaction was incubated for 1 h at room temperature and quenched by addition of 4 mL of cold acetone (-80 °C) and stored overnight at -20 °C.

For gel-based analysis, 100 µL of all samples (1 mg/mL) were additionally clicked to rhodamine azide and visualized as described in the previous section.

Moreover, one additional sample was prepared for *B. subtilis* replicates, for which the soluble and insoluble fraction (500 µL each) of the lysate was combined before the click reaction and further processing.

4.5.8. RP-ABPP Experiments in Dynorphin A-Treated *P. aeruginosa*

MOPS medium (50 mM MOPS, pH 7.2, 20 mM NH_4Cl, 20 mM di-sodium succinate, 1 mM $MgSO_4$, 10 mM KCl, 4 mM K_2HPO_4 and 3.5 µM $FeSO_4$) was inoculated (1:100) with a *P. aeruginosa* overnight culture (37 °C, 220 rpm) in LB medium and incubated at 37 °C with shaking at 220 rpm. At OD_{600} = 0.8-1.0, cells were harvested by centrifugation (6,000 g, 4 °C, 10 min) and washed with ice-cold PBS. Cells were resuspended to OD_{600} = 1 in 40 mL PBS and incubated at 37 °C with shaking at 220 rpm. 4 µL of dynorphin A (1-13) (100 mM stock in DMSO; final concentration: 10 µM) or DMSO were added and incubated for either 1, 5 or 15 min at 37 °C with shaking at 220 rpm. The cells were harvested by centrifugation (6,000 g, 4 °C, 10 min), washed with ice-cold PBS and resuspended to OD_{600} = 40 in 1 mL of HA-yne buffer (20 mM HEPES, pH 4.0, 125 mM HA-yne, 1% (w/v) LDAO). The samples were lysed, separated and washed as described above. Soluble and insoluble fractions were resuspended in 1 mL 0.8% SDS in PBS by sonication (10 s, 10% int.) and protein concentration of both fractions was determined by BCA assay and adjusted to 0.5 mg/mL with 0.8% SDS in PBS. 1 mL of each sample was clicked to desthiobiotin azide by addition of 60 µL TBTA ligand (0.9 mg/mL in 4:1 *t*BuOH/DMSO), 20 µL desthiobiotin azide (5 mM stock in DMSO, final concentration: 100 µM), 20 µL TCEP (13 mg/mL in water) and 20 µL $CuSO_4$ (12.5 mg/mL in water). The

click reaction was incubated for 1 h at room temperature and quenched by addition of 4 mL of cold acetone (-80 °C) and stored overnight at -20 °C.

4.5.9. isoDTB-ABPP Experiments in Hormone-Treated *P. aeruginosa*

MOPS medium (50 mM MOPS, pH 7.2, 20 mM NH_4Cl, 20 mM di-sodium succinate, 1 mM $MgSO_4$, 10 mM KCl, 4 mM K_2HPO_4 and 3.5 µM $FeSO_4$) was inoculated (1:100) with a *P. aeruginosa* overnight culture (37 °C, 220 rpm) in LB medium and incubated at 37 °C with shaking at 220 rpm. At OD_{600} = 0.8-1.0, cells were harvested by centrifugation (6,000 g, 4 °C, 10 min) and washed with ice-cold PBS. Cells were resuspended to OD_{600} = 1 in 40 mL PBS and incubated at 37 °C with shaking at 220 rpm.

Dynorphin A treatment: 4 µL of Dynorphin A (1-13) (100 mM in DMSO; final concentration: 10 µM) or DMSO were added and incubated for 1 min or 30 min at 37 °C with shaking at 220 rpm. Estradiol (E2)/ testosterone (TT) treatment: 4 µL of E2 or TT (100 µM in EtOH; final concentration: 10 nM) or EtOH were added and incubated for 2 min at 37 °C with shaking at 220 rpm.

The cells were harvested by centrifugation (6,000 g, 4 °C, 10 min), washed with ice-cold PBS and resuspended to OD_{600} = 40 in 1 mL of HA-yne buffer (20 mM HEPES, pH 4.0, 125 mM HA-yne, 1% (w/v) LDAO). The samples were lysed, washed and separated as described above. Soluble and insoluble fractions were resuspended in 1 mL 0.8% SDS in PBS by sonication (10 s, 10% int.) and protein concentration of both fractions was determined by BCA assay and adjusted to 0.5 mg/mL with 0.8% SDS in PBS. Dynorphin A-treated samples were clicked to the light isoDTB tag and DMSO treated samples were clicked to the heavy isoDTB tag by addition of 60 µL TBTA ligand (0.9 mg/mL in 4:1 *t*BuOH/DMSO), 20 µL of the respective isoDTB tag (5 mM stock in DMSO; final concentration: 100 µM), 20 µL TCEP (13 mg/mL in water) and 20 µL $CuSO_4$ (12.5 mg/mL in water). The click reaction was incubated for 1 h at room temperature and quenched by combination of light and heavy isoDTB-tagged samples into 8 mL of cold acetone (-80 °C). Precipitated samples were stored overnight at -20 °C.

4.5.10. MS Sample Preparation for PhoB Spike-in RP-ABPP Experiments (Protein Enrichment)

Precipitates were centrifuged (9,000 g, 4 °C, 10 min) and washed twice by respuspension in 1 mL MeOH (-80 °C) by sonication (10 s, 10% int.), centrifugation (9,000 g, 4 °C, 10 min) and removal of the supernatant. Pellets were dissolved in 300 µL 8 M urea in 0.1 M triethylammonium bicarbonate (TEAB) by sonication (10 s, 10% int.). 900 µL 0.1 M TEAB were added to obtain a urea concentration of 2 M. This solution was added to 1.2 mL of washed streptavidin agarose beads (50 µL initial slurry; A9207, *Sigma Aldrich*) in 0.2% nonyl phenoxypolyethoxylethanol (NP-40 alternative), which were previously washed by addition of 0.2% NP-40 alternative in PBS (4 × 1 mL), centrifugation (400 rpm, 2 min) and removal of the supernatant. The samples were incubated by rotation at room temperature for 1 h.

To remove unbound proteins, the beads were centrifuged (1,000 g, 2 min) and the supernatant was removed. The beads were resuspended in 600 µL 0.1% NP-40 alternative in PBS and transferred to a centrifuge column (11894131, *Fischer Scientific*). The beads were washed with 0.1% NP-40 alternative (2 × 600 µL), PBS (3 × 600 µL) and ddH_2O (3 × 600 µL) and then resuspended in 600 µL 8 M urea in 0.1 M TEAB. After transfer to a Protein LoBind tube, centrifugation (1,000 g, 2 min) and removal of the supernatant, the beads were resuspended in 300 µL 8 M urea in 0.1 M TEAB.

After reduction of disulfides by addition of 15 µL dithiothreitol (DTT; 31 mg/mL) and incubation at 37 °C with shaking at 850 rpm for 45 min, free thiols were alkylated by adding 15 µL iodoacetamide (IAA; 74 mg/mL) and incubation in the dark at 25 °C with shaking at 850 rpm for 30 min. Remaining IAA was quenched by addition of 15 µL DTT (31 mg/mL) and incubation at 25 °C with shaking at 850 rpm for 30 min. 900 µL 0.1 M TEAB were added to obtain a urea concentration of 2 M for trypsin digestion. 2 µL of 0.5 mg/mL sequencing grade modified trypsin (1 µg; *Promega*) were added and samples were incubated at 37 °C with shaking at 220 rpm overnight. After centrifugation (400 rpm, 2 min) and removal of the supernatant, the beads were washed three times by addition of 50 µL Tris-HCl buffer (50 mM, pH 7.5), centrifugation (1,000 g, 2 min) and removal of the supernatant. The beads were reuspended in 100 µL Tris-HCl buffer, followed by

addition of 16 µL of 0.04 mg/mL sequencing grade AspN (0.64 µg; *Promega*) and incubation at 37 °C with shaking at 220 rpm for 7 h.

The beads were resuspended in 500 µL 0.1% NP-40 alternative in PBS and transferred to a centrifuge column (11894131, *Fischer Scientific*). The beads were washed with 0.1% NP-40 alternative (2 × 600 µL), PBS (3 × 600 µL) and ddH_2O (3 × 600 µL). The peptides were eluted by addition of 200 µL elution buffer (0.1% formic acid (FA) in 1:1 acetonitrile (ACN)/H_2O) and two more elution steps with 100 µL elution buffer, followed by centrifugation (5,000 g, 3 min). The solvent was removed using a vacuum centrifuge and samples were stored at -80°C until further processing. The samples were dissolved by addition of 30 µL 1% FA in H_2O and sonication for 3 min. The samples were filtered through pre-equilibrated 0.22 µm PVDF filters (UVC30GVNB, *Merck*) and transferred into MS vials for LC-MS/MS analysis.

4.5.11. MS Sample Preparation for RP-ABPP and isoDTB-ABPP Experiments (Peptide Enrichment)

Precipitates were centrifuged (9,000 g, 4 °C, 10 min) and washed twice by respuspension in 1 mL MeOH (-80 °C) by sonication (10 s, 10% int.), centrifugation (9,000 g, 4 °C, 10 min) and removal of the supernatant. Pellets were dissolved in 300 µL 8 M urea in 0.1 M triethylammonium bicarbonate (TEAB) by sonication (10 s, 10% int.). After reduction of disulfides by addition of 15 µL dithiothreitol (DTT; 31 mg/mL) and incubation at 37 °C with shaking at 850 rpm for 45 min, free thiols were alkylated by adding 15 µL iodoacetamide (IAA; 74 mg/mL) and incubation in the dark at 25 °C with shaking at 850 rpm for 30 min. Remaining IAA was quenched by addition of 15 µL DTT (31 mg/mL) and incubation at 25 °C with shaking at 850 rpm for 30 min. 900 µL 0.1 M TEAB were added to obtain a urea concentration of 2 M for trypsin digestion. 20 µL of 0.5 mg/mL sequencing grade modified trypsin (10 µg; *Promega*) were added and samples were incubated at 37 °C with shaking at 220 rpm overnight. This solution was added to 1.2 mL of washed streptavidin agarose beads (50 µL initial slurry; A9207, *Sigma Aldrich*) in 0.2% nonyl phenoxypolyethoxylethanol (NP-40 alternative), which were previously washed by addition of 0.2% NP-40 alternative in PBS (4 × 1 mL), centrifugation (400 rpm, 2 min) and

removal of the supernatant. The samples were incubated by rotation at room temperature for 1 h.

To remove unbound peptides, the beads were centrifuged (1,000 g, 2 min) and the supernatant was removed. The beads were resuspended in 600 µL 0.1% NP-40 alternative in PBS and transferred to a centrifuge column (11894131, *Fischer Scientific*). The beads were washed with 0.1% NP-40 alternative (2 × 600 µL), PBS (3 × 600 µL) and ddH_2O (3 × 600 µL). The peptides were eluted by addition of 200 µL elution buffer (0.1% formic acid (FA) in 1:1 ACN/H_2O) and two more elution steps with 100 µL elution buffer, followed by centrifugation (5,000 g, 3 min). The solvent was removed using a vacuum centrifuge and samples were stored at -80°C until further processing. The samples were dissolved by addition of 30 µL 1% FA in H_2O and sonication for 3 min. The samples were filtered through pre-equilibrated 0.22 µm PVDF filters (UVC30GVNB, *Merck*) and transferred into MS vials for LC-MS/MS analysis.

4.5.12. LC-MS/MS Analysis

Samples (injection volume: 5 µL) were analyzed with an Ultimate 3000 nano HPLC system (*Dionex*) coupled to a Q Exactive Plus mass spectrometer (*Thermo Fisher Scientific*). Samples were loaded on an Acclaim C18 PepMap100 trap column (75 µm ID x 2 cm), washed with 0.1% TFA and separated on an Acclaim C18PepMapRSLC column (75 µm ID x 50 cm) with a flow of 300 nL/min using buffer A (0.1% FA in H_2O) and buffer B (0.1% FA in ACN): 5% B for 7 min, 5-40% B in 105 min, 40-60% B in 10 min, 60-90% B in 10 min, 90% B for 10 min, 90-5% B in 0.1 min, 5% B for 9.9 min. The Q Exactive Plus mass spectrometer was operated in a TOP10 data dependent acquisition mode (DDA). Full MS (MS1) scans were acquired at a resolution of 70,000, a scan range of m/z = 300-1500 Th, an automomatic gain control (AGC) target of 3e6, and a maximum injection time of 80 ms. The ten most intense precursors (Top10) were selected for MS2 scan acquisition at a resolution of 17,500, an AGC target of 1e5, and a maximum injection time of 100 ms. Precursors with unassigned charge or a charge of +1 were excluded and dynamic exclusion was set to 60 s. Quadrupole isolation of the precursor was set to a window of 1.6 Th. Fragment ions were generated using higher-energy dissociation (HCD) with a normalized collision energy (NCE) of 27% and detected in the orbitrap.

4.5.13. Target-ID Data Analysis

MS raw data were analyzed using MaxQuant software (version 1.6.2.10).[97] Standard settings were used with the following changes and additions: The normal FASTA database without manual changes was downloaded from UniProt[132] (*B. subtilis* 168 taxon identifier: 224308, date of download: 20.09.2018). No labels were used. The proteolytic enzyme was set to Trypsin/P with up to two missed cleavages. *N*-terminal acetylation and oxidation of methionine were selected as further variable modifications and carbamidomethylated cysteine as fixed modification. The maximum number of modifications per peptide was 5. Label-free quantification (LFQ) options were set to a minimal ratio count: 2, min unique peptides: 2 and razor protein FDR enabled. The "Re-quantify" option was enabled and contaminants were included. Peptides were searched with a minimum peptide length of 6 and a maximum peptide mass of 4,600 Da. "Second peptides" was enabled and "Dependent peptides" was disabled. "Match between runs" was enabled with a Match time window of 0.7 min and an alignment window of 20 min. A minimal Andromeda score[96] of 40 and a delta score of 6 was set for modified peptides. An FDR of 0.01 was used for Protein FDR, PSM FDR and XPSM FDR. Technical replicates were analyzed in the same MaxQuant analysis. For statistical analysis, the protein groups table was loaded into Perseus (version 1.6.5.0).[128] Upon $\log_2$ transformation of LFQ intensities, contaminants and reverse hits were removed. Data was filtered for two valid values in at least one group and missing value imputation was performed over the total matrix. Statistical evaluation was performed by a two-sied two sample Student's *t*-test.

4.5.14. Open Search with FragPipe

An open search was performed with FragPipe (version 9.4) to screen the mass shifts found on peptides with settings as follows: Precursor mass tolerance: -150 to 1000 Da, fragment mass tolerance: 10 ppm, isotope error: 0, enzyme name: trypsin, cut after: KR, but not before: P, cleavage: enzymatic, missed cleavages: 2, peptide length: 7 to 50, peptide mass range 500 to 5000 Da, variable modifications: M Ox, *N*-terminal acetylation, fixed modifications: C carbamidomethylation. Remaining settings were left as default. PeptideProphet options were set to nonparam, expectscore, decoyprobs, masswidth: 1000.0, clevel: -2, decoy rev. ProteinProphet was set to maxppmdiff: 2000000. Crystal-C

was enabled. Generate report was allowed with filter: sequential, razor, prot 0.01. PTM-Shepherd was enabled with the following settings: smoothing factor: 2, localization background 4, prominence ratio 0.3, peak picking width: 0.002 Da.

4.5.15. RP-ABPP Data Analysis

MS raw data were analyzed using MaxQuant software (version 1.6.2.10).[97] Standard settings were used with the following changes and additions: The normal FASTA databases without manual changes were downloaded from UniProt[132] (*B. subtilis* 168 taxon identifier: 224308, date of download: 20.09.2018; *P. aeruginosa* PAO1 taxon identifier: 208964, date of download: 22.05.2019). No labels were used. The proteolytic enzyme was set to Trypsin/P with up to three missed cleavages. Variable modifications with HA-yne and desthiobiotin azide were allowed on Asp, Glu; Asn and Gln:

- HA-yne and desthiobiotin azide on Asp or Glu: $C_{24}H_{43}N_7O_5$ (509.3326 Da)

- HA-yne and desthiobiotin azide on Asn or Gln: $C_{24}H_{42}N_6O_6$ (510.3166 Da)

Optional, the following diagnostic peaks were specified on Asp and Glu (elementary composition as in Figure 16):

- 197.13 Da, 240.17 Da, 495.33 Da, 513.34 Da, 528.35 Da

N-terminal acetylation and oxidation of methionine were selected as further variable modifications and carbamidomethylated cysteine as fixed modification. The maximum number of modifications per peptide was 5. The “Re-quantify” option was enabled. Contaminants were included. Peptides were searched with a minimum peptide length of 6 and a maximum peptide mass of 4,600 Da. “Second peptides” was enabled and “Dependent peptides” was disabled. “Match between runs” was enabled with a Match time window of 0.7 min and an alignment window of 20 min. A minimal Andromeda score[96] of 40 and a delta score of 6 was set for modified peptides. An FDR of 0.01 was used for Protein FDR, PSM FDR and XPSM FDR. Technical replicates were analyzed in the same MaxQuant analysis.

The “DTB-PEG-N3-Sites.txt” files generated by MaxQuant analysis for modification with HA-yne and the desthiobiotin azide tag were used for further analysis. All peptides for

"reverse" sequences and "potential contamination" were removed. The data were filtered to only include peptides with a localization probability of at least 75% for a single amino acid residue. Within these peptides, for each potentially electrophilic amino acid, the number of sequences was counted that is modified on one specific residue. Identical sequences with HA-yne modification at different positions are possible and these are counted as separate sites, if they exceed the 75% localization probability cutoff. The sum of all modified sites within our cutoff from biologically independent replicates was reported.

4.5.16. isoDTB Data Analysis

MS raw data were analyzed using MaxQuant software (version 1.6.2.10).[97] Standard settings were used with the following changes and additions: The normal FASTA databases without manual changes were downloaded from UniProt[132] (*P. aeruginosa* PAO1 taxon identifier: 208964, date of download: 22.05.2019). No labels were used. The proteolytic enzyme was set to Trypsin/P with up to three missed cleavages. Variable modifications with HA-yne and either the light or heavy isoDTB tag were allowed on Asp and Glu:

- HA-yne and light isoDTB tag on Asp or Glu: $C_{26}H_{44}N_{10}O_5$ (576.3496 Da)

- HA-yne and heavy isoDTB tag on Asp or Glu: $C_{22}{}^{13}C_4H_{44}N_8{}^{15}N_2O_5$ (582.3571 Da)

Optional, the following diagnostic peaks were specified on Asp and Glu (elementary composition as in Figure 21):

- light: 197.13 Da, 226.16 Da, 254.15 Da, 283.17 Da, 311.17 Da, 328.20 Da, 562.35 Da, 578.34 Da, 580.36 Da, 595.37 Da

- heavy: 197.13 Da, 228.16 Da, 257.15 Da, 288.18 Da, 317.18 Da, 334.20 Da, 568.35 Da, 584.35 Da, 586.35 Da, 601.37 Da

N-terminal acetylation and oxidation of methionine were selected as further variable modifications and carbamidomethylated cysteine as fixed modification. The maximum number of modifications per peptide was 5. The "Re-quantify" option was enabled. Contaminants were included. Peptides were searched with a minimum peptide length of 7 and a maximum peptide mass of 4,600 Da. "Second peptides" was enabled and

"Dependent peptides" was disabled. "Match between runs" was enabled with a Match time window of 0.7 min and an alignment window of 20 min. A minimal Andromeda score[96] of 40 and a delta score of 6 was set for modified peptides. An FDR of 0.01 was used for Protein FDR, PSM FDR and XPSM FDR. Technical replicates were analyzed in the same MaxQuant analysis.

The "isoDTB light HA-yne (DE)Sites.txt" and "isoDTB heavy HA-yne (DE)Sites.txt" files generated by MaxQuant analysis for modification with HA-yne and isoDTB tags were used for further analysis. All peptides for "reverse" sequences and "potential contamination" were removed. The data were filtered to only include peptides with a localization probability of at least 75% for a single amino acid residue. Within these peptides, for each potentially electrophilic amino acid, the number of sequences was counted that is modified on one specific residue. Identical sequences with HA-yne modification at different positions are possible and these are counted as separate sites, if they exceed the 75% localization probability cutoff. The sum of all modified sites within our cutoff from biologically independent replicates was reported.

4.5.17. Adjustment of FASTA Databases for Quantitative isoDTB-ABPP Data Analysis[169]

The challenge for the quantification of modified aspartates and glutamates in this project was to quantify the relative abundance of peptides modified at one residue with HA-yne and the light and heavy isoDTB tags, respectively. We have previously reported this procedure for addressing a single modified amino acid, cysteine,[110] and also applied it for two modified amino acids, aspartate and glutamate.[169] To the best of our knowledge, relative quantification of two "variable modifications" relative to one another is not possible using MaxQuant software at this point. Therefore, we set out to use the "label" function in MaxQuant for quantification. Nevertheless, while this function allows very reliable relative quantification of light- and heavy-labeled peptides, this function assumes every amino acid of a certain type (e.g. aspartate and glutamate) to be modified with the label. Therefore, peptides with two or more of these residues are only detected and quantified, if all of these residues have reacted with the probe and the isoDTB tags. However, the peptides that are modified at one residue with the probe and the isoDTB tags but are unmodified at the others are not detectable. For this reason, we utilized our

workaround as described previously,[169] in order to achieve this quantification. We utilized "U" respectively "O", which normally stand for selenocysteine and pyrrolysine, as a placeholder amino acid for the modified residue ("U" used for glutamates and "O" used for aspartates). To do so, we deleted all selenocysteine- or pyrrolysine-containing proteins from the FASTA database, which were very few or nonexistent, respectively. We then individually replaced each glutamate in the FASTA database with a "U" and additionally every aspartate individually with an "O" generating n different sequences with a single "U" or "O" for a protein with n aspartates and glutamates. For each individual replacement, we created an entry in the FASTA database, which was named in the format "UniProt code"_"E""number of the glutamate" respectively "UniProt code"_"D""number of the aspartate". The unmodified sequence was deleted from the FASTA database, except if the protein did not contain any aspartate or glutamate, in which case the unmodified entry was renamed to "UniProt Code"_"0" and kept in the database. In this way, for each aspartate and glutamate in the database, we created a unique sequence, in which it is marked as the modified residue (by being replaced by the placeholder "U" or "O") and all other aspartates and glutamates are marked as unmodified (are remaining "D" or "E" in the database). Therefore, we were able to make sure that there is always only one modified residue in each peptide to be detected and quantified. Therefore, this allows us to detect and quantify all peptides that contain several aspartates and glutamates but are only modified with the probe and the isoDTB tags at one of them. During MaxQuant analysis, we define the labels in a way to not only add the modification with the tag but also to transfer the placeholder "U" or "O" back to a glutamate or aspartate. During downstream data analysis, the "U" or "O" in the sequence is changed back to the indicator for a modified glutamate ("E*") or aspartate ("D*").

4.5.18. isoDTB-ABPP Data Analysis for Quantification

MS raw data were analyzed using MaxQuant software (version 1.6.2.10).[97] Standard settings were used with the following changes and additions analogous to our previous study:[169] The modified FASTA database with individual substitutions of aspartates and glutamates with the placeholder "O" or "U" was used ("PA8_DO_EU.fasta"). Labels were

set on the placeholder amino acids “O” and “U” for the light isoDTB tag as light label and the heavy isoDTB tag as heavy label. The following labels were used:

- HA-yne and light isoDTB tag on “O” as placeholder for D: $C_{18}H_{30}N_8O_6$

- HA-yne and heavy isoDTB tag on “O” as placeholder for D: $C_{14}{}^{13}C_4H_{30}N_6{}^{15}N_2O_6$

- HA-yne and light isoDTB tag on “U” as placeholder for E: $C_{28}H_{46}N_{10}O_7Se_{-1}$

- HA-yne and heavy isoDTB tag on “U” as placeholder for E: $C_{24}{}^{13}C_4H_{46}N_8{}^{15}N_2O_7Se_{-1}$

Multiplicity of 2 and maximum number of labeled amino acids of 1 was set. The proteolytic enzyme was set to Trypsin/P with up to three missed cleavages. The “Re-quantify” option was enabled. *N*-terminal acetylation and oxidation of methionine were selected as further variable modifications and carbamidomethylated cysteine as fixed modification. Contaminants were included. Peptides were searched with a minimum peptide length of 7 and a maximum peptide mass of 4,600 Da. “Second peptides” was enabled and “Dependent peptides” was disabled. “Match between runs” was enabled with a Match time window of 0.7 min and an alignment window of 20 min. A minimal Andromeda score[96] of 40 and a delta score of 6 was set for modified peptides. An FDR of 0.01 was used for Protein FDR, PSM FDR and XPSM FDR. Technical replicates and all competitive data were analyzed in the same MaxQuant analysis.

The “peptides.txt” file of the MaxQuant analysis was used for further analysis. All peptide sequences without a modified aspartate or glutamate (placeholder “O” or “U”) and with an Andromeda Score[96] below 40 were deleted. Also all peptides for “reverse” sequences and “potential contamination” were removed. Only the columns “Sequence”, “Leading Razor Protein”, “Start Position” and the columns for “Ratio H/L” for all experiments were kept. The “Leading Razor Protein” was renamed to the UniProt Code without the indicator for the number of the aspartate or glutamate. All individual ratios were filtered out if they were “NaN”, and all other values were transformed into the $\log_2$-scale. For each peptide, the data were filtered out, if there were not at least two data points for individual technical replicates or if the standard deviation between the technical replicates exceeded a value of 1.41. For each peptide, an identifier was generated in the form “UniProt Code”_”D”” residue number of the modified aspartate” or “UniProt Code”_”E””

residue number of the modified glutamate". The data for all peptides with the same identifier, and therefore the same modified aspartate or glutamate, were combined. Here, the median of the data was used. The data were filtered out if the standard deviation exceeded a value of 1.41. Each modified aspartate or glutamate was kept in the dataset once with the shortest peptide sequence as the reported sequence. For each modified residue, all values of replicates were combined, but the individual values are also reported. The values were combined as the median and the data were filtered out, if there were not at least two data points or if the standard deviation exceeded a value of 1.41. These are the final ratios $\log_2$ (ratio L/H) that are reported. For all comparisons between different MaxQuant runs, the data were combined into one table based on the modified residue.

All individual values (4 biological replicates: soluble and insoluble) for each modified residue were loaded into Perseus (version 1.6.5.0)[128] and analyzed using a one-sample *t*-test against a value of $\log_2$ (ratio L/H) = 0. Sites were considered as significantly regulated, if the statistical significance was $p < 0.05$ and the median ratio was $\log_2$ (ratio L/H) > 2.

Ratios and *p*-values of the modified peptides were matched with the corresponding UniProt data (*P. aeruginosa* PAO1 taxon identifier: 208964) and the corresponding categorized protein abundance data obtained from PaxDb[41] and listed in Table S1.

4.5.19. PRM Method Development

Based on the results of the quantitative data dependent acquisition (DDA) isoDTB experiments, the most interesting HA-yne modified peptides with the highest light to heavy MS1 ratios (L/H) were chosen for PRM measurements. The corresponding peptides from the response regulators CprR and ParR were selected for fragmentation, showing the highest or a so far uncharacterized MS1 ratio (light to heavy), respectively. Additionally, two peptides (from response regulators GacA and PhoP) with an MS1 ratio of roughly one, were chosen as controls. Precursors for fragmentation were selected based on their respective most intense charge state from the DDA measurements analyzed by MS1 Filtering using Skyline (version 20.2.1.286).[157] Experimental spectral libraries were built within Skyline using DDA and PRM isoDTB data processed with

MaxQuant and are available for download from Panorama Public[170] (https://panoramaweb.org/pAsp-isoDTB-PAO1.url). For retention time comparison, PROCAL retention time peptides (*JPT Peptide Technologies*) were used, consisting of 40 non-naturally occurring peptides. PROCAL peptides were spiked into the samples (final quantity: 100 fmol/peptide). For 34 PROCAL peptides only MS1-chromatogram information was acquired in PRM mode, while five PROCAL peptides were also selected for fragmentation. For further information see Table S2 and https://panoramaweb.org/pAsp-isoDTB-PAO1.url.

4.5.20. PRM LC-MS/MS Analysis

For PRM measurements, the same samples from the isoDTB experiments were used. Additionally, PROCAL retention time peptides were spiked into the samples (v/v 1:6) directly before measurement. 6 µL of sample were injected in order to obtain similar intensities as in previous DDA measurements and 100 fmol/peptide of the PROCAL retention time peptides.

PRM measurements were performed using the same instruments and LC-setup as described in section “LC-MS/MS Analysis”, but the Q Exactive Plus (*Thermo Fisher Scientific*) was operated in PRM mode. Full MS (MS1) scans were acquired at a resolution of 70,000, a scan range of m/z = 300-1500 Th, an automatic gain control (AGC) target of 3e6, and a maximum injection time of 80 ms. Targeted MS2 scans were acquired at a resolution of 17,500, an AGC target of 1e5, and a maximum injection time of 100 ms. The number of targeted precursors was adjusted to maintain a maximum cycle time of 2 s for at least 8 points across the peak in a non-scheduled PRM measurement. In total, 4 different HA-yne-modified peptides from proteins CprR, ParR, GacA and PhoP (light/heavy isoDTB version) and 5 PROCAL peptides were targeted (Table S2). Quadrupole isolation of the precursor was set to a window of 1.6 Th. Fragment ions were generated using higher-energy dissociation (HCD) with a normalized collision energy (NCE) of 27% and detected in the orbitrap.

4.5.21. PRM Data Analysis

PRM data analysis was performed using the Skyline-daily (64-bit) software (version 20.2.1.286).[157] For all target peptides, the 6 most intense fragment ions (top6) were automatically picked by Skyline using the generated experimental spectral library. Raw PRM data were also processed by MaxQuant in order to visualize in Skyline the exact time point of successful peptide identification for any given MS2 spectrum. Peak picking, peak integration and transition interferences were reviewed and integration boundaries were adjusted manually in Skyline, if necessary. Mass accuracy information ("average mass error [ppm]"), correlation of fragment ion intensities between the detected light and heavy peptides ("dot product L/H") and correlation of fragment ion intensities between the detected peptides measured by PRM and the experimental library spectrum from Skyline ("library dot product" separately for light and heavy) were exported from Skyline. Peptide identifications with a dot product L/H > 0.9 and a library dot product > 0.85 were included for the overall ratio (L/H) calculation. The ratio of the respective MS2 peak areas ("total area fragment" L/H) was used for the ratio (L/H) calculation. For further information, see Table S2 and https://panoramaweb.org/pAsp-isoDTB-PAO1.url.

5 Abbreviations

ABPP	Activity-based protein profiling
ACN	Acetonitrile
AcP	Acetyl phosphate
AfBPP	Affinity-based protein profiling
AGC	Automomatic gain control
AMR	Antimicrobial resistance
AR	Adaptive resistance
Asn	Asparagine
Asp	Aspartic acid
BCA	Bicinchoninic acid
BSA	Bovine serum albumin
C	Cysteine
calc.	Calculated
$CDCl_3$	Deuterated chloroform
CID	Collision-induced dissociation
d	Doublet
D	Aspartic acid
Da	Dalton
DBHA	Desthiobiotin-containing hydroxylamine probe
dd	Double distilled
DDA	Data-dependent acquisition
DCM	Dichloromethane
DDM	*n*-Dodecyl-β-D-Maltopyranoside
DIA	Data-independent acquisition

DIAD	Diisopropyl azodicarboxylate
DMSO	Dimethyl sulfoxide
DTB-PEG_3-N_3	Desthiobiotin-azide
DTT	Dithiothreitol
Dyn	Dynorphin A
E	Glutamic acid
E2	Estradiol
ECL	Enhanced chemiluminescence
EDTA	Ethylenediaminetetraacetic acid
eq.	Equivalent/s
ESI	Electrospray ionization
Et_2O	Diethyl ether
ETD	Electron-transfer dissociation
EtOAc	Ethyl acetate
FA	Formic acid
FDR	False discovery rate
G	Glycine
Gln	Glutamine
Glu	Glutamic acid
H	Histidine
HA-yne	Hydroxylamine alkyne probe
HEPES	4-(2-Hydroxyethyl)-1-piperazineethanesulfonic acid
HCD	Higher-energy collision induced dissociation
HK	Histidine kinase

HPLC	High-performance liquid chromatography
HR-MS	High-resolution mass spectrometry
HRP	Horseradish peroxidase
IAA	Iodoacetamide
IMAC	Immobilized metal affinity chromatography
IPMS	Intact protein mass spectrometry
IPTG	Isopropyl-β-D-1-thiogalactopyranoside
iRT	Indexed retention time
isoDTB	Isotopically labeled desthiotbiotin azide
isoTOP	Isotopic tandem orthogonal proteolysis
K	Lysine
LB	Lysogeny broth
LC	Liquid chromatography
LDAO	Lauryldimethylamine oxide
LFQ	Label-free quantification
LPS	Lipopolysaccharide
m	Multiplet
M	Methionine
m/z	Mass-to-charge ratio
Mb	Megabase
MeOH	Methanol
MOPS	3-(*N*-morpholino)propanesulfonic acid
MS	Mass spectrometry
MS1	MS1 scan, full MS scan

MS2	MS2 scan
MS/MS	Tandem mass spectrometry
NCE	Normalized collision energy
NMR	Nuclear magnetic resonance
NP-40	Nonyl phenoxypolyethoxylethanol
O	Pyrrolysine
OD	Optical density
P	Proline
pAsp	Phosphoaspartate
PBS	Phosphate buffered saline
PEG	Polyethylene glycol
PPh_3	Triphenylphosphine
PRM	Parallel reaction monitoring
PSM	Peptide spectrum match
PTM	Post-translational modification
R	Arginin
RP	Reverse-polarity
RR	Response regulator
RT	Room temperature
s	Singlet
S	Serine
SDS-PAGE	Sodium dodecyl sulfate-polyacrylamide gel electrophoresis
SRM	Selected reaction monitoring
t	Triplet

T	Threonine
TBTA	Tris((1-benzyl-4-triazolyl)methyl)amine
*t*BuOH	*tert*-Butyl alcohol
TCEP	Tris(2-carboxyethyl)phosphine
TCS	Two-component system
TEAB	Tetraethylammonium bromide
TEV	Tobacco etch virus
TFA	Trifluoroacetic acid
THF	Tetrahydrofuran
TLC	Thin-layer chromatography
TMT	Tandem mass tags
TT	Testosterone
U	Selenocysteine
V	Valine
WHO	World Health Organization
wt	Wild type
Y	Tyrosine

6 References

1. Fleming, A., Penicillin. Noble Lectures. **1945**. https://www.nobelprize.org/uploads/2018/06/fleming-lecture.pdf (accessed Sep 8, 2021).

2. Laxminarayan, R., Duse, A., Wattal, C., Zaidi, A. K., Wertheim, H. F., Sumpradit, N., Vlieghe, E., Hara, G. L., Gould, I. M., Goossens, H., Greko, C., So, A. D., Bigdeli, M., Tomson, G., Woodhouse, W., Ombaka, E., Peralta, A. Q., Qamar, F. N., Mir, F., Kariuki, S., Bhutta, Z. A., Coates, A., Bergstrom, R., Wright, G. D., Brown, E. D., Cars, O. Antibiotic resistance-the need for global solutions. *Lancet Infect. Dis.*, **2013**, *13*, 1057-1098.

3. Falagas, M. E., Bliziotis, I. A., Kasiakou, S. K., Samonis, G., Athanassopoulou, P., Michalopoulos, A. Outcome of infections due to pandrug-resistant (PDR) Gram-negative bacteria. *BMC Infect. Dis.*, **2005**, *5*, 24.

4. Falagas, M. E., Bliziotis, I. A. Pandrug-resistant Gram-negative bacteria: the dawn of the post-antibiotic era? *Int. J. Antimicrob. Agents*, **2007**, *29*, 630-636.

5. O'Neill, J. Antimicrobial Resistance: Tackling a Crisis for the Health and Wealth of Nations. *Review on Antimicrobial Resistance*, **2014**.

6. CDC. Antibiotic Resistance Threats in the United States, 2019. Atlanta, GA: U.S. Department of Health and Human Services, CDC; **2019**.

7. Nelson, R. E., Hatfield, K. M., Wolford, H., Samore, M. H., Scott, R. D., Reddy, S. C., Olubajo, B., Paul, P., Jernigan, J. A., Baggs, J. National Estimates of Healthcare Costs Associated With Multidrug-Resistant Bacterial Infections Among Hospitalized Patients in the United States. *Clin. Infect. Dis.*, **2021**, *72*, S17-S26.

8. Towse, A., Hoyle, C. K., Goodall, J., Hirsch, M., Mestre-Ferrandiz, J., Rex, J. H. Time for a change in how new antibiotics are reimbursed: Development of an insurance framework for funding new antibiotics based on a policy of risk mitigation. *Health Policy*, **2017**, *121*, 1025-1030.

9. Bundesministerium für Gesundheit, DART 2020 - Deutsche Antibiotika-Resistenzstrategie. **2021**. https://www.bundesgesundheitsministerium.de/themen/praevention/antibiotika-resistenzen/antibiotika-resistenzstrategie.html (accessed Oct 23, 2021).

10. Balasegaram, M., Piddock, L. J. V. The Global Antibiotic Research and Development Partnership (GARDP) Not-for-Profit Model of Antibiotic Development. *ACS Infect. Dis.*, **2020**, *6*, 1295-1298.

11. Outterson, K., Rex, J. H., Jinks, T., Jackson, P., Hallinan, J., Karp, S., Hung, D. T., Franceschi, F., Merkeley, T., Houchens, C., Dixon, D. M., Kurilla, M. G., Aurigemma, R., Larsen, J. Accelerating global innovation to address antibacterial resistance: introducing CARB-X. *Nat. Rev. Drug. Discov.*, **2016**, *15*, 589-590.

12. AMR action fund, New AMR Action Fund Worldwide launch – Press Release. **2020**. https://www.amractionfund.com/resources/new-amr-action-fund-worldwide-launch-press-release (accessed Oct 23, 2021).

13. Babic, N., Kovacic, F. Predicting drug targets by homology modelling of *Pseudomonas* aeruginosa proteins of unknown function. *PLoS One*, **2021**, *16*, e0258385.

14. Diggle, S. P., Whiteley, M. Microbe Profile: *Pseudomonas* aeruginosa: opportunistic pathogen and lab rat. *Microbiology (Reading)*, **2020**, *166*, 30-33.

15. Silby, M. W., Winstanley, C., Godfrey, S. A., Levy, S. B., Jackson, R. W. *Pseudomonas* genomes: diverse and adaptable. *FEMS Microbiol. Rev.*, **2011**, *35*, 652-680.

16. Lyczak, J. B., Cannon, C. L., Pier, G. B. Lung infections associated with cystic fibrosis. *Clin. Microbiol. Rev.*, **2002**, *15*, 194-222.

17. Bhagirath, A. Y., Li, Y., Somayajula, D., Dadashi, M., Badr, S., Duan, K. Cystic fibrosis lung environment and *Pseudomonas* aeruginosa infection. *BMC Pulm. Med.*, **2016**, *16*, 174.

18. Cole, S. J., Records, A. R., Orr, M. W., Linden, S. B., Lee, V. T. Catheter-Associated Urinary Tract Infection by *Pseudomonas* aeruginosa Is Mediated by Exopolysaccharide-Independent Biofilms. *Infect Immun*, **2014**, *82*, 2048-2058.

19. Gonzalez, M. R., Fleuchot, B., Lauciello, L., Jafari, P., Applegate, L. A., Raffoul, W., Que, Y. A., Perron, K. Effect of Human Burn Wound Exudate on *Pseudomonas* aeruginosa Virulence. *mSphere*, **2016**, *1*.

20. Tacconelli, E., Carrara, E., Savoldi, A., Harbarth, S., Mendelson, M., Monnet, D. L., Pulcini, C., Kahlmeter, G., Kluytmans, J., Carmeli, Y., Ouellette, M., Outterson, K., Patel, J., Cavaleri, M., Cox, E. M., Houchens, C. R., Grayson, M. L., Hansen, P., Singh, N., Theuretzbacher, U., Magrini, N., Group, W. H. O. P. P. L. W. Discovery, research, and development of new antibiotics: the WHO priority list of antibiotic-resistant bacteria and tuberculosis. *Lancet Infect. Dis.*, **2018**, *18*, 318-327.

21. Winstanley, C., O'Brien, S., Brockhurst, M. A. *Pseudomonas* aeruginosa Evolutionary Adaptation and Diversification in Cystic Fibrosis Chronic Lung Infections. *Trends Microbiol.*, **2016**, *24*, 327-337.

22. Jain, M., Ramirez, D., Seshadri, R., Cullina, J. F., Powers, C. A., Schulert, G. S., Bar-Meir, M., Sullivan, C. L., McColley, S. A., Hauser, A. R. Type III secretion phenotypes of *Pseudomonas* aeruginosa strains change during infection of individuals with cystic fibrosis. *J. Clin. Microbiol.*, **2004**, *42*, 5229-5237.

23. Winstanley, C., Fothergill, J. L. The role of quorum sensing in chronic cystic fibrosis *Pseudomonas* aeruginosa infections. *FEMS Microbiol. Lett.*, **2009**, *290*, 1-9.

24. Singh, P. K., Schaefer, A. L., Parsek, M. R., Moninger, T. O., Welsh, M. J., Greenberg, E. P. Quorum-sensing signals indicate that cystic fibrosis lungs are infected with bacterial biofilms. *Nature*, **2000**, *407*, 762-764.

25. Jimenez, P. N., Koch, G., Thompson, J. A., Xavier, K. B., Cool, R. H., Quax, W. J. The multiple signaling systems regulating virulence in *Pseudomonas* aeruginosa. *Microbiol. Mol. Biol. Rev.*, **2012**, *76*, 46-65.

26. Deziel, E., Comeau, Y., Villemur, R. Initiation of biofilm formation by *Pseudomonas* aeruginosa 57RP correlates with emergence of hyperpiliated and highly adherent phenotypic variants deficient in swimming, swarming, and twitching motilities. *J. Bacteriol.*, **2001**, *183*, 1195-1204.

27. Tyrrell, J., Harvey, B. J. Sexual dimorphism in the microbiology of the CF 'Gender Gap': Estrogen modulation of *Pseudomonas* aeruginosa virulence. *Steroids*, **2020**, *156*, 108575.

28. Pedersen, S. S., Hoiby, N., Espersen, F., Koch, C. Role of alginate in infection with mucoid *Pseudomonas* aeruginosa in cystic fibrosis. *Thorax*, **1992**, *47*, 6-13.

29. O'Sullivan, B. P., Freedman, S. D. Cystic fibrosis. *Lancet*, **2009**, *373*, 1891-1904.

30. Kopel, F. B. Gastrointestinal manifestations of cystic fibrosis. *Gastroenterology*, **1972**, *62*, 483-491.

31. Rossi, E., La Rosa, R., Bartell, J. A., Marvig, R. L., Haagensen, J. A. J., Sommer, L. M., Molin, S., Johansen, H. K. *Pseudomonas* aeruginosa adaptation and evolution in patients with cystic fibrosis. *Nat. Rev. Microbiol.*, **2021**, *19*, 331-342.

32. Burkhart, M., Nährlich, L., Zahlen, Daten & Fakten für Patienten & Angehörige. **2020**. https://www.muko.info/fileadmin/user_upload/angebote/qualitaetsmanagement/register/berichtsbaende/patientenberichtsband_2020.pdf (accessed Oct 28, 2021).

33. The Canadian Cystic Fibrosis Registry, 2019 Annual Data Report. **2019**. https://www.cysticfibrosis.ca/registry/2019AnnualDataReport.pdf (accessed Apr 18, 2021).

34. Rosenfeld, M., Davis, R., FitzSimmons, S., Pepe, M., Ramsey, B. Gender gap in cystic fibrosis mortality. *Am. J. Epidemiol.*, **1997**, *145*, 794-803.

35. Mooney, C., McKiernan, P. J., Raoof, R., Henshall, D. C., Linnane, B., McNally, P., Glasgow, A. M. A., Greene, C. M. Plasma microRNA levels in male and female children with cystic fibrosis. *Sci. Rep.*, **2020**, *10*, 1141.

36. Chotirmall, S. H., Smith, S. G., Gunaratnam, C., Cosgrove, S., Dimitrov, B. D., O'Neill, S. J., Harvey, B. J., Greene, C. M., McElvaney, N. G. Effect of estrogen on *pseudomonas* mucoidy and exacerbations in cystic fibrosis. *N. Engl. J. Med.*, **2012**, *366*, 1978-1986.

37. Sweezey, N. B., Ratjen, F. The cystic fibrosis gender gap: potential roles of estrogen. *Pediatr. Pulmonol.*, **2014**, *49*, 309-317.

38. Zaborina, O., Lepine, F., Xiao, G., Valuckaite, V., Chen, Y., Li, T., Ciancio, M., Zaborin, A., Petrof, E. O., Turner, J. R., Rahme, L. G., Chang, E., Alverdy, J. C. Dynorphin activates quorum sensing quinolone signaling in *Pseudomonas* aeruginosa. *PLoS Pathog.*, **2007**, *3*, e35.

39. Wright, M. H., Fetzer, C., Sieber, S. A. Chemical Probes Unravel an Antimicrobial Defense Response Triggered by Binding of the Human Opioid Dynorphin to a Bacterial Sensor Kinase. *J. Am. Chem. Soc.*, **2017**, *139*, 6152-6159.

40. Ganz, T. The role of antimicrobial peptides in innate immunity. *Integr. Comp. Biol.*, **2003**, *43*, 300-304.

41. Wang, G. Human antimicrobial peptides and proteins. *Pharmaceuticals (Basel)*, **2014**, *7*, 545-594.

42. Fernandez, L., Gooderham, W. J., Bains, M., McPhee, J. B., Wiegand, I., Hancock, R. E. Adaptive resistance to the "last hope" antibiotics polymyxin B and colistin in *Pseudomonas* aeruginosa is mediated by the novel two-component regulatory system ParR-ParS. *Antimicrob. Agents Chemother.*, **2010**, *54*, 3372-3382.

43. McPhee, J. B., Lewenza, S., Hancock, R. E. Cationic antimicrobial peptides activate a two-component regulatory system, PmrA-PmrB, that regulates resistance to polymyxin B and cationic antimicrobial peptides in *Pseudomonas* aeruginosa. *Mol. Microbiol.*, **2003**, *50*, 205-217.

44. Fernandez, L., Jenssen, H., Bains, M., Wiegand, I., Gooderham, W. J., Hancock, R. E. The two-component system CprRS senses cationic peptides and triggers adaptive

resistance in *Pseudomonas* aeruginosa independently of ParRS. *Antimicrob. Agents Chemother.*, **2012**, *56*, 6212-6222.

45. Gao, R., Stock, A. M. Biological insights from structures of two-component proteins. *Annu. Rev. Microbiol.*, **2009**, *63*, 133-154.

46. Santos, J. L., Shiozaki, K. Fungal histidine kinases. *Sci. STKE,* **2001**, *2001*, re1.

47. Galperin, M. Y., Makarova, K. S., Wolf, Y. I., Koonin, E. V. Phyletic Distribution and Lineage-Specific Domain Architectures of Archaeal Two-Component Signal Transduction Systems. *J. Bacteriol.*, **2018**, *200*.

48. Alvarez, A. F., Barba-Ostria, C., Silva-Jimenez, H., Georgellis, D. Organization and mode of action of two component system signaling circuits from the various kingdoms of life. *Environ. Microbiol.*, **2016**, *18*, 3210-3226.

49. Bhaya, D., Takahashi, A., Grossman, A. R. Light regulation of type IV pilus-dependent motility by chemosensor-like elements in Synechocystis PCC6803. *Proc. Natl. Acad. Sci. U. S. A.*, **2001**, *98*, 7540-7545.

50. Bassler, B. L., Wright, M., Silverman, M. R. Sequence and function of LuxO, a negative regulator of luminescence in Vibrio harveyi. *Mol. Microbiol.*, **1994**, *12*, 403-412.

51. Beier, D., Gross, R. Regulation of bacterial virulence by two-component systems. *Curr. Opin. Microbiol.*, **2006**, *9*, 143-152.

52. Mascher, T., Helmann, J. D., Unden, G. Stimulus perception in bacterial signal-transducing histidine kinases. *Microbiol. Mol. Biol. Rev.*, **2006**, *70*, 910-938.

53. Gao, R., Mack, T. R., Stock, A. M. Bacterial response regulators: versatile regulatory strategies from common domains. *Trends. Biochem. Sci.*, **2007**, *32*, 225-234.

54. Appleby, J. L., Parkinson, J. S., Bourret, R. B. Signal transduction via the multi-step phosphorelay: not necessarily a road less traveled. *Cell*, **1996**, *86*, 845-848.

55. Allihn, P. W. A., Hackl, M. W., Ludwig, C., Hacker, S. M., Sieber, S. A. A tailored phosphoaspartate probe unravels CprR as a response regulator in *Pseudomonas* aeruginosa interkingdom signaling. *Chem. Sci.*, **2021**, *12*, 4763-4770.

56. Galperin, M. Y. Diversity of structure and function of response regulator output domains. *Curr. Opin. Microbiol.*, **2010**, *13*, 150-159.

57. Dyer, C. M., Vartanian, A. S., Zhou, H., Dahlquist, F. W. A molecular mechanism of bacterial flagellar motor switching. *J. Mol. Biol*, **2009**, *388*, 71-84.

58. Chang, Y., Zhang, K., Carroll, B. L., Zhao, X., Charon, N. W., Norris, S. J., Motaleb, M. A., Li, C., Liu, J. Molecular mechanism for rotational switching of the bacterial flagellar motor. *Nat. Struct. Mol Biol.*, **2020**, *27*, 1041-1047.

59. West, A. H., Martinez-Hackert, E., Stock, A. M. Crystal structure of the catalytic domain of the chemotaxis receptor methylesterase, CheB. *J. Mol. Biol*, **1995**, *250*, 276-290.

60. Barends, T. R., Hartmann, E., Griese, J. J., Beitlich, T., Kirienko, N. V., Ryjenkov, D. A., Reinstein, J., Shoeman, R. L., Gomelsky, M., Schlichting, I. Structure and mechanism of a bacterial light-regulated cyclic nucleotide phosphodiesterase. *Nature*, **2009**, *459*, 1015-1018.

61. Burbulys, D., Trach, K. A., Hoch, J. A. Initiation of sporulation in *B. subtilis* is controlled by a multicomponent phosphorelay. *Cell*, **1991**, *64*, 545-552.

62. Grebe, T. W., Stock, J. B. The histidine protein kinase superfamily. *Adv. Microb. Physiol.*, **1999**, *41*, 139-227.

63. De Hertogh, B., Lantin, A. C., Baret, P. V., Goffeau, A. The archaeal P-type ATPases. *J. Bioenerg. Biomembr.*, **2004**, *36*, 135-142.

64. Pedersen, P. L., Carafoli, E. Ion Motive Atpases .1. Ubiquity, Properties, and Significance to Cell-Function. *Trends in Biochemical Sciences*, **1987**, *12*, 146-150.

65. Nishigaki, I., Chen, F. T., Hokin, L. E. Studies on the characterization of the sodium-potassium transport adenosine triphosphatase. XV. Direct chemical characterization of the acyl phosphate in the enzyme as an aspartyl beta-phosphate residue. *J. Biol. Chem.*, **1974**, *249*, 4911-4916.

66. Attwood, P. V., Besant, P. G., Piggott, M. J. Focus on phosphoaspartate and phosphoglutamate. *Amino Acids*, **2011**, *40*, 1035-1051.

67. Katchalsky, A., Paecht, M. Phosphate Anhydrides of Amino Acids. *Journal of the American Chemical Society*, **1954**, *76*, 6042-6044.

68. Koshland, D. E. Effect of Catalysts on the Hydrolysis of Acetyl Phosphate - Nucleophilic Displacement Mechanisms in Enzymatic Reactions. *J. Am. Chem. Soc.*, **1952**, *74*, 2286-2292.

69. Phillips, D. R., Fife, T. H. Acid-Catalyzed Hydrolysis of Acyl Phosphates. *J. Am. Chem. Soc.*, **1968**, *90*, 6803-6809.

70. Black, S., Wright, N. G. beta-Aspartokinase and beta-aspartyl phosphate. *J. Biol. Chem.*, **1955**, *213*, 27-38.

71. Degani, C., Boyer, P. D. A borohydride reduction method for characterization of the acyl phosphate linkage in proteins and its application to sarcoplasmic reticulum adenosine triphosphatase. *J. Biol. Chem.*, **1973**, *248*, 8222-8226.

72. Barth, A., Mantele, W. ATP-Induced phosphorylation of the sarcoplasmic reticulum Ca2+ ATPase: molecular interpretation of infrared difference spectra. *Biophys. J.*, **1998**, *75*, 538-544.

73. Lahiri, S. D., Zhang, G., Dunaway-Mariano, D., Allen, K. N. Caught in the act: the structure of phosphorylated beta-phosphoglucomutase from Lactococcus lactis. *Biochemistry*, **2002**, *41*, 8351-8359.

74. Wemmer, D. E., Kern, D. Beryllofluoride binding mimics phosphorylation of aspartate in response regulators. *J. Bacteriol.*, **2005**, *187*, 8229-8230.

75. Sourjik, V., Schmitt, R. Phosphotransfer between CheA, CheY1, and CheY2 in the chemotaxis signal transduction chain of Rhizobium meliloti. *Biochemistry*, **1998**, *37*, 2327-2335.

76. Lukat, G. S., McCleary, W. R., Stock, A. M., Stock, J. B. Phosphorylation of bacterial response regulator proteins by low molecular weight phospho-donors. *Proc. Natl. Acad. Sci. U. S. A.*, **1992**, *89*, 718-722.

77. Thingholm, T. E., Larsen, M. R. Phosphopeptide Enrichment by Immobilized Metal Affinity Chromatography. *Methods Mol. Biol.*, **2016**, *1355*, 123-133.

78. Lipmann, F., Tuttle, L. C. A Specific Micromethod for the Determination of Acyl Phosphates. *J. Biol. Chem.*, **1945**, *159*, 21-28.

79. Chang, J. W., Montgomery, J. E., Lee, G., Moellering, R. E. Chemoproteomic Profiling of Phosphoaspartate Modifications in Prokaryotes. *Angew. Chem. Int. Ed.*, **2018**, *57*, 15712-15716.

80. Evans, M. J., Cravatt, B. F. Mechanism-based profiling of enzyme families. *Chem. Rev.*, **2006**, *106*, 3279-3301.

81. Liu, Y., Patricelli, M. P., Cravatt, B. F. Activity-based protein profiling: the serine hydrolases. *Proc. Natl. Acad. Sci. U. S. A.*, **1999**, *96*, 14694-14699.

82. Jessani, N., Liu, Y., Humphrey, M., Cravatt, B. F. Enzyme activity profiles of the secreted and membrane proteome that depict cancer cell invasiveness. *Proc. Natl. Acad. Sci. U. S. A.*, **2002**, *99*, 10335-10340.

83. Speers, A. E., Adam, G. C., Cravatt, B. F. Activity-based protein profiling in vivo using a copper(I)-catalyzed azide-alkyne [3+2] cycloaddition. *Journal of the American Chemical Society*, **2003**, *125*, 4686-4687.

84. Greenbaum, D., Medzihradszky, K. F., Burlingame, A., Bogyo, M. Epoxide electrophiles as activity-dependent cysteine protease profiling and discovery tools. *Chem Biol*, **2000**, *7*, 569-581.

85. Greenbaum, D., Baruch, A., Hayrapetian, L., Darula, Z., Burlingame, A., Medzihradszky, K. F., Bogyo, M. Chemical approaches for functionally probing the proteome. *Mol. Cell. Proteomics*, **2002**, *1*, 60-68.

86. Matthews, M. L., He, L., Horning, B. D., Olson, E. J., Correia, B. E., Yates, J. R., 3rd, Dawson, P. E., Cravatt, B. F. Chemoproteomic profiling and discovery of protein electrophiles in human cells. *Nat. Chem.*, **2017**, *9*, 234-243.

87. Kolb, H. C., Finn, M. G., Sharpless, K. B. Click Chemistry: Diverse Chemical Function from a Few Good Reactions. *Angew. Chem. Int. Ed.*, **2001**, *40*, 2004-2021.

88. Rostovtsev, V. V., Green, L. G., Fokin, V. V., Sharpless, K. B. A stepwise huisgen cycloaddition process: copper(I)-catalyzed regioselective "ligation" of azides and terminal alkynes. *Angew. Chem. Int. Ed.*, **2002**, *41*, 2596-2599.

89. Ma, N., Zhang, Z. M., Lee, J. S., Cheng, K., Lin, L., Zhang, D. M., Hao, P., Ding, K., Ye, W. C., Li, Z. Affinity-Based Protein Profiling Reveals Cellular Targets of Photoreactive Anticancer Inhibitors. *ACS Chem. Biol.*, **2019**, *14*, 2546-2552.

90. Hofmann, K., Kiso, Y. An approach to the targeted attachment of peptides and proteins to solid supports. *Proc. Natl. Acad. Sci. U. S. A.*, **1976**, *73*, 3516-3518.

91. Bogdanov, B., Smith, R. D. Proteomics by FTICR mass spectrometry: top down and bottom up. *Mass Spectrom. Rev.*, **2005**, *24*, 168-200.

92. Lakemeyer, M., Bertosin, E., Moller, F., Balogh, D., Strasser, R., Dietz, H., Sieber, S. A. Tailored Peptide Phenyl Esters Block ClpXP Proteolysis by an Unusual Breakdown into a Heptamer-Hexamer Assembly. *Angew. Chem. Int. Ed.*, **2019**, *58*, 7127-7132.

93. Catherman, A. D., Skinner, O. S., Kelleher, N. L. Top Down proteomics: facts and perspectives. *Biochem. Biophys. Res. Commun.*, **2014**, *445*, 683-693.

94. Melby, J. A., Roberts, D. S., Larson, E. J., Brown, K. A., Bayne, E. F., Jin, S., Ge, Y. Novel Strategies to Address the Challenges in Top-Down Proteomics. *J. Am. Soc. Mass. Spectrom.*, **2021**, *32*, 1278-1294.

95. Eng, J. K., McCormack, A. L., Yates, J. R. An approach to correlate tandem mass spectral data of peptides with amino acid sequences in a protein database. *J. Am. Soc. Mass. Spectrom.*, **1994**, *5*, 976-989.

96. Cox, J., Neuhauser, N., Michalski, A., Scheltema, R. A., Olsen, J. V., Mann, M. Andromeda: a peptide search engine integrated into the MaxQuant environment. *J. Proteome Res.*, **2011**, *10*, 1794-1805.

97. Cox, J., Mann, M. MaxQuant enables high peptide identification rates, individualized p.p.b.-range mass accuracies and proteome-wide protein quantification. *Nat. Biotechnol.*, **2008**, *26*, 1367-1372.

98. Kong, A. T., Leprevost, F. V., Avtonomov, D. M., Mellacheruvu, D., Nesvizhskii, A. I. MSFragger: ultrafast and comprehensive peptide identification in mass spectrometry-based proteomics. *Nat. Methods*, **2017**, *14*, 513-520.

99. Pappireddi, N., Martin, L., Wuhr, M. A Review on Quantitative Multiplexed Proteomics. *Chembiochem*, **2019**, *20*, 1210-1224.

100. Cox, J., Hein, M. Y., Luber, C. A., Paron, I., Nagaraj, N., Mann, M. Accurate proteome-wide label-free quantification by delayed normalization and maximal peptide ratio extraction, termed MaxLFQ. *Mol. Cell. Proteomics*, **2014**, *13*, 2513-2526.

101. Ong, S. E., Mann, M. A practical recipe for stable isotope labeling by amino acids in cell culture (SILAC). *Nat. Protoc.*, **2006**, *1*, 2650-2660.

102. Hsu, J. L., Huang, S. Y., Chow, N. H., Chen, S. H. Stable-isotope dimethyl labeling for quantitative proteomics. *Anal. Chem.*, **2003**, *75*, 6843-6852.

103. Thompson, A., Schafer, J., Kuhn, K., Kienle, S., Schwarz, J., Schmidt, G., Neumann, T., Johnstone, R., Mohammed, A. K., Hamon, C. Tandem mass tags: a novel quantification strategy for comparative analysis of complex protein mixtures by MS/MS. *Anal. Chem.*, **2003**, *75*, 1895-1904.

104. Wiese, S., Reidegeld, K. A., Meyer, H. E., Warscheid, B. Protein labeling by iTRAQ: a new tool for quantitative mass spectrometry in proteome research. *Proteomics*, **2007**, *7*, 340-350.

105. Li, J., Cai, Z., Bomgarden, R. D., Pike, I., Kuhn, K., Rogers, J. C., Roberts, T. M., Gygi, S. P., Paulo, J. A. TMTpro-18plex: The Expanded and Complete Set of TMTpro Reagents for Sample Multiplexing. *J. Proteome Res.*, **2021**, *20*, 2964-2972.

106. Ting, L., Rad, R., Gygi, S. P., Haas, W. MS3 eliminates ratio distortion in isobaric multiplexed quantitative proteomics. *Nat. Methods*, **2011**, *8*, 937-940.

107. Savitski, M. M., Nielsen, M. L., Zubarev, R. A. ModifiComb, a new proteomic tool for mapping substoichiometric post-translational modifications, finding novel types of modifications, and fingerprinting complex protein mixtures. *Mol. Cell. Proteomics*, **2006**, *5*, 935-948.

108. Hirsch, J. D., Eslamizar, L., Filanoski, B. J., Malekzadeh, N., Haugland, R. P., Beechem, J. M., Haugland, R. P. Easily reversible desthiobiotin binding to streptavidin, avidin, and other biotin-binding proteins: uses for protein labeling, detection, and isolation. *Anal. Biochem.*, **2002**, *308*, 343-357.

109. Weerapana, E., Speers, A. E., Cravatt, B. F. Tandem orthogonal proteolysis-activity-based protein profiling (TOP-ABPP)--a general method for mapping sites of probe modification in proteomes. *Nat. Protoc.*, **2007**, *2*, 1414-1425.

110. Zanon, P. R. A., Lewald, L., Hacker, S. M. Isotopically Labeled Desthiobiotin Azide (isoDTB) Tags Enable Global Profiling of the Bacterial Cysteinome. *Angew. Chem. Int. Ed.*, **2020**, *59*, 2829-2836.

111. Patricelli, M. P., Nomanbhoy, T. K., Wu, J., Brown, H., Zhou, D., Zhang, J., Jagannathan, S., Aban, A., Okerberg, E., Herring, C., Nordin, B., Weissig, H., Yang, Q., Lee, J. D., Gray, N. S., Kozarich, J. W. In situ kinase profiling reveals functionally relevant properties of native kinases. *Chem Biol*, **2011**, *18*, 699-710.

112. Hogrebe, A., von Stechow, L., Bekker-Jensen, D. B., Weinert, B. T., Kelstrup, C. D., Olsen, J. V. Benchmarking common quantification strategies for large-scale phosphoproteomics. *Nat. Commun.*, **2018**, *9*, 1045.

113. Weerapana, E., Wang, C., Simon, G. M., Richter, F., Khare, S., Dillon, M. B., Bachovchin, D. A., Mowen, K., Baker, D., Cravatt, B. F. Quantitative reactivity profiling predicts functional cysteines in proteomes. *Nature*, **2010**, *468*, 790-795.

114. Jaffe, J. D., Keshishian, H., Chang, B., Addona, T. A., Gillette, M. A., Carr, S. A. Accurate inclusion mass screening: a bridge from unbiased discovery to targeted assay development for biomarker verification. *Mol. Cell. Proteomics*, **2008**, *7*, 1952-1962.

115. Smith, R. D. Mass spectrometry in biomarker applications: from untargeted discovery to targeted verification, and implications for platform convergence and clinical application. *Clin. Chem.*, **2012**, *58*, 528-530.

116. Nguyen, C. D. L., Malchow, S., Reich, S., Steltgens, S., Shuvaev, K. V., Loroch, S., Lorenz, C., Sickmann, A., Knobbe-Thomsen, C. B., Tews, B., Medenbach, J., Ahrends, R. A sensitive and simple targeted proteomics approach to quantify transcription factor and membrane proteins of the unfolded protein response pathway in glioblastoma cells. *Sci. Rep.*, **2019**, *9*, 8836.

117. Stahl, D. C., Swiderek, K. M., Davis, M. T., Lee, T. D. Data-controlled automation of liquid chromatography/tandem mass spectrometry analysis of peptide mixtures. *J. Am. Soc. Mass. Spectrom.*, **1996**, *7*, 532-540.

118. Chambers, A. G., Sweet, S. M. M., Chain, D., Kim, Y. J. Global Extraction from Parallel Reaction Monitoring to Quantify Background Peptides for Improved Normalization and Quality Control in Targeted Proteomics. *Anal. Chem.*, **2021**, *93*, 13434-13440.

119. VanBogelen, R. A., Olson, E. R., Wanner, B. L., Neidhardt, F. C. Global analysis of proteins synthesized during phosphorus restriction in Escherichia coli. *J. Bacteriol.*, **1996**, *178*, 4344-4366.

120. Hsieh, Y. J., Wanner, B. L. Global regulation by the seven-component Pi signaling system. *Curr. Opin. Microbiol.*, **2010**, *13*, 198-203.

121. Creager-Allen, R. L., Silversmith, R. E., Bourret, R. B. A Link between Dimerization and Autophosphorylation of the Response Regulator PhoB. *J. Biol. Chem.*, **2013**, *288*.

122. Makino, K., Amemura, M., Kim, S. K., Nakata, A., Shinagawa, H. Mechanism of Transcriptional Activation of the Phosphate Regulon in Escherichia-Coli. In *Phosphate in Microorganisms: Cellular and Molecular Biology*, eds. A. Torriani-Gorini, E. Yagil and S. Silver. Washington DC, **1994**, pp. 5-12.

123. McCleary, W. R. The activation of PhoB by acetylphosphate. *Mol. Microbiol.*, **1996**, *20*, 1155-1163.

124. Chen, Y., Cong, Y., Quan, B., Lan, T., Chu, X., Ye, Z., Hou, X., Wang, C. Chemoproteomic profiling of targets of lipid-derived electrophiles by bioorthogonal aminooxy probe. *Redox Biol.*, **2017**, *12*, 712-718.

125. Ortega, D. R., Fleetwood, A. D., Krell, T., Harwood, C. S., Jensen, G. J., Zhulin, I. B. Assigning chemoreceptors to chemosensory pathways in *Pseudomonas* aeruginosa. *Proc. Natl. Acad. Sci. U. S. A.*, **2017**, *114*, 12809-12814.

126. Zhang, Y., Wang, J., Ding, M., Yu, Y. Site-specific characterization of the Asp- and Glu-ADP-ribosylated proteome. *Nat. Methods*, **2013**, *10*, 981-984.

127. Chio, T. I., Demestichas, B. R., Brems, B. M., Bane, S. L., Tumey, L. N. Expanding the Versatility of Microbial Transglutaminase Using alpha-Effect Nucleophiles as Noncanonical Substrates. *Angew. Chem. Int. Ed.*, **2020**, *59*, 13814-13820.

128. Tyanova, S., Temu, T., Sinitcyn, P., Carlson, A., Hein, M. Y., Geiger, T., Mann, M., Cox, J. The Perseus computational platform for comprehensive analysis of (prote)omics data. *Nat. Methods*, **2016**, *13*, 731-740.

129. Ishihama, Y., Schmidt, T., Rappsilber, J., Mann, M., Hartl, F. U., Kerner, M. J., Frishman, D. Protein abundance profiling of the Escherichia coli cytosol. *BMC Genomics*, **2008**, *9*, 102.

130. Wakankar, A. A., Borchardt, R. T. Formulation considerations for proteins susceptible to asparagine deamidation and aspartate isomerization. *J. Pharm. Sci.*, **2006**, *95*, 2321-2336.

131. Rabalski, A. J., Bogdan, A. R., Baranczak, A. Evaluation of Chemically-Cleavable Linkers for Quantitative Mapping of Small Molecule-Cysteinome Reactivity. *ACS Chem. Biol.*, **2019**, *14*, 1940-1950.

132. The UniProt Consortium. UniProt: a worldwide hub of protein knowledge. *Nucleic Acids Res.*, **2019**, *47*, D506-D515.

133. Wang, M., Herrmann, C. J., Simonovic, M., Szklarczyk, D., von Mering, C. Version 4.0 of PaxDb: Protein abundance data, integrated across model organisms, tissues, and cell-lines. *Proteomics*, **2015**, *15*, 3163-3168.

134. Gao, R., Bouillet, S., Stock, A. M. Structural Basis of Response Regulator Function. *Annu. Rev. Microbiol.*, **2019**, *73*, 175-197.

135. O'Shea, J. P., Chou, M. F., Quader, S. A., Ryan, J. K., Church, G. M., Schwartz, D. pLogo: a probabilistic approach to visualizing sequence motifs. *Nat. Methods*, **2013**, *10*, 1211-1212.

136. Hestrin, S. The reaction of acetylcholine and other carboxylic acid derivatives with hydroxylamine, and its analytical application. *J. Biol. Chem.*, **1949**, *180*, 249-261.

137. Jencks, W. P., Gilchrist, M. Reaction of Hydroxylamine with Amides . Kinetic Evidence for Existence of Tetrahedral Addition Intermediate. *J. Am. Chem. Soc.*, **1964**, *86*, 5616-5620.

138. Meister, A., Levintow, L., Greenfield, R. E., Abendschein, P. A. Hydrolysis and transfer reactions catalyzed by omega-amidase preparations. *J. Biol. Chem.*, **1955**, *215*, 441-460.

139. Abdella, P. M., Smith, P. K., Royer, G. P. A new cleavable reagent for cross-linking and reversible immobilization of proteins. *Biochem. Biophys. Res. Commun.*, **1979**, *87*, 734-742.

140. Geiger, T., Clarke, S. Deamidation, isomerization, and racemization at asparaginyl and aspartyl residues in peptides. Succinimide-linked reactions that contribute to protein degradation. *J. Biol. Chem.*, **1987**, *262*, 785-794.

141. Rollins, C., Dahlquist, F. W. The methyl-accepting chemotaxis proteins of E. coli: a repellent-stimulated, covalent modification, distinct from methylation. *Cell*, **1981**, *25*, 333-340.

142. Robinson, A. B., Rudd, C. J. Deamidation of glutaminyl and asparaginyl residues in peptides and proteins. *Curr. Top. Cell. Regul.*, **1974**, *8*, 247-295.

143. Zhu, J. X., Aswad, D. W. Selective cleavage of isoaspartyl peptide bonds by hydroxylamine after methyltransferase priming. *Anal. Biochem.*, **2007**, *364*, 1-7.

144. Dincbas-Renqvist, V., Engstrom, A., Mora, L., Heurgue-Hamard, V., Buckingham, R., Ehrenberg, M. A post-translational modification in the GGQ motif of RF2 from Escherichia coli stimulates termination of translation. *EMBO J.*, **2000**, *19*, 6900-6907.

145. Klotz, A. V., Thomas, B. A. N5-Methylasparagine and Asparagine as Nucleophiles in Peptides - Main-Chain Vs Side-Chain Amide Cleavage. *Journal of Organic Chemistry*, **1993**, *58*, 6985-6989.

146. Wichmann, C., Meier, F., Virreira Winter, S., Brunner, A. D., Cox, J., Mann, M. MaxQuant.Live Enables Global Targeting of More Than 25,000 Peptides. *Mol. Cell. Proteomics*, **2019**, *18*, 982-994.

147. Hendriks, I. A., Akimov, V., Blagoev, B., Nielsen, M. L. MaxQuant.Live Enables Enhanced Selectivity and Identification of Peptides Modified by Endogenous SUMO and Ubiquitin. *J. Proteome Res.*, **2021**, *20*, 2042-2055.

148. Venable, J. D., Dong, M. Q., Wohlschlegel, J., Dillin, A., Yates, J. R. Automated approach for quantitative analysis of complex peptide mixtures from tandem mass spectra. *Nat. Methods*, **2004**, *1*, 39-45.

149. Chapman, J. D., Goodlett, D. R., Masselon, C. D. Multiplexed and data-independent tandem mass spectrometry for global proteome profiling. *Mass Spectrom. Rev.*, **2014**, *33*, 452-470.

150. Bekker-Jensen, D. B., Bernhardt, O. M., Hogrebe, A., Martinez-Val, A., Verbeke, L., Gandhi, T., Kelstrup, C. D., Reiter, L., Olsen, J. V. Rapid and site-specific deep phosphoproteome profiling by data-independent acquisition without the need for spectral libraries. *Nat. Commun.*, **2020**, *11*, 787.

151. Mehta, D., Scandola, S., Uhrig, R. G., Library-free BoxCarDIA solves the missing value problem in label-free quantitative proteomics. *bioRxiv*, **2021**. doi: 10.1101/2020.11.07.372276.

152. Diedrich, J. K., Pinto, A. F., Yates, J. R., 3rd. Energy dependence of HCD on peptide fragmentation: stepped collisional energy finds the sweet spot. *J. Am. Soc. Mass. Spectrom.*, **2013**, *24*, 1690-1699.

153. Wiesner, J., Premsler, T., Sickmann, A. Application of electron transfer dissociation (ETD) for the analysis of posttranslational modifications. *Proteomics*, **2008**, *8*, 4466-4483.

154. Kim, D. I., Cutler, J. A., Na, C. H., Reckel, S., Renuse, S., Madugundu, A. K., Tahir, R., Goldschmidt, H. L., Reddy, K. L., Huganir, R. L., Wu, X., Zachara, N. E., Hantschel, O., Pandey, A. BioSITe: A Method for Direct Detection and Quantitation of Site-Specific Biotinylation. *J. Proteome Res.*, **2018**, *17*, 759-769.

155. Renuse, S., Madugundu, A. K., Jung, J. H., Byeon, S. K., Goldschmidt, H. L., Tahir, R., Meyers, D., Kim, D. I., Cutler, J., Kim, K. P., Wu, X., Huganir, R. L., Pandey, A. Signature Fragment Ions of Biotinylated Peptides. *J. Am. Soc. Mass. Spectrom.*, **2020**, *31*, 394-404.

156. Yan, T., Palmer, A. B., Geiszler, D. J., Polasky, D. A., Armenta, E., Nesvizhskii, A. I., Backus, K. M., Enhancing Cysteine Chemoproteomic Coverage Through Systematic Assessment of Click Chemistry Product Fragmentation. *chemRxiv*, **2021**. doi: 10.33774/chemrxiv-2021-4b291.

157. MacLean, B., Tomazela, D. M., Shulman, N., Chambers, M., Finney, G. L., Frewen, B., Kern, R., Tabb, D. L., Liebler, D. C., MacCoss, M. J. Skyline: an open source document editor for creating and analyzing targeted proteomics experiments. *Bioinformatics*, **2010**, *26*, 966-968.

158. Rowland, S. S., Falkler, W. A., Jr., Bashirelahi, N. Identification of an estrogen-binding protein in *Pseudomonas* aeruginosa. *J. Steroid Biochem. Mol. Biol.*, **1992**, *42*, 721-727.

159. Vidaillac, C., Yong, V. F. L., Aschtgen, M. S., Qu, J., Yang, S., Xu, G., Seng, Z. J., Brown, A. C., Ali, M. K., Jaggi, T. K., Sankaran, J., Foo, Y. H., Righetti, F., Nedumaran, A. M., Mac Aogain, M., Roizman, D., Richard, J. A., Rogers, T. R., Toyofuku, M., Luo, D., Loh, E., Wohland, T., Czarny, B., Horvat, J. C., Hansbro, P. M., Yang, L., Li, L., Normark, S., Henriques Normark, B., Chotirmall, S. H. Sex Steroids Induce Membrane Stress Responses and Virulence Properties in *Pseudomonas* aeruginosa. *mBio*, **2020**, *11*.

160. Segall, J. E., Manson, M. D., Berg, H. C. Signal processing times in bacterial chemotaxis. *Nature*, **1982**, *296*, 855-857.

161. Pazy, Y., Wollish, A. C., Thomas, S. A., Miller, P. J., Collins, E. J., Bourret, R. B., Silversmith, R. E. Matching biochemical reaction kinetics to the timescales of life: structural determinants that influence the autodephosphorylation rate of response regulator proteins. *J. Mol. Biol*, **2009**, *392*, 1205-1220.

162. Thomas, S. A., Brewster, J. A., Bourret, R. B. Two variable active site residues modulate response regulator phosphoryl group stability. *Mol. Microbiol.*, **2008**, *69*, 453-465.

163. Stokes, D. L., Green, N. M. Structure and function of the calcium pump. *Annu. Rev. Biophys. Biomol. Struct.*, **2003**, *32*, 445-468.

164. Lutsenko, S., Kaplan, J. H. Organization of P-type ATPases: significance of structural diversity. *Biochemistry*, **1995**, *34*, 15607-15613.

165. Tone, T., Nakayama, K., Takatsu, H., Shin, H. W. ATPase reaction cycle of P4-ATPases affects their transport from the endoplasmic reticulum. *Febs Letters*, **2020**, *594*, 412-423.

166. Lapek, J. D., Jr., Tombline, G., Kellersberger, K. A., Friedman, M. R., Friedman, A. E. Evidence of histidine and aspartic acid phosphorylation in human prostate cancer cells. *Naunyn Schmiedebergs Arch Pharmacol*, **2015**, *388*, 161-173.

167. Morgan, R. K., Cohen, M. S. A Clickable Aminooxy Probe for Monitoring Cellular ADP-Ribosylation. *ACS Chem. Biol.*, **2015**, *10*, 1778-1784.

168. Xu, X., Liu, Y., Park, C. M. Rhodium(III)-catalyzed intramolecular annulation through C-H activation: total synthesis of (+/-)-antofine, (+/-)-septicine, (+/-)-tylophorine, and rosettacin. *Angew. Chem. Int. Ed.*, **2012**, *51*, 9372-9376.

169. Bach, K., Beerkens, B. L. H., Zanon, P. R. A., Hacker, S. M. Light-Activatable, 2,5-Disubstituted Tetrazoles for the Proteome-wide Profiling of Aspartates and Glutamates in Living Bacteria. *ACS. Cent. Sci.*, **2020**, *6*, 546-554.

170. Sharma, V., Eckels, J., Schilling, B., Ludwig, C., Jaffe, J. D., MacCoss, M. J., MacLean, B. Panorama Public: A Public Repository for Quantitative Data Sets Processed in Skyline. *Mol. Cell. Proteomics*, **2018**, *17*, 1239-1244.

7 Appendix

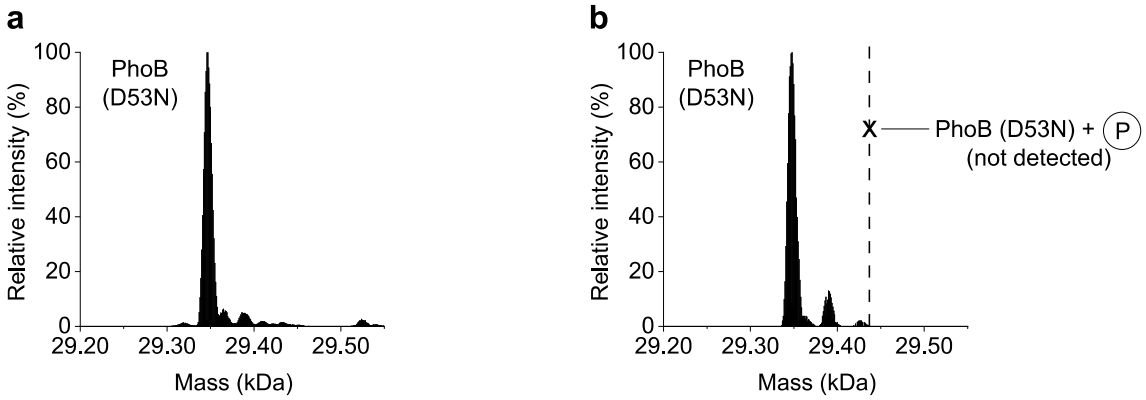

Figure S 1: Verification of site-specific *in vitro* phosphorylation of wt *E. coli* PhoB at D53. IPMS analysis of PhoB D53N mutant before (a) and after (b) acetyl phosphate (AcP) treatment. No phosphorylation was observed for PhoB D53N. Adapted from Allihn *et al.*[55]

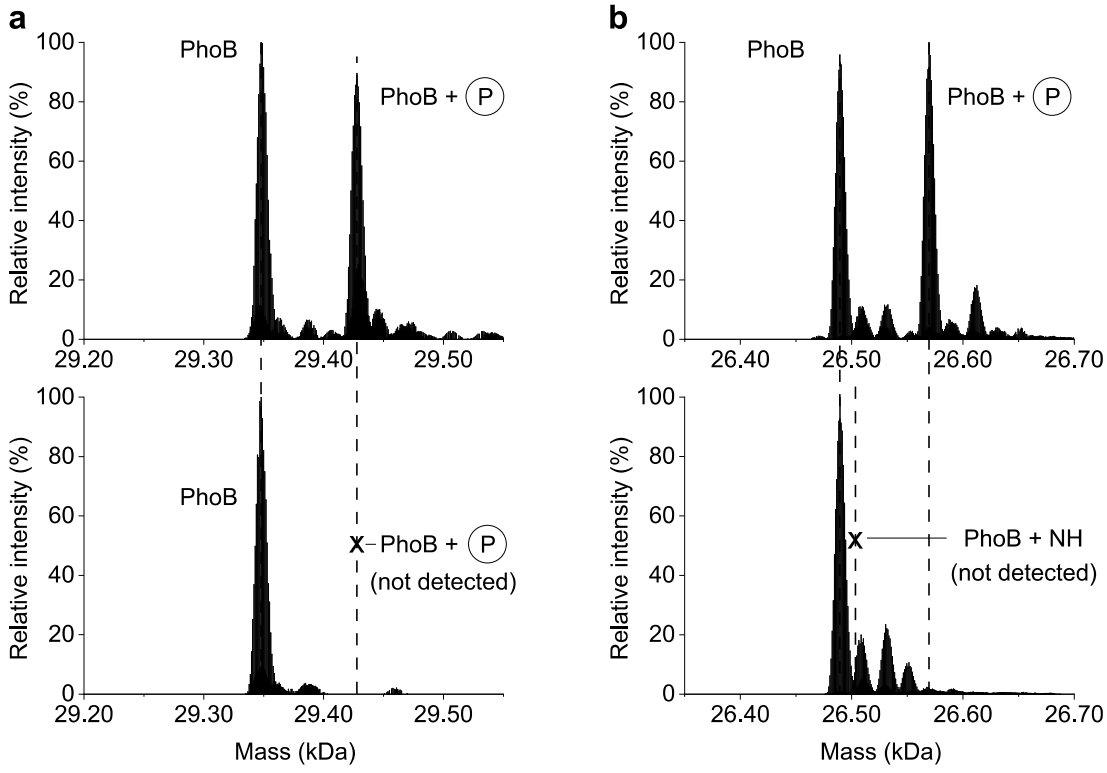

Figure S 2: Hydrolytic cleavage of phosphorylated wt PhoB without and with hydroxylamine treatment at pH = 7. IPMS analysis of phosphorylated wt PhoB incubated without (a) and with 500 mM hydroxylamine (b). Adapted from Allihn *et al.*[55]

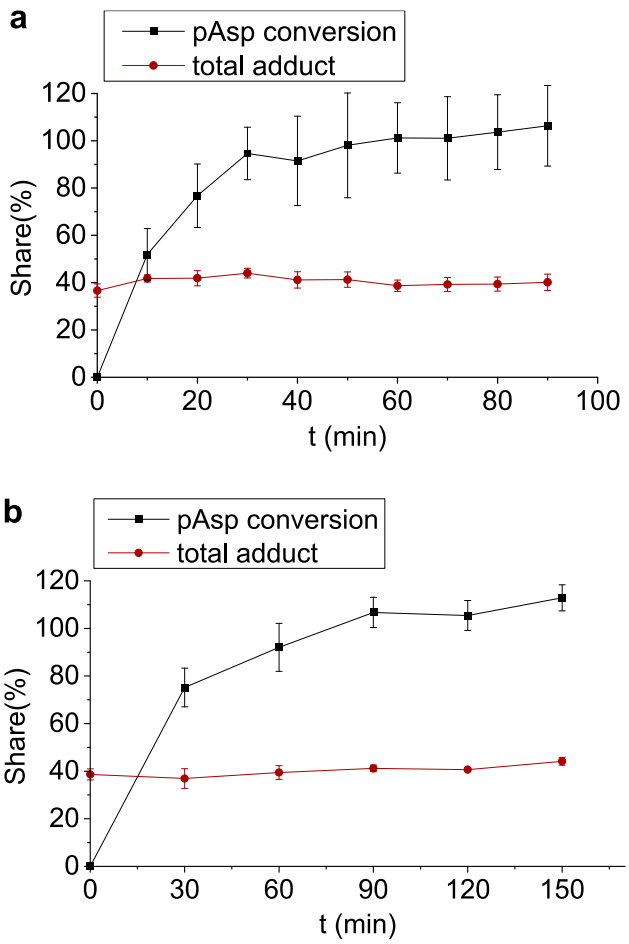

Figure S 3: Reaction kinetics of the conversion of phosphorylated wt PhoB with 500 mM hydroxylamine (a) or HA-yne (b) at pH = 4. Reused from Allihn *et al.*[55]

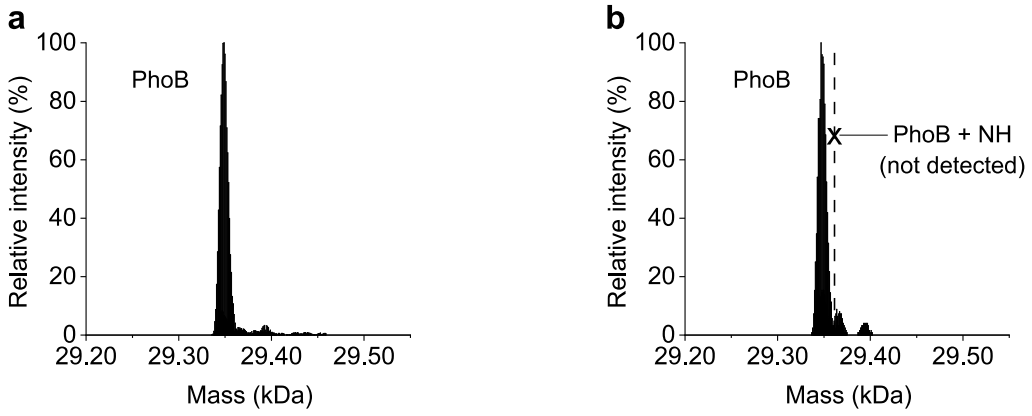

Figure S 4: Control experiment for the exclusion of hydroxylamine conversion with unphosphorylated wt PhoB. IPMS analysis of unphosphorylated wt PhoB before (a) and after (b) treatment with 500 mM Hydroxylamine. No formation of *N*-hydroxyasparagine was observed. Adapted from Allihn *et al.*[55]

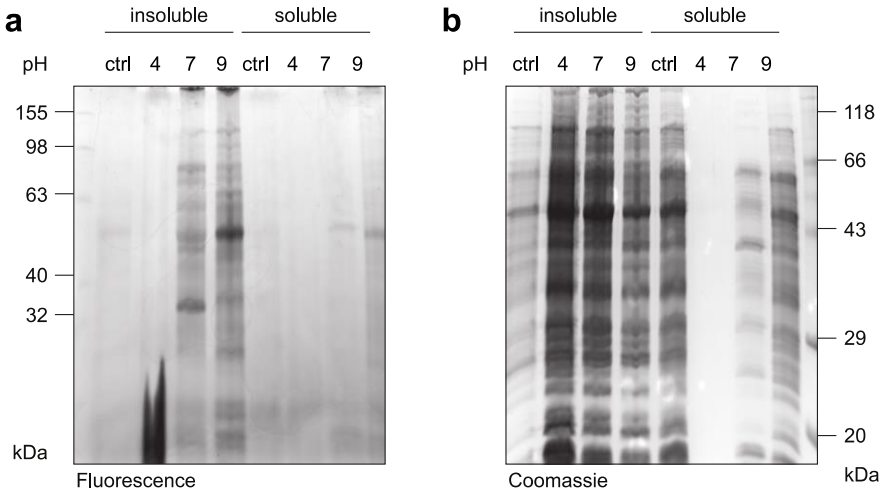

Figure S 5: pH-dependent labeling optimization. Exponentially growing *B. subtilis* were lysed in the presence of 500 mM HA-yne at different pH-values and labeled proteins were clicked to rhodamine azide (ctrl: no HA-yne, 20 mM HEPES, pH = 7). SDS-PAGE analysis was performed by in-gel fluorescence scanning (a) and staining using Coomassie Brilliant Blue (b). The labeling pattern and protein solubility turned out to be strongly pH dependent**.** Reused from Allihn *et al.*[55]

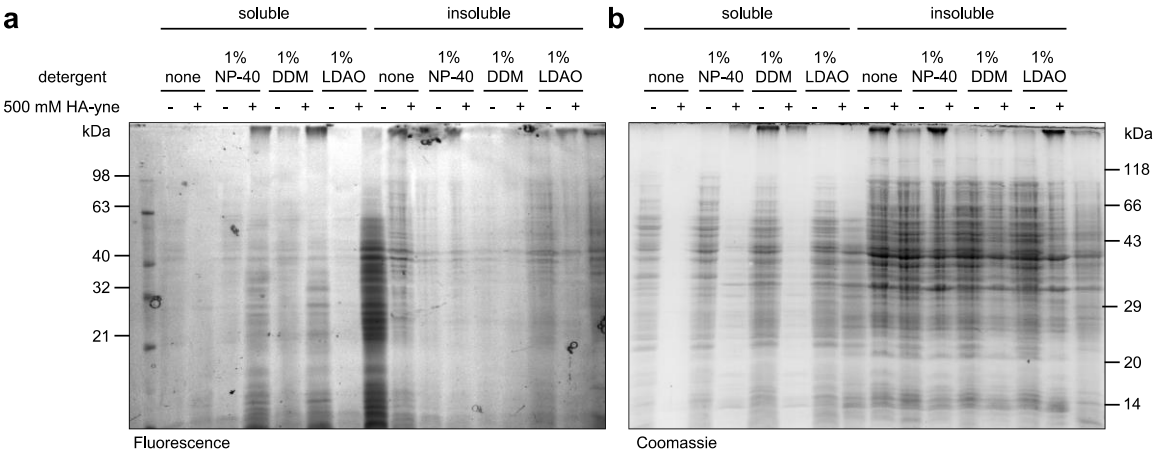

Figure S 6: Optimization of labeling conditions by evaluation of different detergents. Exponentially growing *B. subtilis* were lysed in the presence of 500 mM HA-yne at pH = 4 in labeling buffer containing different detergents. Labeled proteins were clicked to rhodamine azide and SDS-PAGE analysis was performed by in-gel fluorescence scanning (a) and staining using Coomassie Brilliant Blue (b). Addition of 1% (w/v) LDAO revealed the most efficient solubilization of the proteome and the most pronounced labeling pattern. Reused from Allihn *et al.*[55]

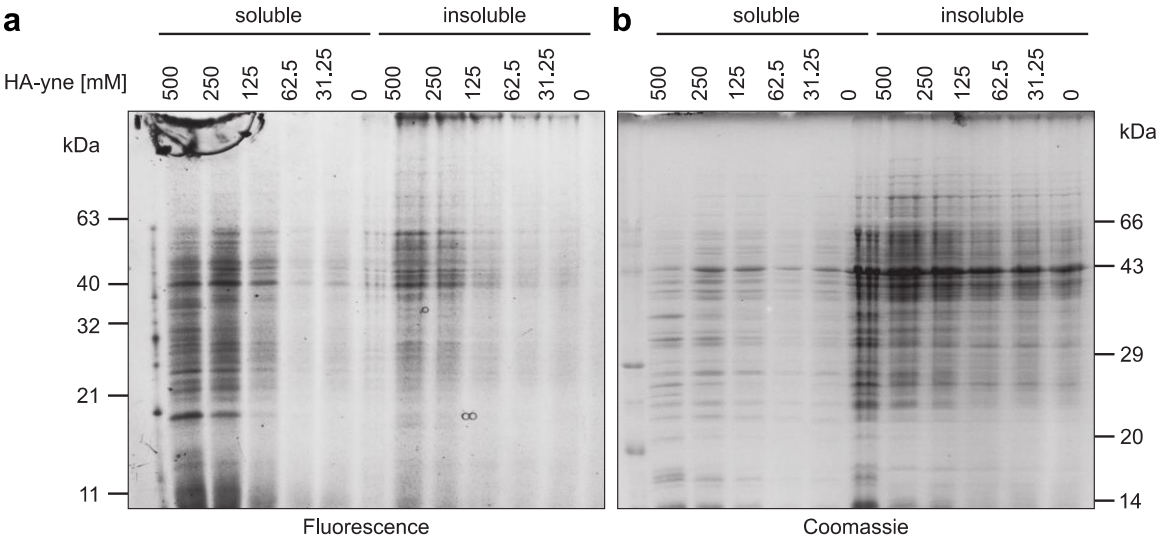

Figure S 7: Dose-dependent labeling optimization. Exponentially growing *B. subtilis* were lysed in the presence of different concentrations of HA-yne at pH = 4 in HEPES buffer containing 1% (w/v) LDAO. Labeled proteins were clicked to rhodamine azide and SDS-PAGE analysis was performed by in-gel fluorescence scanning (a) and staining using Coomassie Brilliant Blue (b). A probe concentration of 125 mM was chosen for RP-ABPP experiments. Reused from Allihn *et al.*[55]

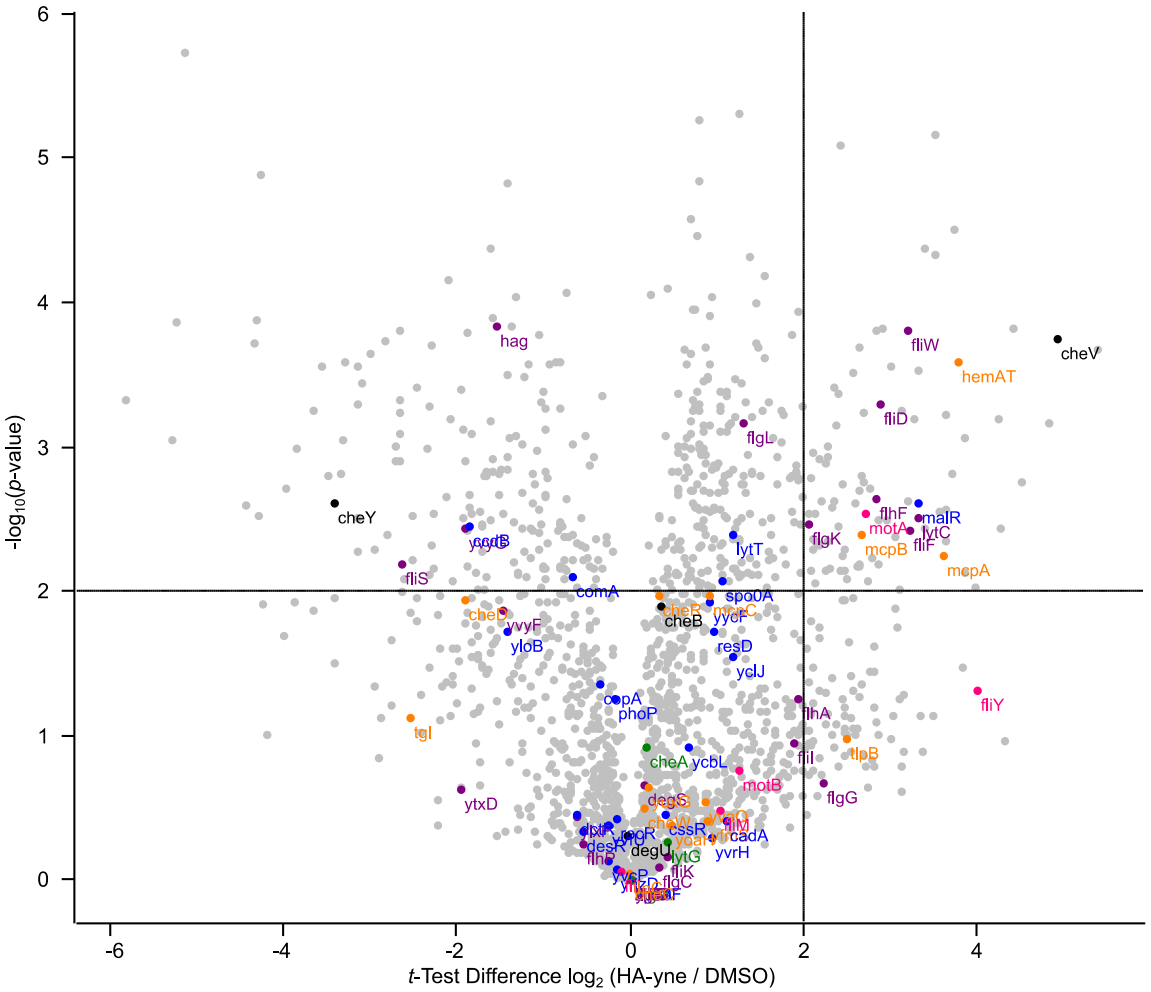

Figure S 8: Target identification using HA-yne in *B. subtilis*. The scatter plot illustrates the statistical significance of protein enrichment as function of the logarithmic ratio of protein enrichment from HA-yne treated and control cells (DMSO). Color codes for UniProt annotations: blue: pAsp, orange: black: pAsp and chemotaxis, orange: methyl-accepting chemotaxis, green: pHis, purple: flagellum.

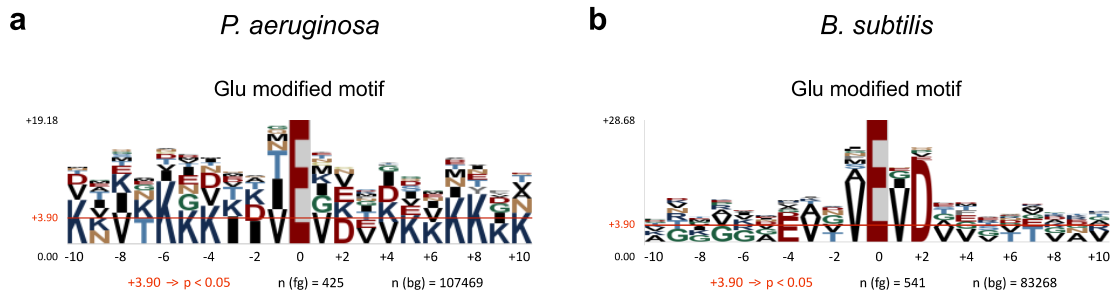

Figure S 9: HA-yne-modified sequence motifs of Glu in *P. aeruginosa* and *B. subtilis* using pLogo.[135] Residues ranging from positions -10 to +10 next to the modification site were included in the analysis. pAsp annotated and HA-yne-modified sequences (fg) were compared with the complete proteomic background (bg) in *P. aeruginosa* or *B. subtilis* from the UniProt database. Red horizontal bars indicate the Bonferroni-corrected statistical significance (p = 0.05). Adapted from Allihn *et al.*[55]

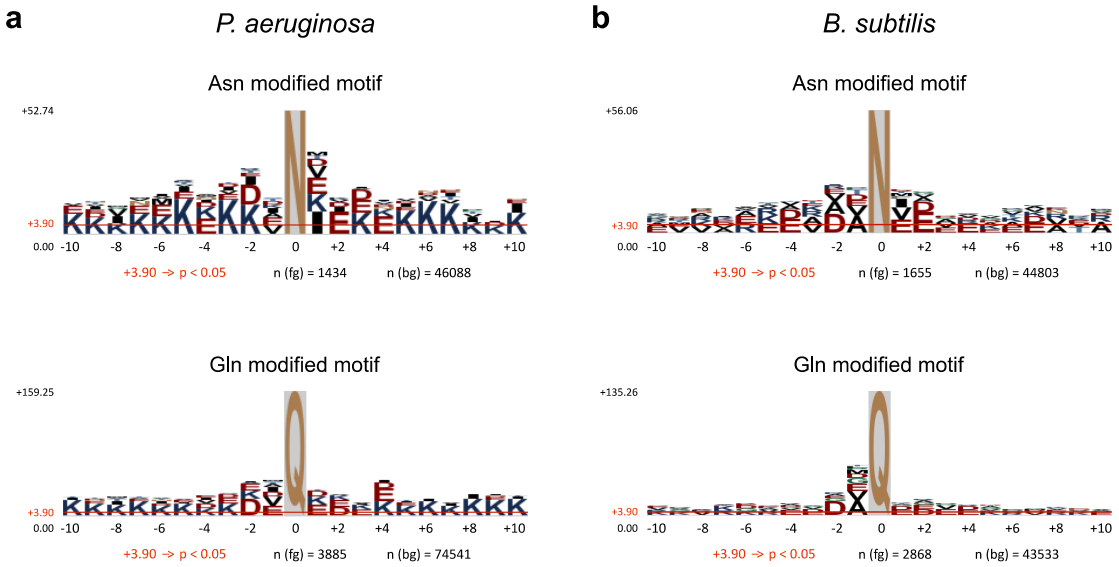

Figure S 10: HA-yne-modified sequence motifs of Asn and Gln in *P. aeruginosa* and *B. subtilis* using pLogo.[135] Residues ranging from positions -10 to +10 next to the modification site were included in the analysis. pAsp annotated and HA-yne-modified sequences (fg) were compared with the complete proteomic background (bg) in *P. aeruginosa* or *B. subtilis* from the UniProt database. Red horizontal bars indicate the Bonferroni-corrected statistical significance (p = 0.05). Adapted from Allihn *et al.*[55]

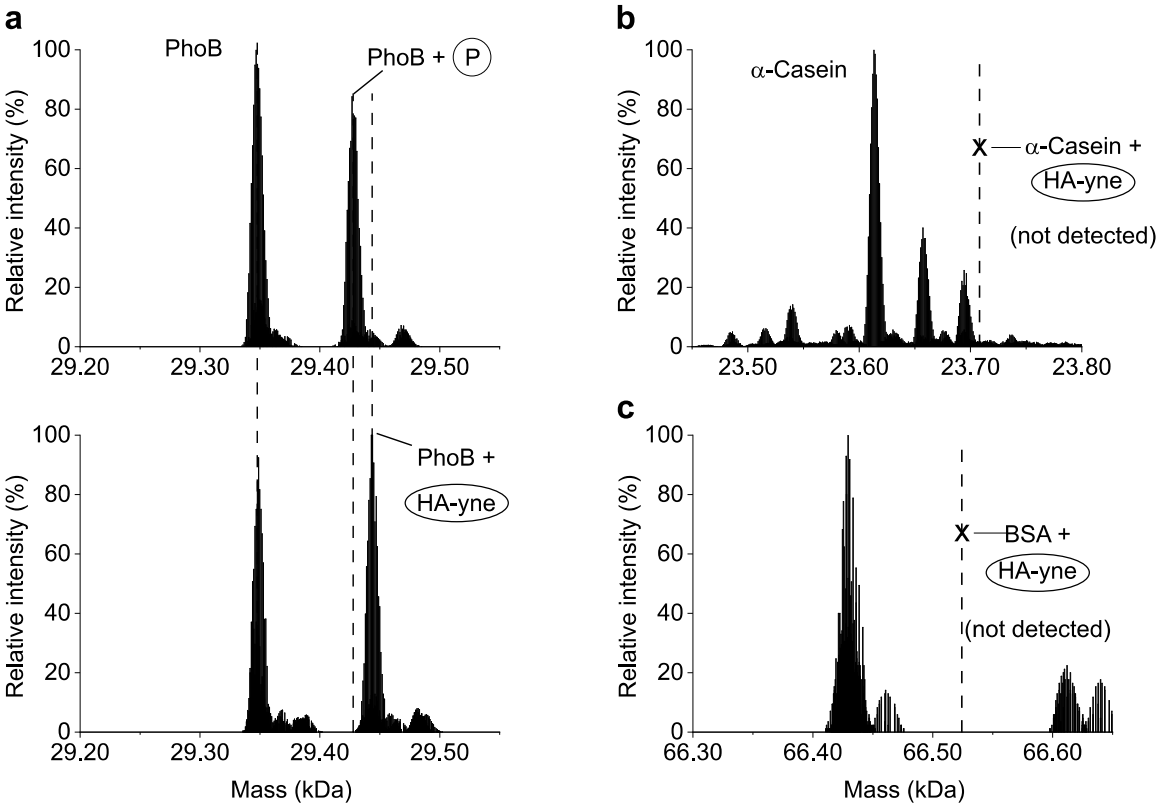

Figure S 11: Assessment of background probe reactivity by IPMS analysis of phosphorylated PhoB, α-Casein and BSA with 125 mM HA-yne at pH = 4. (a) PhoB was in vitro phosphorylated with acetyl phosphate and converted with HA yne. α-Casein (b) and BSA (c) were treated with HA-yne without prior phosphorylation. No background reactions could be observed under the applied conditions. Adapted from Allihn *et al.*[55]

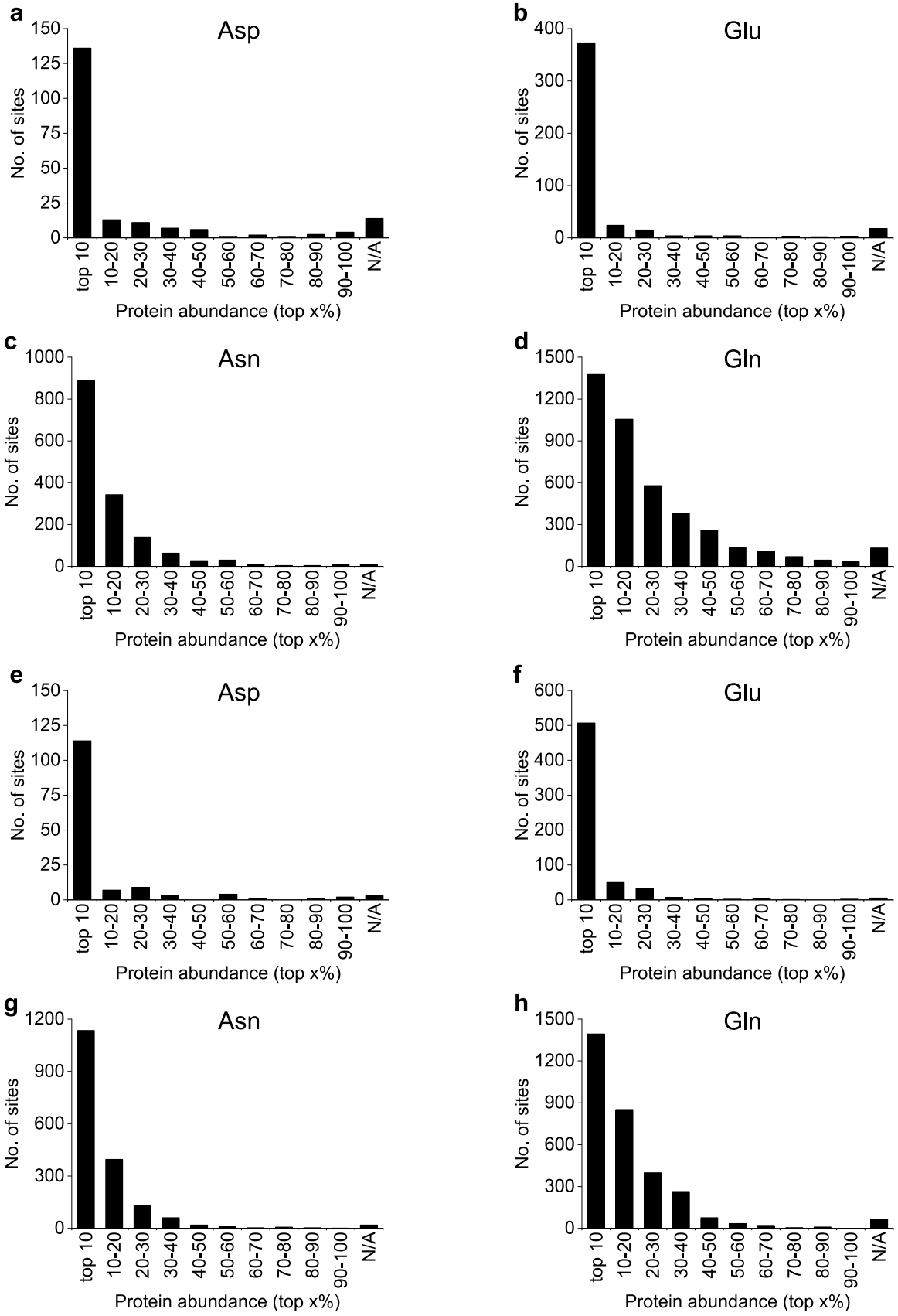
a
Asp
No. of sites
Protein abundance (top x%)
b
Glu
c
Asn
d
Gln
e
Asp
f
Glu
g
Asn
h
Gln
top 10
10-20
20-30
30-40
40-50
50-60
60-70
70-80
80-90
90-100
N/A

Figure S 12: Abundance evaluation of HA-yne modified proteins in labeled proteomes of *P. aeruginosa* (a-d) and *B. subtilis* (e-h). Proteins were ranked according to their abundance in the relative organism and grouped in 10% steps. The last group indicates proteins, for which no abundance data is available (N/A). The number of HA-yne modified peptides was assigned to the relative category. Modification of mainly high abundance proteins suggests background reactivity. Protein abundance data were obtained using the PaxDb database.[133] Reused from Allihn *et al.*[55]

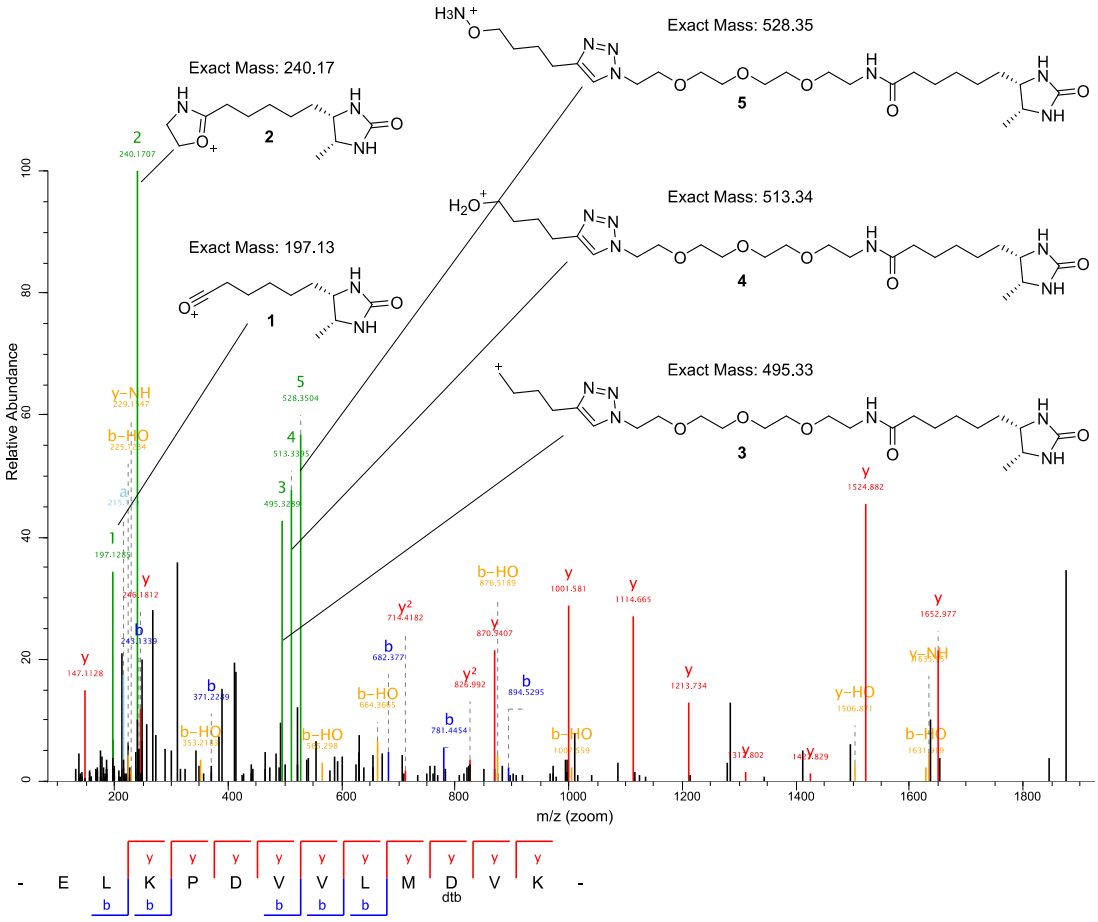

Figure S 13: MS2 spectrum of the pAsp annotated and HA-yne modified peptide from PhoB showing highest intensity of the determined diagnostic peaks.

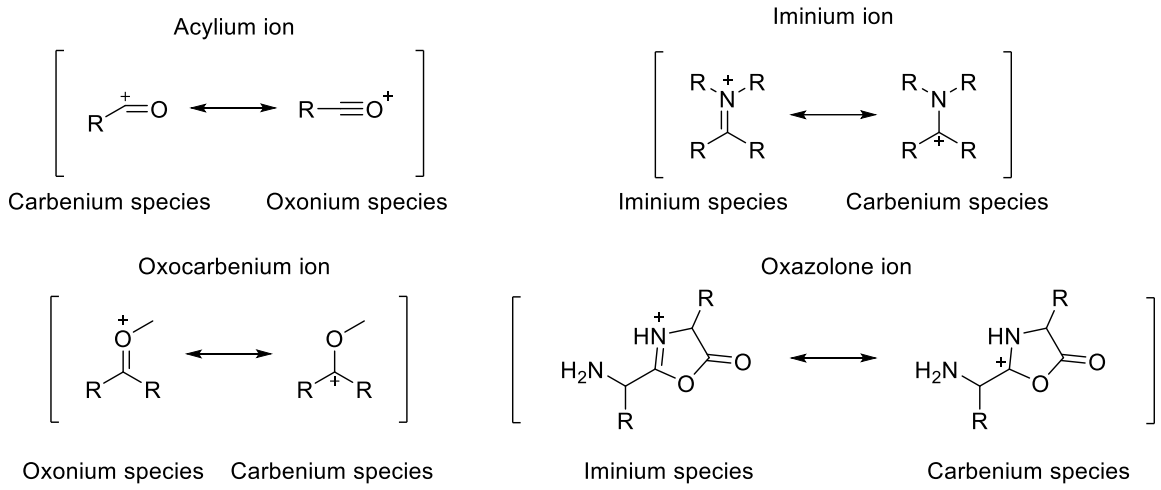

Figure S 14: Overview of the common fragment ion types and their equilibria.

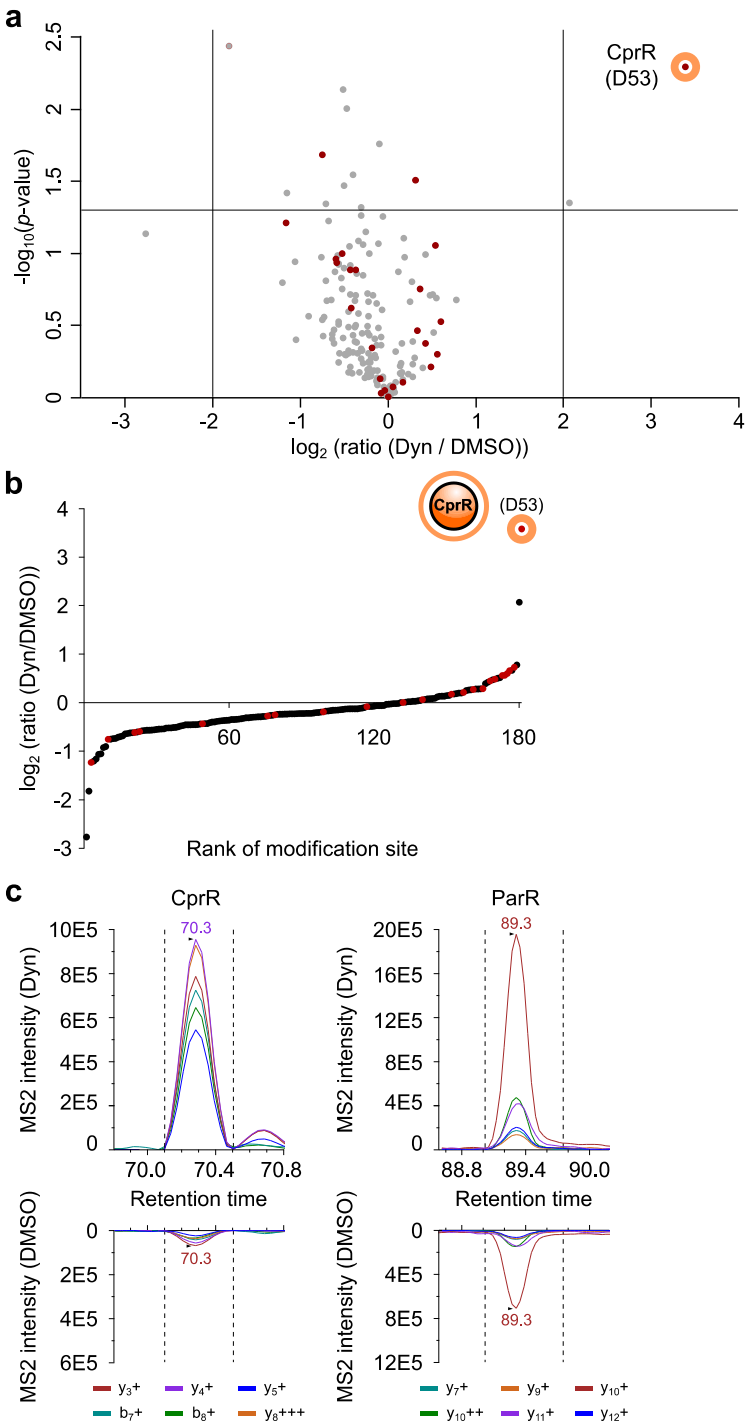

Figure S 15: MS1 (a, b) and MS2 (PRM) quantification (c) for 30 min dynorphin A vs. DMSO treatment. (a) Volcano plot of the isoDTB-ABPP experiment comparing the HA-yne modified sites of DMSO (heavy) and dynorphin (Dyn, light) pretreated samples. Plots show the $\log_2$-fold enrichment of the ratio between light and heavy labeled samples and the probability in a one-sample t-test that the ratio is equal to one ($-\log_{10}(p)$). Red and gray indicate proteins annotated as "phosphoaspartate" in UniProt and all other proteins, respectively. Data were visualized using Perseus software.[128] (b) Waterfall plot representing the ratio between dynorphin A (light) and DMSO (heavy) treated HA-yne modified Asp and Glu residues. Red dots indicate sites, that are also annotated as pAsp sites in UniProt. (c) PRM transitions (Dyn/light vs.

DMSO/heavy) of pAsp annotated and HA-yne modified peptides of response regulators CprR and ParR. Data was analyzed using the Skyline software.9 MS2 ratios of 19.4 and 2.8 were obtained for CprR and ParR, respectively, unraveling CprR as the only protein with highly enhanced modification. Adapted from Allihn *et al.*[55]

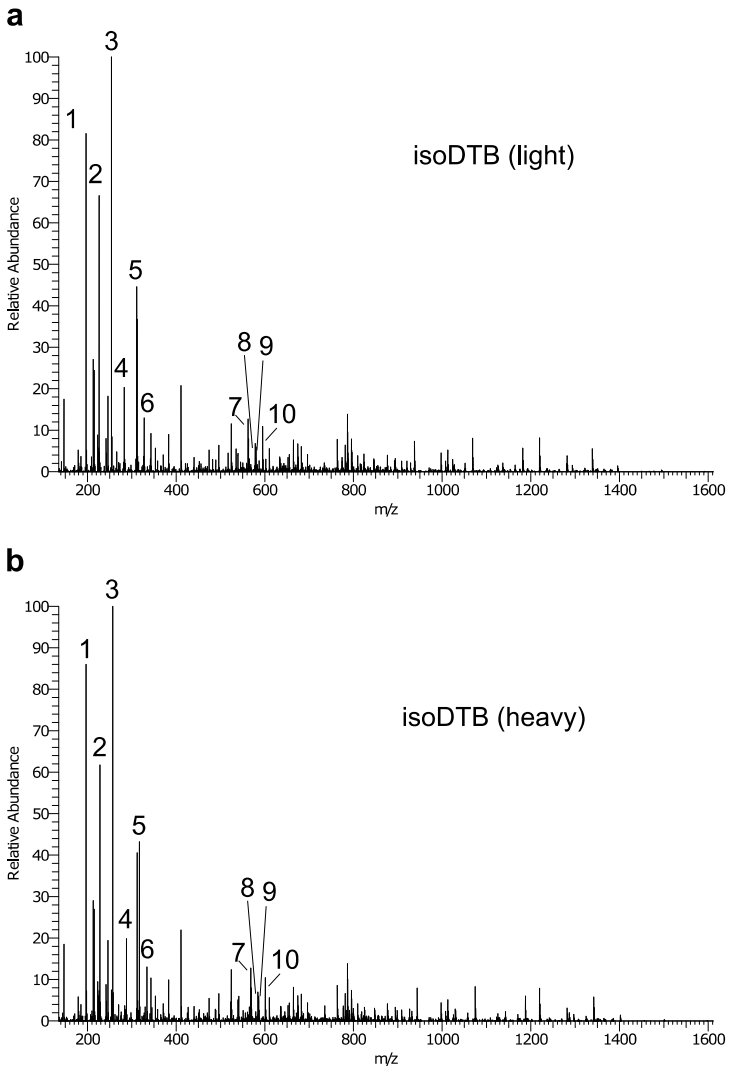

Figure S 16 MS2 spectrum of the RR GacA for assessment of the reoccurrence of diagnostic peaks. Interestingly, especially the tag-specific fragments (1-6) show extraordinary high intensity. The diagnostic peaks have almost identical relative abduncancies in both light (a) and heavy samples (b).

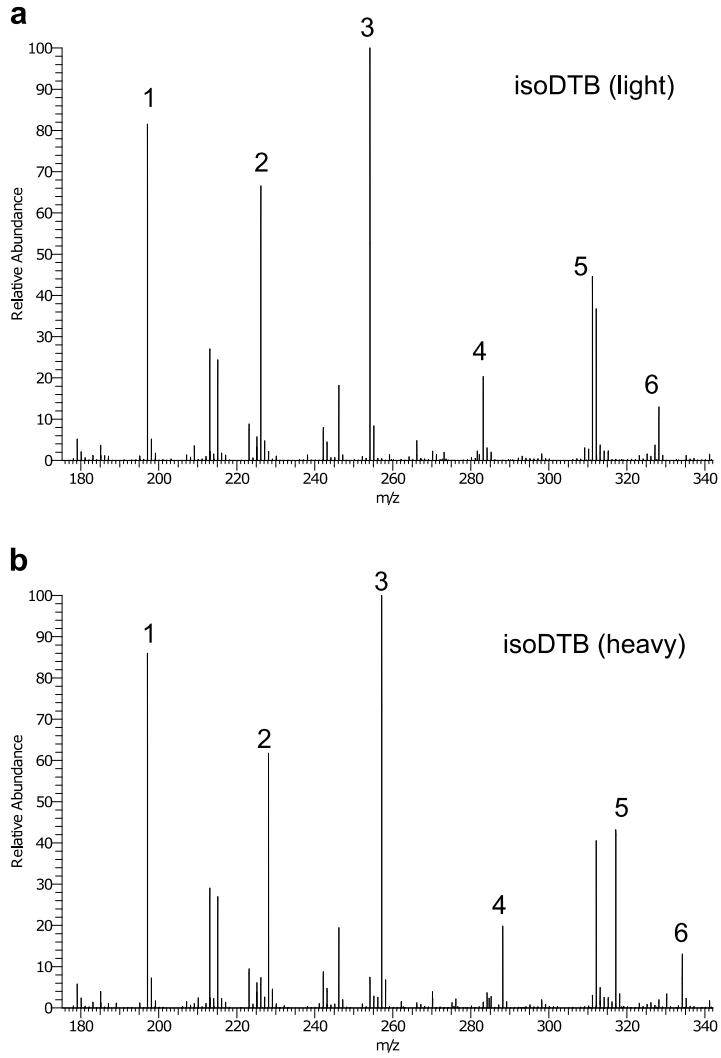

Figure S 17: Tag-specific fragments. Zoom of the MS2 spectrum of the RR GacA for assessment of the reoccurrence of diagnostic peaks. All tag-specific fragments are highly abundant in both channels.

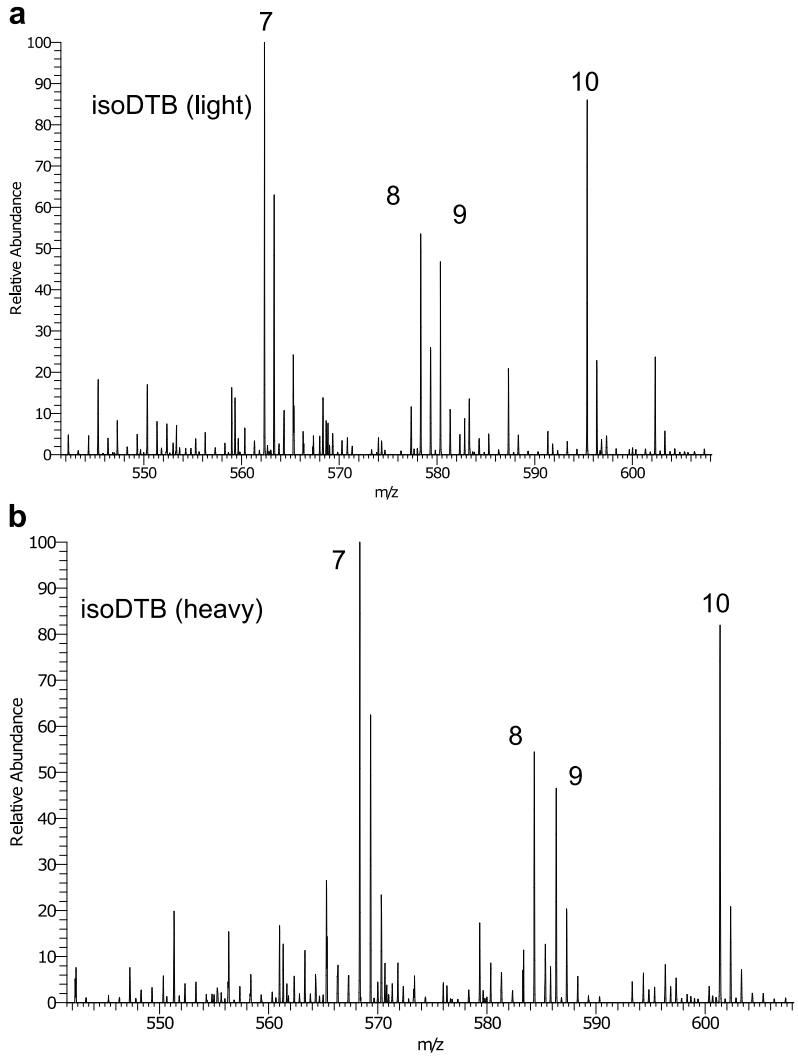

Figure S 18: Probe specific fragments. Zoom of the MS2 spectrum of the RR GacA for assessment of the reoccurrence of diagnostic peaks. All probe-specific fragments are abundant in both channels.

8 License Agreement

A tailored phosphoaspartate probe unravels CprR as a response regulator in *Pseudomonas aeruginosa* interkingdom signaling

P. W. A. Allihn, M. W. Hackl, C. Ludwig, S. M. Hacker and S. A. Sieber, *Chem. Sci.*, 2021, **12**, 4763 **DOI:** 10.1039/D0SC06226J